# INCIPIENT BEARING FAULT DETECTION FOR ELECTRIC MACHINES USING STATOR CURRENT NOISE CANCELLATION

A Dissertation
Presented to
The Academic Faculty

By

Wei Zhou

In Partial Fulfillment
Of the Requirements for the Degree
Doctor of Philosophy in the
School of Electrical and Computer Engineering

Georgia Institute of Technology

December 2007

# INCIPIENT BEARING FAULT DETECTION FOR ELECTRIC MACHINES USING STATOR CURRENT NOISE CANCELLATION

Approved by:


Dr. Thomas G. Habetler, Advisor
School of Electrical and Computer Engineering
*Georgia Institute of Technology*

Dr. Ronald G. Harley
School of Electrical and Computer Engineering
*Georgia Institute of Technology*

Dr. Deepakraj M. Divan
School of Electrical and Computer Engineering
*Georgia Institute of Technology*

Dr. Thomas Michaels
School of Electrical and Computer Engineering
*Georgia Institute of Technology*

Dr. Rhett Mayor
School of Mechanical Engineering
*Georgia Institute of Technology*


Date Approved: November 12, 2007

# ACKNOWLEDGEMENTS

I am very appreciative to my advisor, Dr. Thomas Habetler, for his continual guidance and support. He has been a source of motivation and inspiration throughout the course of this work. I am also grateful to Dr. Ronald Harley and Dr. Deepak Divan, for their time and invaluable input into my research. I have benefited immensely from their knowledge and experience. I would also like to thank Dr. Thomas Michaels and Dr. Rhett Mayor for their time, input, and for serving on my thesis committee.

I would like to acknowledge Eaton Corporation for providing the financial support necessary to conduct this work. I would also like to acknowledge the ECE machine shop. Special thanks to Lorand Csizar, who was always available and willing to help with the laboratory setup.

I wish to thank the faculty members and my colleagues in the Power group for their assistance and support during my PhD study at Georgia Tech. I want to especially thank Dr. Sakis Meliopoulos, Dr. Miroslav Begovic, Dr. Bin Lu, Dr. Jose Aller, Stefan Grubic, Dr. Long Wu, Dr. Zhi Gao, Wei Qiao, Yi Yang, Yang Song, Dr. Xianghui Huang, Youngcook Lee, Dr. Satish Rajagopalan, Dr. Salman Mohagheghi, Dr. Ramzy Obaid, Yamille del Valle, Jean Carlos Hernandez Mejia, Harjeet, Yi Du, Pinjia Zhang, and Yao Duan. I also want to thank Dr. Jason Stack, whose work provided an excellent introduction to this area for me.

I am deeply indebted to my parents and brothers for a lifetime of support, encouragement, and education. I also want to thank my sisters-in-law, my nephew, and my niece for their love. The most wonderful thing during these years in the pursuit of the Ph.D. Degree was meeting Ms. Lifei Kong. I would like to thank her, now my wife, for her love and support that has helped to make everything I have accomplished possible.

# TABLE OF CONTENTS

# LIST OF TABLES

# LIST OF FIGURES

# SUMMARY

The objective of this work is to develop a non-intrusive and inexpensive detection method for generalized-roughness bearing faults in electric machines, with particular interest in identifying faults at an early stage. This involves several steps. First, available condition monitoring methods for bearings are analyzed and compared. The main objective of this comparison is to find the method that is the least intrusive and can be realized with the lowest costs. Second, based on the selected monitoring method, a fault index is developed. And thirdly, based on this fault index, a threshold is built that indicates the state of the bearing's degradation. Since bearing faults account for approximately one half of all electric machine failures, this topic is of practical importance.

Since the method is supposed to be non-intrusive and low-cost, the stator current of the electric machines is chosen as the main media to perform the monitoring process. To fully appreciate the advantages of stator current-based monitoring, a brief review of different bearing condition monitoring methods is presented, with emphasis on their implementation requirements. These monitoring methods include vibration, temperature, chemical, acoustic emission, sound, laser, and current monitoring. The comparison of these methods shows that current-based monitoring is the future trend of bearing condition monitoring, while vibration-based monitoring is most widely used at the present time.

A comprehensive survey of literature available on existing current-based bearing fault detection techniques is presented. The survey shows that most of the methods are not suitable for detecting generalized-roughness bearing faults. It also reveals the major disadvantages of current-based monitoring: the fault signatures injected by generalize-roughness bearing faults, especially by those at an early stage, are subtle, and no physical equations are available to describe the fault signatures.

To address those disadvantages, the bearing fault detection problem is examined under the signal processing theory. The examination illustrates that the problem is a low signal-to-noise ratio (SNR), where noise refers to dominant components in stator current that are not related to bearing faults, and signal refers to those components that are injected by bearing faults. To effectively solve the problem, it is proposed that a noise cancellation algorithm be used.

A survey of different noise cancellation algorithms is performed in order to choose an appropriate noise cancellation algorithm. Due to its optimum property in the sense of producing the best estimate of a noise-interfered signal and its ability to fully use the frequency properties of the noise and the signal, the Wiener filtering technique is selected among all the algorithms available. Once the noise cancellation is accomplished, the remaining components are related to bearing faults. Specifically, the RMS of the noise-cancelled stator current is chosen as the fault index.

To verify the effectiveness of the proposed method, online experiments at constant-load and variable-load conditions are performed. An experimental method, known as the shaft current method, is employed to generate bearing faults online; the generated bearing faults are characteristic of generalized roughness on bearing surfaces and are similar to the realistic bearing faults. The industrial vibration standard is applied to provide information on the bearing condition as a reference. Since load has drastic impacts on the performance of the bearing fault detection, a strategy is proposed to minimize the effects of variable-load conditions. For this purpose, the noise cancellation algorithm is applied to different load levels separately, and stator current-based speed estimation is used to indicate the level of the load. The noise cancellation results for those experiments are compared to those of the existing Mean Spectral Deviation (MSD) method. The correlation between the stator current measurements and the machine vibration is also evaluated.

It is desired to evaluate the bearing condition solely based on the value of the fault index in real time. This is achieved by establishing a threshold on the fault index such that when the fault index frequently exceeds this threshold, the bearing is in a deteriorated condition. This issue is addressed in detail in the dissertation. First, the difficulties relating the fault signatures in the stator current to the fault severity evaluation are discussed. Then, to minimize the difficulties, it is proposed that statistical methods such as the Statistical Process Control (SPC) should be applied to compute the threshold. Finally, the data from the on-line experiments is analyzed and the results show that the threshold computed by SPC serves the purpose of detecting a deteriorated bearing.

In contrast to most of the existing current monitoring techniques, there are many desirable features of the method developed in this research. The method is specifically designed to detect generalized-roughness bearing faults. Furthermore, the method is easy to implement, since it does not require information about the machine parameters and bearing dimensions. Neither does the implementation require a high-resolution spectrum analyzer. These features make the method promising for practical use.

# CHAPTER 1

# INTRODUCTION AND OBJECTIVE OF RESEARCH

## 1.1 PROBLEM STATEMENT

Electrical machines are extensively used and are at the core of most engineering systems. Unanticipated machine failures incur huge costs for industries. Condition monitoring of electrical machines provides the health status of electric machines and recognizes machine faults at an early stage. Based on condition monitoring, appropriate maintenance can be scheduled and the collapse of industrial processes from machine failures can be avoided. Machine failures include stator, rotor, and bearing failures. Bearing failures account for approximately 41% of all machine failures [1]. Therefore it is of practical importance to monitor bearing conditions in electrical machines.

There are many bearing condition monitoring methods, including vibration monitoring, temperature monitoring, chemical monitoring, acoustic emission monitoring, current monitoring, etc. Except for current monitoring, all these monitoring methods require expensive sensors or specialized tools and are usually intrusive. In current monitoring, no additional sensors are necessary. This is because the basic electrical quantities associated with electromechanical plants such as currents and voltages are readily measured by tapping into the existing voltage and current transformers that are always installed as part of the protection system. As a result, current monitoring is non-intrusive and may even be implemented in the motor control center remotely from the motors being monitored. Therefore, current monitoring offers significant implementation and economic benefits.

Another advantage of current monitoring is that an overall electric machine condition monitoring package is possible, given the fact that the detection of other machine faults and the estimation of machine speed and efficiency have been well achieved via stator current.

Most existing current-based bearing condition monitoring techniques are designed to detect the four characteristic bearing fault frequencies: a) the inner raceway fault frequency, b) the outer raceway fault frequency, c) the cage fault frequency, and d) the ball fault frequency. Such techniques are most effective for detecting bearing faults that are generated off-line, for example, by drilling a hole on either part of a bearing. However, for many realistic bearing faults that develop during operation in industrial settings, especially at an early stage, these characteristic fault frequencies do not appear. These realistic faults are often characterized by generalized roughness on bearing surfaces which results in subtle fault signatures. Consequently, most existing current-based techniques may not be suitable for generalized-roughness fault detection.

In addition to the fact that the fault signatures caused by realistic bearing faults are typically subtle, no fundamental relationship is available to describe the fault signatures in terms of on-line measurable parameter. This makes it difficult to assess the fault severity based on the fault signatures in the stator current even if a fault is recognized. Due to these difficulties, there is *no* current-based bearing fault detection technique presently employed in industry.

## 1.2 OBJECTIVE OF RESEARCH

The main objective of this research is to develop a new current-based bearing condition monitoring method. Such a method should be able to detect incipient bearing faults that are characterized by generalized roughness on the bearing surfaces. Other preferred

characteristics of such a method include easy implementation and minimal requirements for external information or devices. For example, it is desired that the bearing condition can still be monitored without the information about bearing dimensions. It is also desired that the use of high-resolution power spectrum analyzers, which are employed in most of the existing monitoring schemes, be avoided.

To meet this objective, the fault signatures for generalized-roughness faults have to be extracted. Since they are usually subtle in magnitude and with unpredictable frequencies, in this research it is not attempted to locate specific frequencies in the stator current to discover the fault signatures. Instead, the problem will be closely inspected using signal processing theory and advanced signal processing technologies will be applied to solve the problem.

Once the fault signatures are extracted and the fault-related components are isolated, the proposed technique should be able to evaluate the condition of the bearings in real-time using the magnitude of the components. For this purpose, it is desired to have a threshold on the magnitude of these components in order to distinguish between normal bearing conditions and degraded bearing conditions. When the measured magnitude exceeds the threshold, a warning message about a possible degraded bearing will be generated to attract the operator's attention. The warning threshold will be determined by considering many factors. For example, the magnitude of the fault-related components may differ among applications. All of these problems will be fully addressed in this work.

Experiments are needed to validate a bearing condition monitoring scheme. A special experimental setup is employed to generate bearing faults *in situ.* The faults generated by using this setup are characterized by generalized roughness on the bearing surfaces; thus, compared to off-line created bearing faults, they are more representative of realistic faults.

On-line experiments will be conducted and the data collected from those experiments will be used to validate the algorithms proposed in this research. This is one of the most distinctive features of this study, compared to most existing studies where the involved bearing faults are created off-line and characterized by distinct, single-point defects on the bearing surfaces.

## 1.3 OUTLINE OF DISSERTATION

This dissertation is organized as follows: in Chapter 2, background information is provided and existing bearing condition monitoring schemes are discussed. This includes the introduction of bearing fault classifications, the survey on different condition monitoring methods (vibration-, temperature-, chemical-, and acoustic-based, etc.), and the review of existing vibration-based and current-based techniques. The limits and shortcomings of these existing techniques are pointed out in order to define the scope of this research: the development of a current-based monitoring scheme that is suitable to detect generalized-roughness bearing faults.

In Chapter 3, a survey on noise cancellation algorithms is presented, which is the basis for the new monitoring concept introduced in Chapter 4. According to this concept, the bearing fault detection can be treated as a low signal-to-noise ratio (SNR) problem and a noise cancellation algorithm is appropriate to solve the problem. The survey in Chapter 3 is, therefore, performed in an attempt to select the best algorithm for bearing fault detection purposes. Common noise cancellation structures and algorithms are examined under the need of the current-based bearing fault detection in this chapter.

In Chapter 4, a new method to extract bearing fault signatures in stator current is

introduced. The method is based on the concept of treating non-bearing-fault-related components as noise. Since those fault-unrelated components are actually dominant in the stator current, the problem is formulated as a low signal-to-noise-ratio (SNR) problem, where the signal refers to the fault-related components. The components carrying fault signatures are extracted via stator current noise cancellation by using the Wiener filtering technique. The invention and development of the method is a major contribution of this work [71 - 74]. The related theoretical analysis is also presented in this chapter.

Chapter 5 presents the experimental validation of the method under constant-load conditions. The experimental method to generate *in situ* bearing faults is introduced. The results of applying the proposed noise cancellation method to those experiments are discussed. In addition, the noise cancellation results are compared to those from the existing methods. The correlation between the noise cancellation results and the vibration measurements is also investigated.

Chapter 6 proposes a scheme to apply the noise cancellation method to variable-load conditions. Current-based speed detection is employed to differentiate load levels and the noise cancellation method is applied to each load level separately. The results from the on-line experiments are presented.

Chapter 7 describes the determination of the warning threshold based on the magnitude of fault-related components, where the fault-related components are obtained by using the noise cancellation method described in Chapter 4. The warning threshold serves as the maximum allowed magnitude of those components under healthy bearing conditions. Considering the many critical factors involved, it is proposed that statistical methods are appropriate to determine the warning threshold. It is then demonstrated that the statistical process control (SPC) theory can be applied to calculate the warning threshold. The results obtained by applying the SPC for those on-line experiments are also presented in this

chapter.

Finally, major conclusions and contributions are summarized in Chapter 8. Recommendations for future work are also presented at the end of the chapter.

# CHAPTER 2

# SURVEY OF BEARING CONDITION MONITORING METHODS

## 2.1 BEARING INTRODUCTION AND BEARING FAULTS CATEGORIZATION

This chapter is organized as follows: in Section 2.1, a brief introduction of bearing and bearing faults is presented; in Section 2.2, different bearing condition monitoring methods are reviewed; in Sections 2.3 and 2.4, representative techniques in vibration monitoring and current monitoring are summarized; and in Section 2.5, a summary of this chapter is presented.

Bearings are a common element of electric machines. They are employed to permit rotary motion of the shafts. Though modern manufacturing has increased the reliability of bearings, bearings are subject to fail. In fact, bearings are the single largest cause of machine failures. According to some statistical data, bearing faults account for over 41% of all motor failures, while rotor cage faults and stator insulation faults account for 10% and 35%, respectively [1].

Among the different types of bearings, rolling element bearings are most frequently used in typical applications. The most common rolling element bearing used in motors is the single-row deep-groove ball bearing, as shown in Figure 2.1. This bearing is made up of four parts: the balls, the inner raceway, the outer raceway, and the cage.

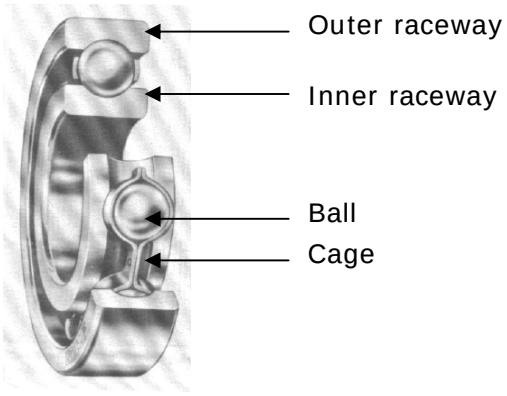


**Figure 2.1The structure of a typical ball bearing.**

**(Figure courtesy Harris *Rolling Bearing Analysis*)**

Corresponding to the four parts there are four characteristic fault frequencies as defined by the following equations:

$$F_I = \text{inner raceway fault frequency} = \frac{N_B}{2} F_R \left(1 + \frac{D_B \cos(\theta)}{D_P}\right), \tag{2.1}$$

$$F_O = \text{outer raceway fault frequency} = \frac{N_B}{2} F_R \left(1 - \frac{D_B \cos(\theta)}{D_P}\right), \tag{2.2}$$

$$F_C = \text{cage fault frequency} = \frac{1}{2} F_R \left(1 - \frac{D_B \cos(\theta)}{D_P}\right), \tag{2.3}$$

$$F_B = \text{ball fault frequency} = \frac{D_P}{2D_B} F_R \left(1 - \frac{D_B^2 \cos^2(\theta)}{D_P^2}\right). \tag{2.4}$$

In these equations, $F_R$ is the machine speed, $N_B$ is the number of balls, $D_B$ is the ball diameter, $D_P$ is the ball pitch diameter, and the angle $\theta$ is the ball contact angle.

The thorough derivation of the above equations can be found in [2] or in [3]. According to these equations, the characteristic fault frequencies are determined by the geometry of the bearing and the machine speed. If the bearing has 6 – 12 rolling elements, the inner raceway fault frequency and the outer raceway fault frequency can be estimated by the following equations, respectively [4].

$$F_I = 0.6 N_B F_R \,, \tag{2.5}$$

$$F_O = 0.4 N_B F_R \,. \tag{2.6}$$

Most current-based bearing fault detection techniques focus on the four characteristic fault frequencies [5-9]. However, the four characteristic fault frequencies don't exist in many realistic bearing faults [9-11]. This has led to the notion of classifying bearing faults according to the fault signatures that are produced [10]. From this notion, bearing faults can be categorized into two types: single-point defects or generalized roughness. Single-point defects are usually created off-line in a lab or a workshop, for example, by drilling a hole in either part of the bearing. Generalized roughness faults are most often generated on-line (*in situ*) and are characterized by the degraded bearing surfaces, but they do not necessarily exhibit distinguishing defects.

For single-point defects, the characteristic fault frequencies exist in machine vibration and can be reflected into the stator current. Therefore, the faults can be identified by detecting the characteristic fault frequencies. For generalized roughness faults, the characteristic fault frequencies may not exist in machine vibration or in the stator current. These faults may cause broadband changes in machine vibration and can be detected by rudimentary techniques based on the general guidelines laid out in ISO 10816 [12, 13]. However, the exact effects they have on the stator current are still not very clear at the present time, though some preliminary research shows that they may cause similar broadband changes in the stator current as in machine vibration [10]. Since generalized roughness faults are most often neglected in the literature despite the fact that they widely exist in industries, this research will mainly focus on the detection of this type of fault.

## 2.2 BEARING CONDITION MONITORING METHODS

In an effort to fully appreciate the advantages of current-based bearing condition monitoring techniques, a brief review of different bearing condition monitoring methods is presented. These monitoring methods include vibration monitoring, temperature monitoring, chemical monitoring, acoustic emission monitoring, sound pressure monitoring, laser monitoring, and current monitoring. They are reviewed in the following subsections, with emphasis on their implementation considerations.

### 2.2.1 BEARING CONDITION MONITORING VIA MACHINE VIBRATION

The bearing condition can be very well monitored via machine vibration. This is because bearing faults, whether single-point defects or generalized roughness, will typically produce salient fault signatures in machine vibration. Vibration has to be measured by using vibration sensors, such as accelerometers and vibration velocity transducers. Measurements should be taken on the bearings, bearing support housing, or other structural parts that significantly respond to the dynamic forces and characterize the overall vibration of the machine [12, 13].

It has been recognized for many years that machine vibration is a very reliable indicator for bearing faults. Therefore, vibration monitoring is popular in practice, and well-accepted standards are available such as ISO 10816 [12, 13]. However, the major disadvantage of vibration monitoring is cost. For example, a regular vibration sensor costs several hundred dollars. A high product cost can be incurred just by employing the necessary vibration sensors for a large number of electric machines. Another disadvantage of vibration monitoring is that it requires access to the machine. For accurate measurements, sensors

should be mounted tightly on the electric machines, and expertise is required in the mounting. In addition, sensors themselves are subject to fail. This could be a problem given that the typical lifetime of a bearing is several years.

### 2.2.2 Bearing Condition Monitoring via Chemical Analysis

When lubricating oils are degraded by heat, they produce a large number of chemical products in the form of gas, liquid, and solid states. Also, when bearings are degraded, wear debris is likely to be generated and released. Therefore, lubrication oils carry not only the products of their own degradation, but also those from the wear of bearings [14]. Thus the bearing health can be monitored by performing chemical analysis on the lubrication oil.

Though the detection of oil degradation and wear debris could provide useful information about the bearing condition, the detection can be performed only when the lubricating oil is available. Therefore, chemical monitoring is only applicable for large machines (above 50 kW) with oil-lubricated bearings and larger size machines possessing sleeve bearings with a continuous oil supply. For small and medium size machines, since greases are usually encapsulated inside bearings, chemical analysis methods are not practical.

### 2.2.3 Bearing Condition Monitoring via Temperature Measurement

Bearing temperatures should not exceed certain levels at rated conditions. For example, in the petroleum and chemical industry, the IEEE 841 standard specifies that the stabilized bearing temperature rise at rated load should not exceed 45$^{o}$C (50$^{o}$C on two-pole motors) [15]. The bearing temperature rise can be caused by degradation of the grease or the bearing. Some other factors that can cause the bearing temperature rise include winding temperature rise, motor operating speed, temperature distribution within the motor, etc [16]. Therefore, the bearing temperature measurement can provide useful information about the

machine health and the bearing health [17].

The major disadvantage of temperature monitoring is that it takes effort to place embedded temperature detectors in bearings. Even if the bearing temperature is available and a temperature rise is recognized, further investigation is required to determine the cause of the temperature rise. Therefore, temperature monitoring is not very popular today, though this is a traditional way to monitor bearing conditions.

### 2.2.4 Bearing Condition Monitoring via Acoustic Emission

In high-noise environments, the standard vibration monitoring may encounter some difficulties. This is because the low-frequency vibrations associated with small bearing defects contribute negligible energy to the system in comparison to the surrounding noise. For example, the success of vibration monitoring as a bearing diagnostic system for gas turbines, aircraft transmissions, and liquid rocket engines has been disappointing [18]. However, in such environments, the stress wave emissions in high-frequency regions (above 100 kHz) can still provide clear indications of the defects and thus provide an earlier and more reliable indication of bearing degradation. The high-frequency stress waves, i.e., acoustic emission, can be sensed by acoustic emission transducers.

Compared to classical vibration monitoring, acoustic emission monitoring can provide higher signal-to-noise ratio in high-noise environments; however, it also experiences high system costs. In addition, specialized expertise is required in measuring acoustic emission.

### 2.2.5 Bearing Condition Monitoring via Sound Pressure

Since bearing degradation can affect noise emission from the bearing, sound pressure has

been utilized for bearing condition monitoring [19, 20]. The sounds recorded in the research are within the frequency range from 0 Hz to 20 kHz. As in vibration, the characteristic fault frequencies may be identified in the noise excited by bearing defects.

Since bearing noise can be recorded by using microphones, and even screeching from bad bearings can be heard by human ears, sound monitoring seems less intrusive than other conventional methods. However, in sound monitoring, background noise and the unwanted noise from other bearings must be shielded; otherwise, the bearing noise of interest will be corrupted, which could yield incorrect results. Therefore, sound monitoring is not applicable for processing facilities having many electric machines in one room until the above issue is resolved.

### 2.2.6 Bearing Condition Monitoring via Laser Displacement Measurement

Though vibration displacements are usually calculated from vibration accelerations that are measured via accelerometers, there might be some calculation errors in this process. To eliminate such errors, there is research being done that uses a laser sensor to directly read bearing displacements caused by bearing defects [21]. Though this is an alternative way to obtain bearing vibrations, it requires that the laser displacement sensor be placed on the bearing surface, which is usually not easy to implement.

### 2.2.7 Bearing Condition Monitoring via Stator Current

The basic electrical quantities associated with electromechanical plants are readily measured by tapping in to the existing voltage and current transformers that are always installed as part of the protection system [14]. These are standard practice, and therefore no additional sensors are necessary in current monitoring. As a result, current monitoring is

non-invasive and may even be implemented in the motor control center remotely from the motors being monitored. Therefore, current monitoring can provide significant economic and implementation benefits. Another advantage of current monitoring is that an overall machine condition monitoring package is possible, given that the detection of other machine faults and the estimation of machine speed and efficiency can be fairly well achieved via stator current.

The major disadvantage of current-based bearing monitoring is that bearing-fault signatures are very subtle in the stator current where the dominant components are supply frequency components. For single-point defects, the subtle fault signatures can be discovered by monitoring the characteristic fault frequencies, as illustrated in previous research. However, little attention has yet been given to generalized roughness faults. Therefore, a challenge will be to apply current monitoring in the detection of these faults.

Despite the diversity of bearing monitoring strategies, vibration monitoring and current monitoring are popular. Therefore, a review of state-of-the-art techniques in these two areas is presented in the following sections.

## 2.3 VIBRATION-BASED BEARING FAULT DETECTION TECHNIQUES

Considerable research has been carried out in the development of various algorithms for bearing fault detection via machine vibration. Those algorithms can be classified into time domain, frequency domain, and other algorithms including shock pulse monitoring. They are reviewed in the following subsections.

### 2.3.1 TIME-DOMAIN METHODS

A commonly used vibration monitoring method is to measure the RMS value of the vibration level over a pre-selected bandwidth. This is often called overall level monitoring. The ISO 10816 vibration standard indicates that the RMS value of vibration velocity over a frequency range from 10 Hz to 1 kHz should be used to evaluate the condition of the machine (see Table 2.1) [12, 13]. Another useful set of criteria is that given in the Canadian Government specification CDA/MS/NVSH107. This specification suggests a broader bandwidth, namely, from 10 Hz to 10 kHz, but still relies on overall velocity vibration measurement.

**Table 2.1 Specifications in ISO 10816 [12, 13].**

| RMS vibration velocity (mm/s) | Class I (up to 15 kW) | Class II (15 kW to 75 kW) | Class III (large prime movers with rigid foundation) | Class IV (large prime movers with soft foundation) |
|---|---|---|---|---|
| 0.28 | Normal | Normal | Normal | Normal |
| 0.45 | | | | |
| 0.71 | | | | |
| 1.12 | Acceptable | | | |
| 1.8 | | Acceptable | | |
| 2.8 | Unacceptable | | Acceptable | |
| 4.5 | | Unacceptable | | Acceptable |
| 7.1 | Destructive | | Unacceptable | |
| 11.2 | | Destructive | | Unacceptable |
| 18 | | | Destructive | |
| 28 | | | | Destructive |
| 45 | | | | |

In addition to the basic RMS value (the 2nd order moment), there are other statistical moments that are helpful to detect bearing defects, especially those at an early stage. They are the crest factor, the skew value (the normalized 3rd moment), the kurtosis (the normalized 4th moment). Intuitively, the RMS value gives the intensity of the signal, the skew value measures the degree of symmetry of the shape of the probabilistic distribution curve, and the kurtosis measures the Gaussianity of the distribution of the signal. For the signal $x(n)$, $n = 1,..., N$ its rth-order moment about its mean $\bar{x}$ is $M_r = \frac{1}{N}\sum_{k=1}^{N}(x_k - \bar{x})^r$, its RMS

value is $\sqrt{\frac{1}{n}\sum_{k=1}^{N} x_k^2}$, the standard deviation is $\sigma = \sqrt{\frac{1}{n}\sum_{k=1}^{N}\left(x_k - \bar{x}\right)^2}$, the skew value is $\frac{M_3}{\sigma_3}$, the kurtosis is $\frac{M_4}{\sigma_4}$, and the crest factor is $\frac{[\text{max, peak}]}{\text{rms}}$.

Most bearing surfaces exhibit a random distribution of asperities in the direction of the machining process, and the distribution of asperity heights for an undamaged surface of this type can be assumed to be a Gaussian distribution [22]. From this assumption, for a bearing with good quality surfaces, it can be shown that the kurtosis is 3.0 and the odd moments are zero. As the bearing becomes degraded and the interface between two surfaces in motion begins to break down, the shape of the probability density function (PDF) tends to become peaky. As a result, the skew value and the kurtosis increase. The use of these statistical moments to detect the bearing faults can be found in [19, 22].

Though most time-domain methods are effective techniques for detecting bearing faults, they are limited in fault diagnosis. However, frequency-domain methods are more useful for fault diagnosis.

### 2.3.2 FREQUENCY-DOMAIN METHODS

The most well-known bearing-related frequencies in machine vibration are the characteristic fault frequencies defined in Equations (2.1) – (2.6). By monitoring those fault frequencies, the component in fault (the inner race, the outer race, the cage or the balls) can be specified. However, directly monitoring those frequencies may be difficult, because they are low frequencies and can be easily lost in noise. To improve detection performance, other techniques are required. Those techniques include the envelope method, the adaptive noise cancellation method, and the time-frequency method.

The envelope method is also known as the high frequency resonance method. This method extracts the characteristic fault frequency components from the frequency bands that occur in regions of mechanical resonance (usually above 1 kHz and below 50 kHz). Therefore, the low-frequency high-amplitude non-fault signals can be suppressed in this method. Implementing this method involves band-pass filtering and rectifying the time-domain vibration signal, low-pass filtering the rectified signal to form the envelope, and then analyzing the envelope signal. This is shown in the left part of Figure 2.2. The demodulation can be done either by using an analogue band-pass filter and rectifier, or by using digital filters [23, 24]. A problem with envelope analysis is that salient fault information could fall outside the pre-selected frequency band as the fault develops into different stages.

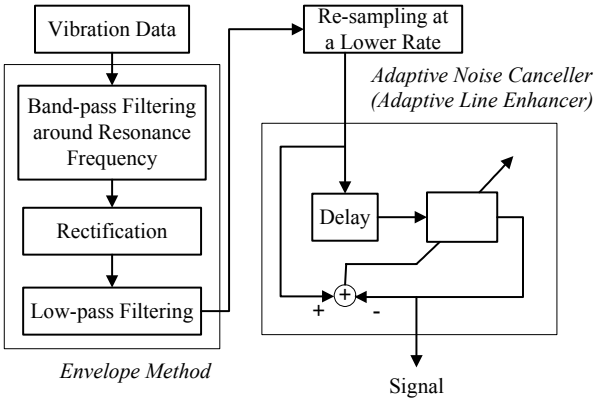


**Figure 2.2 Bearing fault detection by envelope method and adaptive noise cancellation method [25]**

The noise cancellation method is also used in some bearing condition monitoring schemes. As the name *noise cancellation* indicates, noise cancellation can be used to remove unwanted noise and thus increase the signal-to-noise ratio. This is important in the detection of incipient bearing faults; because most difficulties in such detection stem from both the presence of a variety of noises and the wide spectrum of a bearing fault signal [25]. The detection scheme presented in [25] is illustrated in Figure 2.2. First, an envelope signal is obtained by the high-frequency resonance technique (HFRT). Then, this signal passes through an adaptive noise canceller (or adaptive line enhancer, ALE). Since any broadband

noise is not correlated with its delayed version, it will be eliminated by the filter.

Another example of the use of the noise cancellation method in bearing fault detection can be found in [26]. In this research, a reference signal that simulates background noise is the input to an adaptive noise cancellation filter. The output of the filter is used to cancel the background noise in a primary signal. One acoustic emission transducer is positioned on the test bearing housing to measure the primary signal, which includes the bearing fault frequencies, the shaft unbalance frequencies, and background noise. A second transducer is positioned on the frame away from the test bearing to measure the reference signal, which includes the shaft unbalance frequencies and background noise. The experimental results in [26] show that the bearing faults can be identified even when the fault frequencies are similar to the unbalance frequencies.

### 2.3.3 SHOCK PULSE METHOD

As a rolling element bearing degrades, small pits may be developed on bearing surfaces. When these surfaces interact with other parts of the bearing, stress waves, usually called shock pulses, can be generated. These shock pulses are at very high frequencies and can be detected by piezoelectric transducers with high resonant frequency (typical 25 kHz to 35 kHz). A peak holding circuit is employed and the maximum value of shock is then recorded. The condition of the bearing will then be assessed by a quantity known as the shock pulse value, SPV, defined as [14]

$$\mathrm{SPV} = \frac{R}{n^2 F^2} \tag{2.7}$$

where $R$ is the peak value, $n$ is the shaft speed, and $F$ is a factor relating to bearing geometry. Low values indicate bearings in good condition, while high values indicate that bearing damage is likely.

Though a number of commercial instruments are available based on this method, quantitative evaluation using the method remains difficult. Also it works best in conjunction with overall level monitoring method.

### 2.3.4 OTHER METHODS

Other methods in bearing vibration monitoring include the high order spectra (HOS) method [27], the artificial neural network (ANN) method [3], the cepstrum method [28], the hidden Markov modeling (HMM) method [29], and the time signal averaging method. Though these methods have abilities to detect bearing faults in certain applications, they have limitations to be a common tool for bearing fault detection.

## 2.4 CURRENT-BASED BEARING FAULT DETECTION TECHNIQUES

It was verified in [30], published in 1995, that the characteristic bearing-fault frequencies in vibration can be reflected into the stator current. The relationship between the vibration frequencies and the current frequencies for bearing faults can be described by

$$f_{bng} = \left| f_e \pm m \bullet f_v \right| \tag{2.8}$$

where $m = 1, 2, 3, \ldots$, $f_v$ is one of the characteristic vibration frequencies, $f_e$ is the supply frequency, and $f_{bng}$ is the bearing fault frequencies reflected in the stator current.

However, it was discovered in several independent studies [9-11, 31], published from 2004 to 2005, that for many *in situ* generated bearing faults, those characteristic fault frequencies are not observable and may not exist at all in the stator current. This finding led to the classification of bearing faults for bearing fault detection purposes. According to [10],

bearing faults can be categorized into two types: single-point defects and generalized roughness. Single-point defects are usually created off-line, for example, by drilling holes in bearing components. Comparatively, many bearing faults developed through years on-line in industrial processes are generalized-roughness bearing faults, especially at an early stage. Those faults exhibit degraded bearing surfaces, but not necessarily distinct defects.

For single-point defects, the characteristic fault frequencies are a good fault indicator to current-based bearing fault detection [30]. Consequently, single-point defects may be detected by identifying the characteristic fault frequencies in the stator current. For generalized roughness faults, however, those characteristic fault frequencies may not exit. Instead, it is believed that those faults may cause broadband changes on the spectrum of the stator current [10].

It is apparent, then, that the bearing fault signatures are markedly different for different fault types. Therefore, in this chapter, different techniques for bearing fault detection are reviewed under this categorization. Specifically, existing current-based bearing fault detection techniques are categorized as those suitable to detect single-point defects and those suitable to detect generalized-roughness faults.

### 2.4.1 TECHNIQUES TO DETECT SINGLE-POINT DEFECTS

Since the characteristic bearing-fault frequencies are a good indicator of single-point defects, virtually all current-based techniques to detect single-point defects are based on identifying and processing those fault frequencies in the stator current. There are many good techniques available in the literature for single-point defect detection. Representative techniques include the neural-network clustering approach, the adaptive statistical

time-frequency method, the Wavelet packet decomposition method, the statistical discrimination method, and the extended Park's Vector approach, etc. The basic procedure, as well as some related issues, of these techniques is reviewed as follows.

#### 2.4.1.1 The Neural-Network Clustering Approach

This approach is based on an unsupervised neural network and was proposed by Schoen et al. in 1995 [32]. In this technique, stator current is sampled and the spectrum of the stator current is estimated via Fast Fourier Transform (FFT). A rule-based frequency filter then selects frequency components including those at the characteristic fault frequencies and those relating to machine conditions. The amplitudes of those components form the input of the unsupervised neural network for clustering. After the machine is exposed to all the normal operating and load conditions, the clustering is complete and stable. Then, the neural network weights are saved. As bearing faults occur afterwards, new clusters are formed, which indicate a fault condition. A schematic diagram of this method is shown in Figure 2.3. Experiments with a 5-hp motor were performed by the researchers [32] to verify the effectiveness of the technique on bearing fault detection.

This method has led to a significant amount of research in neural network applications in this area. However, rules have to be made in this method, which requires the knowledge of the spectrum distribution of the stator current.

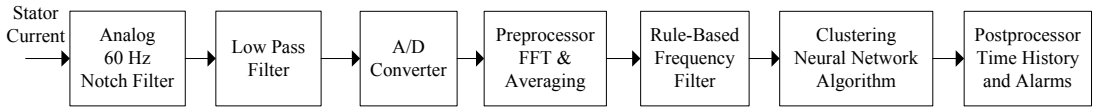


**Figure 2.3 Schematic diagram of current monitoring technique using unsupervised neural network.**

### 2.4.1.2 The Adaptive Statistical Time-Frequency Method

Yazici and Kliman proposed a time-frequency technique in 1999 to detect bearing faults [5]. A schematic diagram of this technique is illustrated in Figure 2.4. This technique treats stator current as a non-stationary signal. First, a time-frequency spectrum is estimated after preprocessing, and feature vectors are extracted from the spectrum. In this research, the feature vectors include frequency components located in the neighborhood of the characteristic fault frequencies (along the frequency axis). Next, the feature space is segmented into various normal conditions of the motor (along the time axis) by a probabilistic method that maximizes the conditional joint distribution probability density function of the feature vectors within a time window. The resulting segments form different operating modes, according to some statistical distance metric. Then, a set of representatives and thresholds is determined for each of the modes. Once the algorithm is trained for all the normal operating conditions, a data base is formed to store all the mode information. For testing data, after the same preprocessing, short-time Fourier transform and feature extraction, the distance between the test feature vector and the representatives of each normal mode is calculated. If this distance is greater than all the mode thresholds, i.e., the test feature vector falls outside the normal modes, then the test measurement is tagged as potential faulty. Experiments with a 3/4-hp motor were performed by the researchers to verify the effectiveness of the technique.

This method provides a useful means to look into the non-stationarity of stator current. However, it involves complicated procedures to calculate the boundaries of those modes.

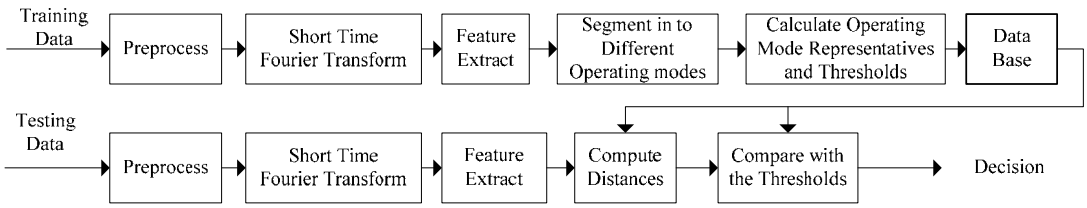


**Figure 2.4 Schematic diagram of current monitoring technique based on time-frequency transform.**

### 2.4.1.3 The Wavelet Packet Decomposition Method

A bearing fault detection scheme based on wavelet packet decomposition was proposed by Eren and Devaney in 2004 [6]. A schematic diagram is shown in Figure 2.5. First, the stator current signal is pre-processed as usual. Next the signal is decomposed linearly within the 0-240 Hz band and decomposed logarithmically for higher-frequency bands to minimize the computational effort while not losing the characteristic fault frequencies. Then, the signal is further decomposed into 7.5-Hz wavelet packets (nodes) over the 0-240 Hz frequency band using a FIR filter-bank structure. After that, the nodes covering the characteristic fault frequencies are selected, and the wavelet coefficients for these nodes are used to calculate the RMS value of these nodes. This is repeated for a set of healthy bearings to form baseline data (In this research eight healthy bearings were used). Specifically, the mean and the standard deviation of the RMS value of the selected nodes from the healthy bearings are calculated and saved as the baseline data. For a testing bearing, the RMS value of the selected nodes is calculated. A significant increase of the RMS value indicates a bearing fault condition. Experiments with a 1-hp motor were performed by the researchers to verify the effectiveness of the technique. This research is extended in [33], where a neural network is used to process the results from the wavelet packet decomposition instead of the statistical method.

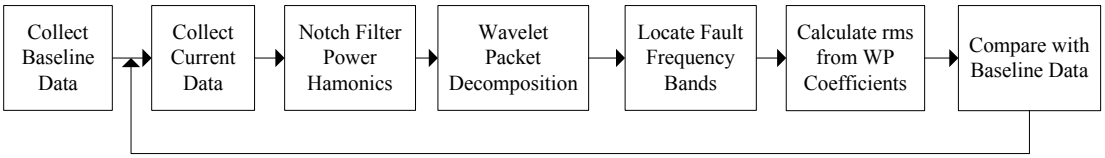


**Figure 2.5 Schematic diagram of current monitoring technique based on wavelet packet decomposition.**

#### 2.4.1.4 The Statistical Discrimination Method

The research in [34] published in 2005 develops a general diagnosis tool for motor condition monitoring. The tool is intended to analyze differences between signals of normal and damaged motors, by using statistical discrimination measures for time-frequency features. The first-order statistics and the second-order statistics of the filter responses are used as the discrimination measures. A notable conclusion from this research is that detection of bearing faults is more difficult at a full-load level than at a no-load level since full load could cause various disturbances. Experiments with a 20-hp motor were performed by the researchers to verify the effectiveness of the technique.

#### 2.4.1.5 The Extended Park's Vector Approach

The research in [39] published in 2005 proposed a bearing fault diagnosis technique based on the extended Park's transform on the three-phase stator currents. The current Park's Vector modulus ($\left|i_d + i_q\right|^2$) was introduced as the fault indicator. It was derived that this modulus contains additional fault components at multiples of the characteristic fault frequencies in the presence of single-point defects. This is compared to the fault components at the modulated frequencies as described by Equation 2.8 in the power spectra of the stator currents themselves. Experiments with a 4-hp motor were performed by the researchers to verify the effectiveness of the technique.

This approach seems simple while effective for detecting single-point defects. However, it requires collecting the stator currents for all three phases at the same time.

It should be noted that the methods (2.4.1.1) – (2.4.1.5) involve inflicting artificial defects to a bearing off-line, and then placing the faulty bearing in a test motor. Two drawbacks exist with this process. First, the off-line generated defects are not very representative of realistic faults [9-11, 31]. Second, disassembling and reassembling a motor can cause unpredictable changes to the stator current spectrum [35]. Therefore, studies on generalized roughness faults, (caused by in situ ageing) are necessary and are of practical importance.

### 2.4.2 TECHNIQUES TO DETECT GENERALIZED ROUGHNESS FAULTS

Generalized-roughness faults are what typically occur in practice. For such faults, new techniques need to be developed to detect those faults, since the characteristic fault frequencies may not exist [9-11, 31]. Currently, few techniques that aim to detect generalized-roughness faults are available in the literature.

A technique called the "mean spectrum deviation (MSD) method" was proposed for this detection purpose in 2004 in [31]. A schematic diagram is shown in Figure 2.6. In this method, stator current is first notch filtered at 60 Hz and 180 Hz by analog filters. Then it is sampled, and further filtered by a bank of digital filters. The frequencies filtered by the digital filters include

a) the supply harmonic frequencies

$$F_{har} = F_e * n \tag{2.9}$$

b) the load variation frequencies and eccentricity frequencies

$$F_{load} = F_{ecc} = F_e\left[1 \pm m(\frac{1-s}{p/2})\right] \tag{2.10}$$

c) the slot harmonics

$$F_{slot} = F_e\left[(m * R \pm N_d)(\frac{1-s}{p/2}) \pm N_w\right] \tag{2.11}$$

d) and the broken bar frequencies

$$F_{brb} = F_e\left[k(\frac{1-s}{p/2}) \pm s\right] \tag{2.12}$$

In these equations, $n, m, k$ are integers, $F_e$ is the fundamental supply frequency (60 Hz), $s$ is the slip, $p$ is the number of poles, $R$ is the number of rotor slots, $N_d$ is the order of the rotating eccentricity (For a static eccentricity, $N_d = 0$ while $N_d = 1$ for a dynamic eccentricity), and $N_w$ is the order of the stator magnetomotive force (MMF) harmonics.

The resulting signal is then modeled as an autoregressive (AR) process driven by white noise, and its power spectrum is estimated from the following equation

$$P_{AR}(e^{j\omega}) = \frac{|b(0)|^2}{\left|1 + \sum_{k=1}^{P} a_P(k) e^{-j\omega k}\right|^2} \tag{2.13}$$

where $a_P(k)$ and $b(0)$ are the model coefficients. The difference between the power spectrum of real-time data and baseline data is computed, and its mean over the entire frequency band of interest is chosen as the fault index. Successful on-line experiments with a 5-hp motor were performed by the researchers to verify the effectiveness of the technique.

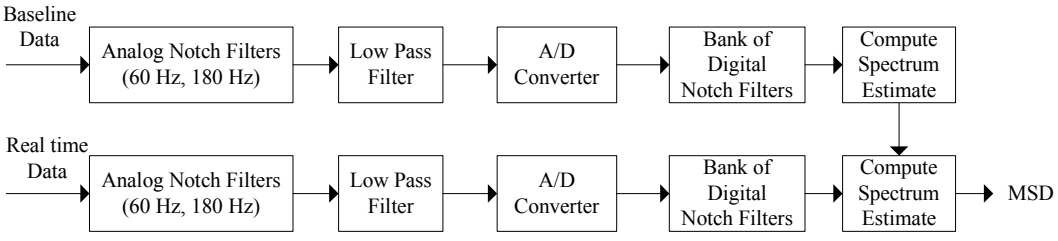


**Figure 2.6 Schematic diagram of the MSD method.**

This method is promising; it is the first current-based technique known in the literature designed to detect generalized roughness bearing faults. However, it has some disadvantages. First, in this method, thorough knowledge of the stator current spectrum distribution is required. Second, it assumes that during the filtering process, no fault information will be lost. However, it is possible that fault information can exist in the components at the frequencies predicted by Equations (2.9)-(2.12) in practice. For example, it has been shown in [11] that contamination of bearings with floor dusts can result in an increase of the components at the eccentricity frequencies predicted by Equation (2.10). Third, machine speed has to be measured or estimated. Machine parameters are also required in this method.

Therefore, the objective of this research is to develop a new improved current-based method to detect bearing faults, including generalized-roughness faults, which overcomes the disadvantages of the existing methods.

## 2.5 SUMMARY

Different bearing condition monitoring methods have been reviewed in this chapter. The notion of categorizing bearing faults as single-point defects or generalized-roughness faults has been discussed. Various vibration- and current-based condition monitoring techniques have been reviewed. The shortcomings of these techniques have been pointed out to define the scope of this research.

# CHAPTER 3

# SURVEY OF NOISE CANCELLATION STRUCTURES AND ALGORITHMS

## 3.1 INTRODUCTION

This chapter is organized in the following manner: in Section 3.1, a brief introduction of noise cancellation and its applications is presented. In Section 3.2, various noise cancellation structures are reviewed. In Section 3.3, various noise cancellation algorithms are reviewed. A summary of the chapter is presented in Section 3.4.

Noise cancellation, also known as Active Noise Control (ANC), utilizes anti-noise to cancel unwanted noise. In most cases, the anti-noise is desired to be equal in magnitude and opposite in phase to the noise; adding the anti-noise and the noise cancels both. Active Noise Control is developing rapidly because, (1) in many cases, passive noise control such as using enclosures, barriers, and silencers either does not have the desired performance or shields interested signals as well, and (2) active noise control permits improvements in noise control, often with potential benefits in size, weight, volume, and cost thanks to favorable DSP systems [36].

Though it is desired to cancel unwanted noise in all noise cancellation applications, the objective of a specific application may be different. In some applications, the target signal consists of noise only, and to cancel the noise is the only objective. Examples include electronic mufflers for exhaust and induction systems, lawn mowers, vacuum cleaners,

transformers, power generators, ear protectors, etc. In many other applications, however, to recover a desired signal corrupted by background noise is as important, if not more so, to cancel the noise. Examples include observing a fetus' heartbeat buried in higher-amplitude background noise from the mother's body, communication between pilots in airplanes, meetings in quiet zones in noisy plants, etc. The objective of noise cancellation for stator current-based bearing fault detection in this research is to recover the bearing fault signal by canceling background noise.

When noise cancellation is used for recovering a desired signal, the characteristics of *both* the desired signal and the background noise need to be considered. Depending on its application, the structure and algorithm of a noise cancellation system may be different as reviewed below.

## 3.2 NOISE CANCELLATION STRUCTURES

From the control standpoint, two broad categories of basic noise cancellation structures are feedforward control and feedback control. In addition to the basic structures, hybrid noise cancellation structures exist and are built upon those basic structures. In the following review, for convenience, feedforward control structures are further categorized as broadband feedforward and narrowband feedforward control in accordance with the frequency properties (broadband or narrowband) of a noise signal.

From an adaptation standpoint, a noise cancellation system can be either non-adaptive or adaptive. A non-adaptive system applies to stationary signals and is easy to implement, while an adaptive system may be desired for non-stationary signals and requires additional sensors. Both the adaptive version and non-adaptive version of the noise cancellation structures are addressed in the following review.

### 3.2.1 BROADBAND FEEDFORWARD NOISE CANCELLATION STRUCTURES

For broadband feedforward structures, in addition to a primary sensor, a secondary sensor is usually employed to collect reference signal data. A generic non-adaptive broadband feedforward noise cancellation structure is shown in Figure 3.1. The processor estimates the primary noise from the reference signal by utilizing the coherence between the primary signal and the reference signal.

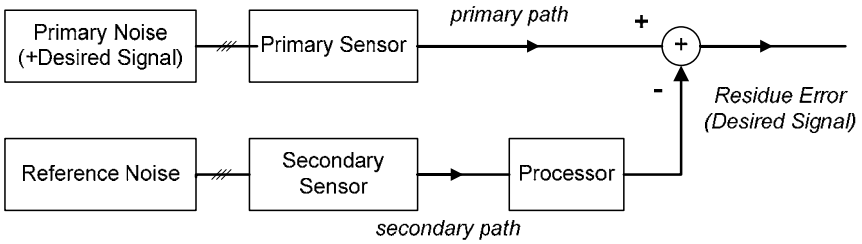


**Figure 3.1 Generic non-adaptive broadband feedforward noise cancellation structure**

For a non-adaptive structure as shown above, an error sensor is not necessary. For an adaptive structure, however, an error sensor is required to measure the difference between a primary signal and the estimated noise, as shown in Figure 3.2. A processor dynamically adjusts the inherent coefficients to minimize the error signal to accommodate the non-stationarity of the primary noise.

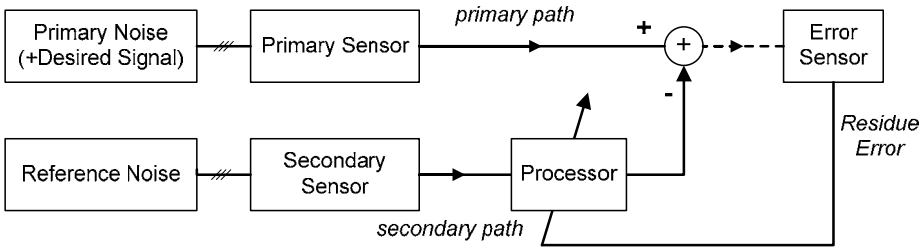


**Figure 3.2 Generic adaptive broadband feedforward noise cancellation structure**

In both of the above structures, it is assumed that a reference noise source is available. Unfortunately, in many applications, a reference signal is neither available nor affordable.

If, however, the noise and the desired signal have different characteristics, it is still possible to achieve good performance by using a delayed version of the primary signal as a reference signal, as shown in Figure 3.3.

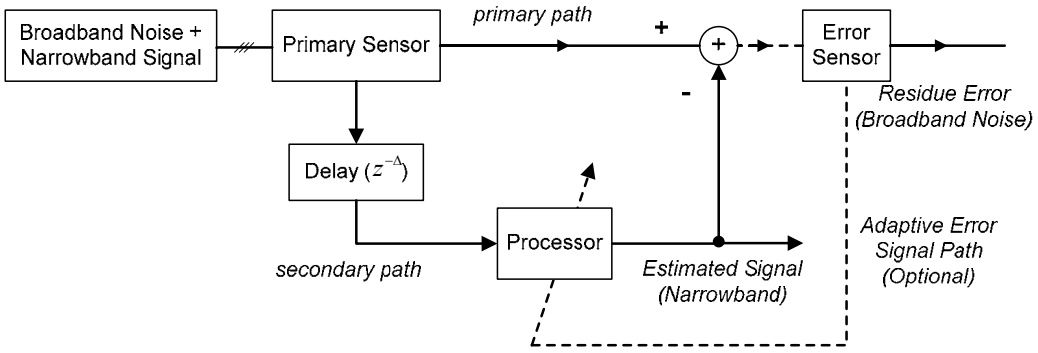


**Figure 3.3 Broadband feedforward noise cancellation without a reference**

As shown in the figure above, noise can be a broadband signal and the signal can be narrowband such as consisting of multiple sinusoids at different frequencies. Through the delaying operation, the broadband noise is filtered out from the output of the processor, since a broadband signal is not correlated with its delayed versions.

In some applications, several practical issues need to be addressed. This is illustrated by a simplified acoustic application shown in Figure 3.4.

The first issue is non-causality caused by the processing time. As illustrated in this figure, after the reference signal is picked up by the reference sensor, the processor will take some time to calculate the correct output to the canceling speaker. If this time delay becomes longer than the acoustic delay (from the reference microphone to the canceling speaker), the processor response is *noncausal*. If the non-causality happens, then the system can effectively control only narrowband or periodic noise [36].

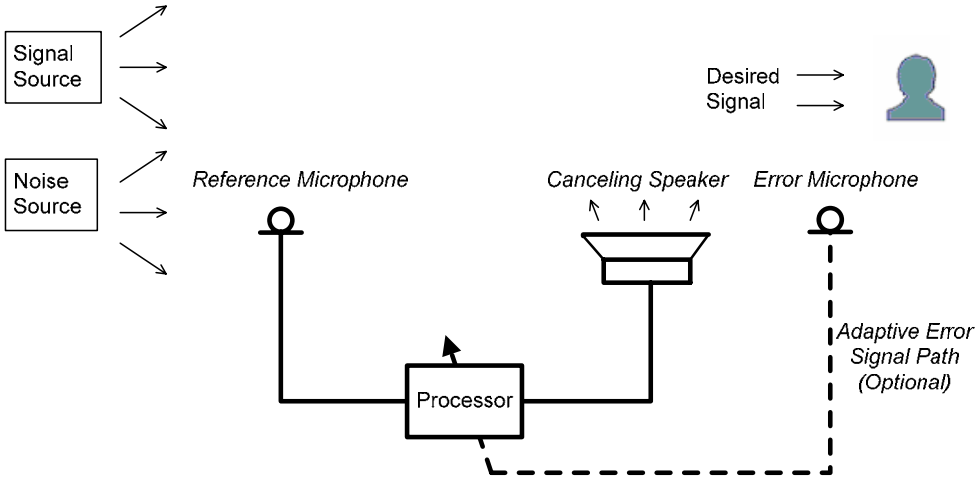


**Figure 3.4 Illustration of an Acoustic Noise Cancellation System**

The second issue concerns the secondary-path effects. In the case of the adaptive realization, the error signal is fed back to the processor as shown in the dashed line in Figure 3.4, and the summing junction in Figure 3.2 represents acoustic superposition in the space from the canceling speaker to the error microphone, where the primary noise is combined with the output of the canceling speaker. Therefore, when modeling this system, it is necessary to compensate for the secondary-path transfer function from the canceling speaker to the error microphone, which includes the digital-to-analog (D/A) converter, reconstruction filter, power amplifier, speaker, acoustic path from speaker to error microphone, error microphone, preamplifier, antialiasing filter, and analog-to-digital (A/D) converter.

In addition to the secondary-path effects as mentioned above, the feedback effects from the canceling speaker to the reference microphone also need to be considered. Otherwise, the reference signal will be corrupted by the antisound that radiates from the canceling speaker, and will result in a degraded system performance.

For the bearing fault detection in this research, all information is processed in the digital

domain once the A/D conversion is completed and no D/A conversions are necessary. Therefore, those practical issues mentioned above are not relevant to this research and are not considered further.

### 3.2.2 NARROWBAND FEEDFORWARD NOISE CANCELLATION STRUCTURES

Narrowband noise exists in many applications, such as noise generated by engines, compressors, motors, fans, and propellers. Generally, an electrical reference signal is obtained by using an appropriate sensor (e.g., a tachometer), which provides the mechanical motion data from such sources. This reference signal contains the fundamental frequency and all of the harmonics of the primary noise. A generic narrowband noise cancellation structure is shown in Figure 3.5.

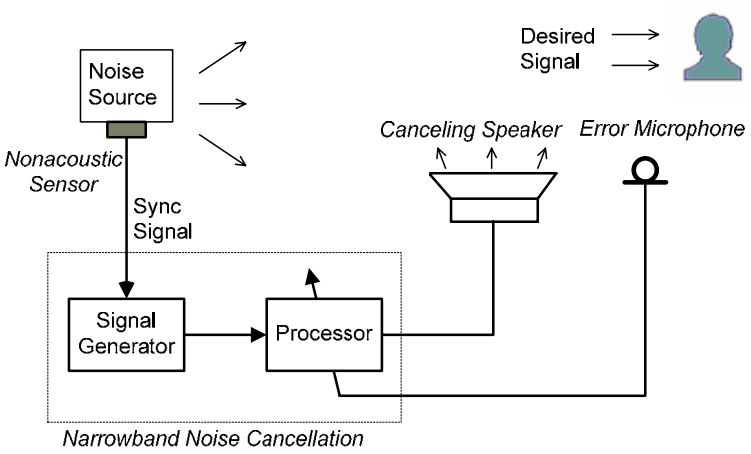


**Figure 3.5 Generic narrowband noise cancellation structure**

As shown in the figure above, a reference signal is internally generated at the frequencies of the signal acquired by the nonacoustic sensor. The processor then adjusts the amplitude and phase of the components in its output signal at those frequencies to match the primary noise, as well as compensates for the secondary path delay and other delays.

There are two types of reference signals that are commonly used in narrowband noise cancellation systems: 1) an impulse train with a period equal to the inverse of the fundamental frequency of the periodic noise, and 2) sinewaves that have the same frequencies as the corresponding harmonic tones to be canceled [36]. Two such methods, called the waveform synthesis method [40] and the adaptive notch filter method [41], are shown in Figure 3.6 and Figure 3.7, respectively.

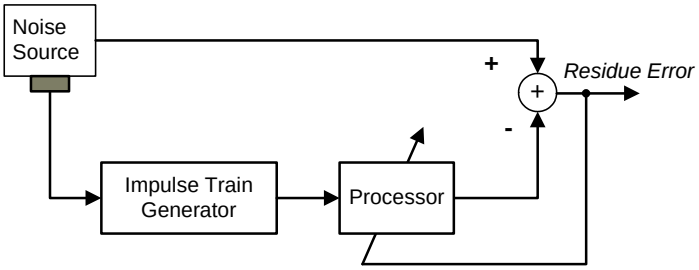


**Figure 3.6 Equivalent diagram of waveform synthesis method**

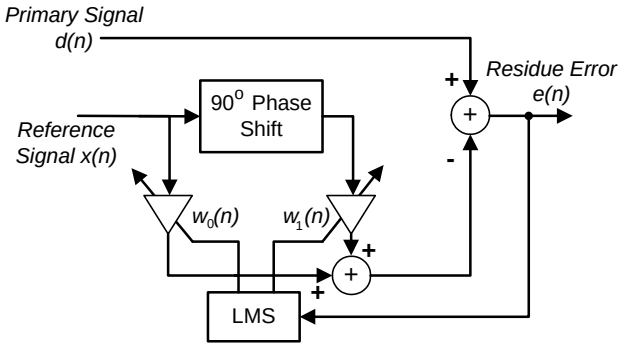


**Figure 3.7 Single-frequency adaptive notch filter method**

The waveform synthesis method stores and dynamically adjusts canceling noise waveform samples; noise cancellation is achieved by retrieving the stored samples for each sampling period, controlled by interrupts generated from the synchronization signal. The adaptive notch filter method generates a canceling signal with a phase opposite to the primary noise phase and a frequency the same as the primary noise frequency, by adaptively adjusting the two taps corresponding to the reference signal and its quadrature version. Since two coefficients are required for each canceling frequency, the order of the adaptive notch filter

can be high in practical applications where noise contains multiple frequencies.

For current-based bearing fault detection, once stator current data is acquired, the same task as the narrowband noise cancellation by using a reference signal can be achieved by using digital notch filters designed at the primary noise frequencies which are *assumed* to be known. This is the essence of the MSD method [38], where the frequencies of the dominant components in the stator current are calculated from the machine theories and a bank of filters at the calculated frequencies are then applied to filter out these components.

### 3.2.3 FEEDBACK NOISE CANCELLATION STRUCTURES

For the feedforward noise cancellation structures above, the reference signal has been the signal collected by a secondary sensor, a delayed version of the primary signal, or internally generated waveforms having frequencies derived from a mechanical motion.

For feedback noise cancellation structures, however, such a reference signal is generated from the output of an error sensor, rather than from the primary noise or a secondary noise reference. Furthermore, the system stability needs to be addressed for a feedback system. It also should be noted that under certain conditions, an adaptive feedback system is equivalent to a feedforward system, as discussed below.

#### 3.2.3.1 Non-Adaptive Feedback Noise Cancellation

The block diagram of a basic non-adaptive feedback noise cancellation system is shown in Figure 3.8. In this figure, $d(n)$ is the primary noise, $e(n)$ is the residual error, $y(n)$ is the secondary anti-noise signal, $W(z)$ is the transfer function of the controller, and $S(z)$ is the

transfer function of the secondary path. Under steady state conditions, the z-transform of the error signal can be expressed as

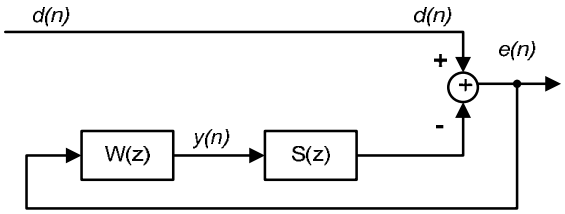


**Figure 3.8 Non-adaptive feedback structure**

$$E(z) = D(z) - S(z)W(z)E(z)\,, \tag{3.1}$$

$$E(z) = \frac{D(z)}{1 + S(z)W(z)} \tag{3.2}$$

Therefore, the closed loop transfer function $H(z)$ from the primary noise to the error signal can be expressed as

$$H(z) = \frac{E(z)}{D(z)} = \frac{1}{1 + S(z)W(z)} \tag{3.3}$$

To minimize $E(z)$, $S(z)W(z)$ is desired to be as large as possible. If the frequency response of $S(z)$ is flat, then this in turn requires the gain of $W(z)$ to increase without limit so that the overall transfer function $H(z)$ is marginal. However, this is rarely the case in practice, since the response of the secondary source usually introduces a significant phase shift and there is some propagation delay from the output of the control filter to the error sensor [42]. If a phase shift of $180^\circ$ occurs, the desired negative feedback becomes positive feedback leading to instability. A careful design of $W(z)$ is required to avoid the situation of instability. A full discussion of the design of the non-adaptive feedback system is available in References [36, 42 - 44].

### 3.2.3.2 Adaptive Feedback Noise Cancellation [36]

A typical adaptive feedback noise cancellation structure is shown in Figure 3.9. As in the previous figure, $d(n)$ is the primary noise, $e(n)$ is the residual error, $y(n)$ is the secondary antinoise signal, $W(z)$ is an adaptive filter, and $S(z)$ is the transfer function of the secondary path. The synthesized reference signal obtained from the error signal is $x(n)$, $\hat{d}(n)$ is the estimate of the primary noise, and $\hat{S}(z)$ is the estimate of $S(z)$. From the figure, the following equations can be obtained:

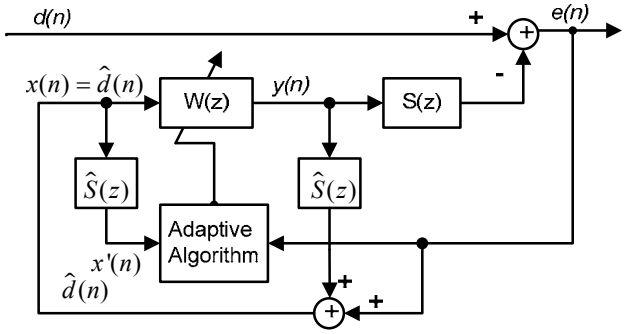


**Figure 3.9 Adaptive feedback structure**

$$D(z) = E(z) + S(z)Y(z) \tag{3.4}$$

$$X(z) = \hat{D}(z) = E(z) + \hat{S}(z)\,Y(z). \tag{3.5}$$

Therefore, the primary noise can be estimated inside the processor, i.e., $x(n) = \hat{d}(n) = d(n)$, if the secondary path can be sufficiently accurately modeled, i.e., if $\hat{S}(z) = S(z)$. This is the reference signal synthesis (regeneration) technique, whereby the secondary signal $y(n)$ is filtered by the secondary-path estimate $\hat{S}(z)$ and then combined with $e(n)$ to regenerate the primary noise. Under the same assumption of $\hat{S}(z) = S(z)$, the overall transfer function $H(z)$ of the feedback noise cancellation system from $d(n)$ to $e(n)$ is

$$H(z)=\frac{E(z)}{D(z)}=\frac{D(z)-\hat{D}(z)\,S(z)W(z)}{D(z)}=\frac{D(z)-D(z)S(z)W(z)}{D(z)}=1-S(z)W(z) \quad (3.6)$$

Thus, under the ideal condition that the secondary path is accurately modeled, the adaptive feedback noise cancellation system shown in the figure above, is equivalent to a feedforward system.

If the secondary path effect is a pure (acoustic or electrical) delay, such as in the case of a simplified, unidirectional acoustic duct, i.e., $S(z)=z^{-\Delta}$, then the overall transfer function is $H(z)=1-z^{-\Delta}W(z)$, and the original system shown in Figure 3.9 is identical to the system shown in Figure 3.10.

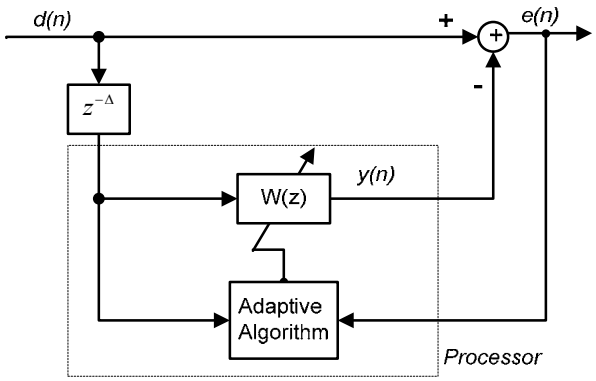


**Figure 3.10 Equivalent system scheme of adaptive feedback noise cancellation system**

It is clear that the system shown in the above figure is identical to the feedforward noise cancellation system without a reference as shown in Figure 3.3.

### 3.2.4 HYBRID NOISE CANCELLATION STRUCTURES

Based on the feedforward and feedback structures, hybrid noise cancellation systems can be built. A generic hybrid system for acoustic noise cancellation is shown in Figure 3.11.

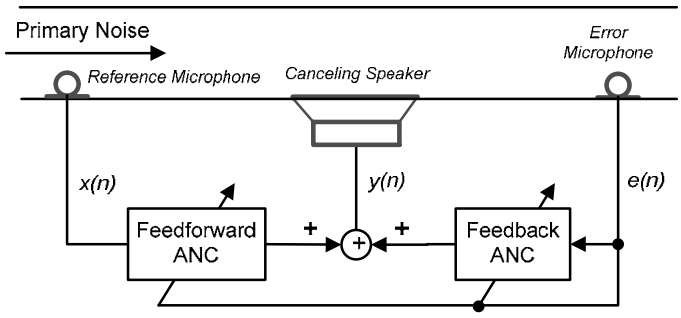


**Figure 3.11 Hybrid noise cancellation system [36]**

In the hybrid system shown above, it is hoped that the acoustic cues of the primary noise source that are not picked up by the reference sensor, will propagate forward and be picked up by the error sensor. The canceling signal fed to the speaker is the sum of the outputs of both the feedforward and feedback controllers.

Usually, a hybrid system can achieve the same performance with a lower order filter compared to either the feedforward or the adaptive feedback system alone [36].

### 3.2.5 OTHER NOISE CANCELLATION STRUCTURES

Some other noise cancellation structures are multiple-channel noise cancellation systems, lattice filter-based noise cancellation systems, subband filter-based noise cancellation systems, and frequency domain noise cancellation systems, etc. [36].

Multiple-channel systems employ several secondary sensors, error sensors, and perhaps even several primary sensors, and are mainly for the noise field in an enclosure or a large-dimension (e.g. 3-dimension) duct that is more complicated than in a usual, narrow duct. Lattice filters and subband filters are employed in some adaptive noise cancellation systems, with a common aim to improve the condition of the reference signal via appropriate filter structures rather than conventional transversal filters. A frequency

domain adaptive filter transforms the primary and reference signals into the frequency domain using the fast Fourier transform (FFT) and processes these signals by an adaptive filter. This frequency-domain technique saves computations by replacing the time-domain convolution by multiplication in the frequency domain.

All of the schemes mentioned above attempt to improve the performance of noise cancellation systems by employing more sensors, subband filters, optimizing filter structures, or reducing computation burdens, rather than by tuning the inherent algorithms that are used to solve the coefficients of those filters. Therefore, they are more related to implementation issues rather than algorithmic issues. For this reason, the details of these schemes are not addressed in this research, and readers are referred to reference material in the bibliography [36-37, 45-47] for more information about these schemes. Instead, the different algorithms employed to solve and adjust the coefficients of the filters in different noise cancellation systems are reviewed in the following section.

## 3.3 NOISE CANCELLATION ALGORITHMS

Several algorithms can be used for noise cancellation purposes. The adaptive transversal filter using the Filtered-X Least Mean Square (FXLMS) algorithm is the most widely used technique for acoustic noise cancellation systems, owing to its simplicity and robustness considering the secondary-path effects and other effects [36]. In addition to the classical LMS algorithm, other algorithms exist, such as the Finite Impulse Response/Infinite Impulse Response (FIR/IIR) Wiener filtering algorithm, the Recursive Least Squares (RLS) algorithm, the fuzzy-neural network (FNN) algorithm, and the Deconvolution algorithm. These algorithms are reviewed in the following sections.

### 3.3.1 THE FIR/IIR WIENER FILTERING ALGORITHM

A digital Wiener filter is an optimum digital filter in the sense of producing the best estimate of the signal in the presence of noise or other interfering signals. This is compared to a classical filter such as a lowpass, highpass, or bandpass filter, in which it is difficult to recover the signal that is corrupted and distorted by noise.

The basic principle of Wiener filtering is illustrated in Fig. 3.12 [37, 46]. The objective of the Wiener filter for noise cancellation purposes is to estimate the primary noise signal, $d(n)$, from the secondary noise signal (reference), $x(n)$.

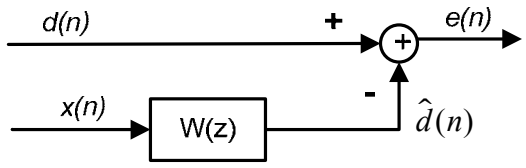


**Figure 3.12 Illustration of the general Wiener filtering problem**

The solution is obtained by minimizing the mean-square error between the desired signal and its estimate:

$$\xi = E\{|\, e(n)\,|^2\}, \text{ where } e(n) = d(n) - \hat{d}(n). \tag{3.7}$$

Assuming the Wiener filter is a ($p$-1)st-order FIR filter, i.e., $W(z) = \sum_{n=0}^{p-1} w(n) z^{-n}$, it follows that $\hat{d}(n) = \sum_{l=0}^{p-1} w(l)x(n-l)$, and $\xi = E\left\{\left| d(n) - \sum_{l=0}^{p-1} w(l)x(n-l)\right|^2\right\}$. By setting the derivative of $\xi$ with respect to $w(k)$ equal to zero for $k = 0,1,..., p-1$, and after some mathematic manipulations, the following equations, known as the *Wiener-Hopf equations,* can be obtained.

$$\sum_{l=0}^{p-1} w(l) r_x(k-l) = r_{dx}(k); k = 0,1,..., p-1, \text{ or in matrix form}$$

$$\begin{bmatrix} r_x(0) & r_x^*(1) & \dots & r_x^*(p-1) \\ r_x(1) & r_x(0) & \dots & r_x^*(p-2) \\ r_x(2) & r_x(1) & \cdots & r_x^*(p-3) \\ \vdots & \vdots & & \vdots \\ r_x(p-1) & r_x(p-2) & \cdots & r_x(0) \end{bmatrix} \begin{bmatrix} w(0) \\ w(1) \\ w(2) \\ \vdots \\ w(p-1) \end{bmatrix} = \begin{bmatrix} r_{dx}(0) \\ r_{dx}(1) \\ r_{dx}(2) \\ \vdots \\ r_{dx}(p-1) \end{bmatrix}, \text{ denoted by } \mathbf{R_x w = r_{dx}} \tag{3.8}$$

where $r_x(k-l) = E\{x(n-l)x^*(n-k)\}$ , $r_{dx}(k) = E\{d(n)x^*(n-k)\}$ are correlation and cross-correlation functions respectively (usually replaced by sample averages during implementation), and $^*$ denotes conjugate.

The solution for an *IIR Wiener filter* can also be obtained, and is in the following form

$$W(z) = \frac{P_{dx}(z)}{P_x(z)} = \frac{1}{\sigma_0^2 Q(z)} \left[ \frac{P_{dx}(z)}{Q^*(1/z^*)} \right], \text{ for a noncausal IIR Wiener filter, and} \tag{3.9}$$

$$W(z) = \frac{1}{\sigma_0^2 Q(z)} \left[ \frac{P_{dx}(z)}{Q^*(1/z^*)} \right]_+ \text{ for a causal IIR Wiener filter.} \tag{3.10}$$

In the above equations, $\sigma_0^2 Q(z) Q^*(1/z^*) = P_x(z)$ is the spectral factorization of the power spectrum of the input signal $x(n)$, $P_{dx}(z)$ is the cross-power spectral density of $x(n)$ and $d(n)$, and $[\bullet]_+$ indicates the "positive-time part" of the sequence whose z-transform is contained within the brackets ($\bullet$) [37, 45].

### 3.3.2 THE STEEPEST DESCENT ALGORITHM

Instead of *setting* the derivatives of $\xi(n)$ as in the Wiener filter algorithm above, the

steepest descent algorithm finds the filter that minimize the error $\xi = E\{|e(n)|^2\}$ by *searching* for the solution using the method of steepest descent, which involves an iterative procedure summarized as follows [37]:

1. Set an initial estimate, $\mathbf{w_0}$, of the optimum weight vector $\mathbf{w}$.
2. Update the estimate at time $n$ by adding a correction that is formed by taking a step of size $\mu$ in the negative gradient direction

$$\mathbf{w_{n+1}} = \mathbf{w_n} + \mu E\{e(n)\mathbf{x}^*\mathbf{(n)}\}, \tag{3.11a}$$

   where $\mathbf{w_n} = [w_n(0), w_n(1),..., w(p)]^T$, and $\mathbf{x(n)} = [x(n), x(n-1),..., x(n-p)]^T$.
3. Repeat Step 2.

In the update equations above, $E\{e(n)\mathbf{x}^*\mathbf{(n)}\}$ is the negative gradient vector of $\xi(n)$ with respect to the weight vector, $\mathbf{w}$. If $x(n)$ and $d(n)$ are jointly wide-sense stationary, then this term becomes

$$E\{e(n)\mathbf{x}^*\mathbf{(n)}\} = E\{[d(n) - \mathbf{w_n^T x(n)}]\mathbf{x}^*\mathbf{(n)}\} = E\{d(n)\mathbf{x}^*\mathbf{(n)}\} - E\{\mathbf{w_n^T x(n)}]\mathbf{x}^*\mathbf{(n)}\} = \mathbf{r_{dx}} - \mathbf{R_x w_n} \tag{3.12}$$

It then follows that,

$$\mathbf{w_{n+1}} = \mathbf{w_n} + \mu(\mathbf{r_{dx}} - \mathbf{R_x w_n}). \tag{3.11b}$$

The equations above show that for jointly wide-sense stationary processes, $x(n)$ and $d(n)$, if a proper step size is assigned, the steepest descent adaptive filter converges to the solution in the Wiener-Hopf equations, i.e.,

$$\lim_{n\to\infty} \mathbf{w_n} = \mathbf{R_x^{-1} r_{dx}}. \tag{3.13}$$

Usually, it can be chosen such that $0 < \mu < 2/\lambda_{\max}$, where $\lambda_{\max}$ is the maximum eigenvalue of $\mathbf{R_x}$.

Although for stationary processes the steepest descent adaptive filter converges to the solution in the Wiener-Hopf equations, it finds difficulty in adaptive filtering applications since the ensemble average, $E\{e(n)\mathbf{x}^*(\mathbf{n})\}$, is generally unknown in practice. Instead, the Least Mean Square (LMS) algorithm is widely used in practice.

### 3.3.3 THE LMS ALGORITHM AND THE NORMALIZED LMS ALGORITHM

Under the same framework as the Steepest Descent Algorithm, *the Least Mean Square (LMS) algorithm* replaces the expectation $E\{e(n)\mathbf{x}^*(\mathbf{n})\}$ in the weight vector update equation by

$$\hat{E}\{e(n)\mathbf{x}^*(\mathbf{n})\} = e(n)\mathbf{x}^*(\mathbf{n}) \tag{3.14}$$

Thus the weight vector update equation becomes

$$\mathbf{w_{n+1}} = \mathbf{w_n} + \mu e(n)\mathbf{x}^*(\mathbf{n}) \tag{3.15}$$

The update equation for the $k$ th coefficient of the filter is simply stated as

$$w_{n+1}(k) = w_n(k) + \mu e(n)x^*(n-k). \tag{3.16}$$

However, to ensure convergence, the selection of the step size $\mu$ is important. A rough selection range can be $0 < \mu < \dfrac{2}{(p+1)E\{|x(n)|^2\}}$ [37].

By replacing $E\{|x(n)|^2\}$ by its estimate, $\hat{E}\{|x(n)|^2\} = \dfrac{1}{p+1}\sum_{k=0}^{p}|x(n-k)|^2$, in the upper bound of $\mu$ and substituting the results in the weight vector update equation, it follows that

$$\mathbf{w_{n+1}} = \mathbf{w_n} + \beta\frac{\mathbf{x}^*(\mathbf{n})}{\|\mathbf{x(n)}\|^2}e(n),\ 0 < \beta < 2 \tag{3.17}$$

This is known as the *Normalized Least Mean Square ( LMS) Algorithm*.

### 3.3.4 DIFFERENT FORMS OF THE RLS ALGORITHM

The Wiener filter algorithms, the gradient descent algorithm, the LMS algorithm, and the Normalized LMS algorithms are all targeted to minimize the *mean square error*:

$$\xi = E\{|\, e(n)\,|^2\}\text{, where } e(n) = d(n) - \hat{d}(n). \tag{3.7}$$

Minimizing the mean-square error produces the same set of filter coefficients for all sequences that have the same statistics, i.e., they have the same auto-correlation and cross-correlation. For some applications, it is desired to minimize the following *least squares error* (or a weighted version of it)

$$\varepsilon(n) = \sum_{i=0}^{n} |\, e(i)\,|^2 \ . \tag{3.18}$$

By doing so, the resulting filter coefficients are optimal for the given data, instead of being statistically optimal for the process.

The Recursive Least Squares (RLS) algorithm is an efficient algorithm for performing this minimization. It does not require the statistics of the underlying processes and offers fast convergence in many applications. According to how the squared errors are weighted, different forms of the RLS algorithm can be obtained: the exponentially weighted RLS, the growing window RLS, the sliding window RLS, etc.

The *exponentially weighted RLS algorithm* tries to minimize the exponentially weighted least squares error

$$\varepsilon(n) = \sum_{i=0}^{n} \lambda^{n-i}\ |\, e(i)\,|^2\ , \tag{3.19}$$

where $0 < \lambda \le 1$ is an exponential weighting (forgetting) factor. The basic procedure to compute the filter coefficients is as follows [37].

1. Set initial estimate values, 0 and $\mathbf{P}(0) = \delta^{-1}\mathbf{I}$, for the filter coefficient vector $\mathbf{w}$

and the inverse auto-correlation matrix $\mathbf{P}$ of the input signal, respectively. Here $\delta$ is a small positive constant.

2. Update the filtered information vector $\mathbf{z}(n) = \mathbf{P}(n-1)\mathbf{x}^*(n)$, the gain vector $\mathbf{g}(n) = \frac{1}{\lambda + \mathbf{x}^T(n)\mathbf{z}(n)}\mathbf{z}(n)$, the *a priori error* $\alpha(n) = d(n) - \mathbf{w}_{n-1}^T\mathbf{x}(n)$, the filter coefficient vector $\mathbf{w}_n = \mathbf{w}_{n-1} + \alpha(n)\mathbf{g}(n)$, and the inverse auto-correlation matrix $\mathbf{P}(n) = \frac{1}{\lambda}\left[\mathbf{P}(n-1) - \mathbf{g}(n)\mathbf{z}^H(n)\right]$.
3. Repeat Step 2.

In the above procedure, if $\lambda = 1$ is set, the algorithm becomes the *growing window RLS algorithm*, since all the errors (the previous and current) are treated equally and therefore the computation window never decreases. In comparison, the *sliding window RLS algorithm* aims to minimize the sum of the squares of $e(i)$ over a *finite* window, i.e., to minimize

$$\varepsilon_L(n) = \sum_{i=n-L}^{n} |e(i)|^2 \text{ , where } L+1 \text{ is the length of the window.} \qquad (3.20)$$

The procedure to compute the filter coefficients is similar to the exponentially weighted RLS algorithm and available in the referenced material in the bibliography [37, 46].

### 3.3.5 NONLINEAR FILTERING APPROACHES

In the Wiener filter algorithm, the steepest descent algorithm, the LMS algorithm, and the RLS algorithm, the error is defined as the difference between the desired signal and its estimate, which is the output of a Wiener filter or adaptive filter. In these algorithms,

$\hat{d}(n) = \sum_{l=0}^{p-1} w(l)x(n-l)$ is used to calculate the error $e(n) = d(n) - \hat{d}(n)$, where $w(l)$, $l = 0,1,...,p-1$, are the filter coefficients. The estimated signal is essentially a linear combination of the input samples.

In many situations, such a linear model has satisfactory performance. However, in situations where the system nonlinearity is significant, a nonlinear filtering approach may be desired.

Nonlinear filtering approaches include the fuzzy-neural network approach, particle swarm optimization, cellular neural networks, etc. Fuzzy-neural networks are hybrids of artificial neural networks and fuzzy logic. Such hybridization combines the human-like reasoning style of fuzzy systems with the learning and connectionist structures of neural networks. Particle swarm optimization was inspired by the social behavior of animals, such as bird flocking or fish schooling, when they search for food. Particle swarm optimization is usually used for optimization in a multi-dimensional search space. Cellular neural networks were inspired by a nonlinear analog circuit which features a multi-dimensional array of neurons and local interconnections among the cells.

There is one study in the literature on the application of discrete-time cellular neural networks combining with particle swarm optimization to image noise cancellation [49]. In comparison, several studies on applying a fuzzy-neural network to noise cancellation have been reported [50-53]. Since particle swarm optimization and cellular neural networks are usually suitable for multi-dimensional problems and do not provide obvious advantages over other methods in noise cancellation for bearing fault diagnosis, only the fuzzy-neural network approach is discussed further in the following section.

### 3.3.6 THE FUZZY-NEURAL NETWORK ALGORITHMS

The basic structure of a fuzzy-neural network is shown in the following figure [51].

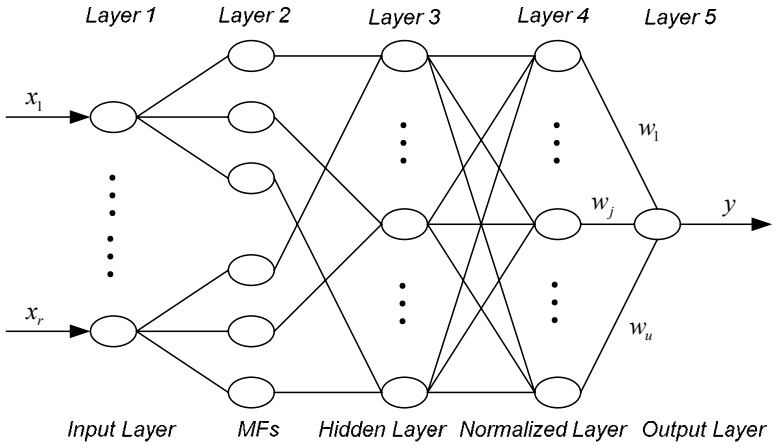


**Figure 3.13 Fuzzy-neural network structure [51]**

The system shown in Fig. 3.13 is based on a modified Radial Basis Function (RBF) neural network and has the following five layers.

Layer 1: Input layer - Each node in this layer represents an input linguistic variable.

Layer 2: Membership function layer - Each node in this layer represents a membership function (MF), which is usually a Gaussian function. The output of the $j$ th membership function, $\mu_{ij}$, given the $i$ th input $x_i$, is calculated as

$$\mu_{ij}(x_i) = \exp\left[-\frac{(x_i - c_{ij})^2}{\sigma_j^2}\right], i = 1,2,...,r \text{ and } j = 1,2,...,u \tag{3.21}$$

where $c_{ij}$ and $\sigma_j$ are the center and the width of the $j$ th Gaussian function of $x_i$, respectively; $r$ and $u$ are the number of the input variables and the number of membership functions, respectively.

Layer 3: Fuzzy rule "If-part" layer - Each node in this layer carries out a possible "If-part" for fuzzy rules, and represents an RBF unit. The number of nodes in this layer is equal to the number of fuzzy rules. For the $j$ th rule $R_j$, its output is

$$\phi_j = \prod_{i=1}^{r} \mu_{ij}(x_i) \tag{3.22}$$

Layer 4: Normalization layer - The output of each node in this layer is the corresponding node in Layer 3 normalized by the sum of all outputs in that layer, i.e.,

$$\psi_j = \frac{\phi_j}{\sum_{k=1}^{u} \phi_k}. \tag{3.23}$$

Layer 5: Output layer and also fuzzy rule "Then-part" layer - This layer carries out the summation of the outputs of Layer 4, i.e.,

$$y = \sum_{k=1}^{u} w_k \psi_k \ , \tag{3.24}$$

where $y$ is the output and $w_k$ is the weight of the $k$ th rule which is a linear combination of input variables, i.e.,

$$w_k = h_{k0} + h_{k1}x_1 + \cdots + h_{kr}x_r \text{, where } h_{ki} \text{ are real-valued parameters.} \tag{3.25}$$

Several learning algorithms for noise cancellation purposes are available, such as the modified dynamic fuzzy neural networks (MDFNN) and enhanced dynamic fuzzy neural networks (EDFNN) learning algorithms in [51, 53], and the self-tuning fuzzy filtered-U algorithm in [54]. To illustrate the problems in Fuzzy Neural Networks (FNNs), the basic procedure of the MDFNN algorithm in [51] is discussed below as an example.

For the $k$ th observation ( $X(k)$ , $y(k)$ ), find the smallest distance, $d_{\min}$, between $X(k)$ and the center $C_j$ ( $C_j = [c_{1j}, c_{2j}, ..., c_{rj}]^T$ ) of the existing RBF units as follows

$$d_j(k) = \left\| X(k) - C_j \right\|, j = 1,2,\ldots,u \tag{3.26}$$

$$d_{\min} = \arg\min(d_j(k)), \tag{3.27}$$

where $X(k) = [x_1, x_2, ..., x_r]^T$ and $y(k)$ are the received samples of the secondary signal

and the primary signal, respectively.

1. If $d_{\min} > k_d$, generate a new rule, with its centers and widths allocated as follows

$$C_i = X(k), \sigma_i = k_{ovlp} d_{\min}, \tag{3.28}$$

where $k_d$ is the threshold for the radius of accommodation boundary, and $k_{ovlp} \in (1.05 - 1.2)$ is an overlap factor.

2. Calculate the error reduction ratio (ERR) for each RBF unit, and delete the RBF units whose ERR is less than a preset threshold $k_{err}$. I.e.,

If $\eta_{erri} < k_{err}$, delete the $i$ th RBF unit,.

where $\eta_{erri}$ is the ERR of the $i$ th RBF unit, calculated according to a computationally complicated procedure described in the material referenced in the bibliography [51].

3. Use the Least Squares Error method to adjust the weight matrix $W$, i.e.,

$$W = YP^T (PP^T)^{-1},$$

where $W = [h_{10},...,h_{u0},h_{11},...,h_{u1},...,h_{1r},...,h_{ur}]$, $Y = [y(1), y(2),..., y(k),...]$, and

$$P = \begin{bmatrix} a_1(1) & \cdots & a_u(1) & a_1(1)x_1(1) & \cdots & a_u(1)x_1(1) & \cdots & a_1(1)x_r(1) & \cdots & a_u(1)x_r(1) \\ \vdots & \cdots & \vdots & \vdots & \cdots & \vdots & \cdots & \vdots & \cdots & \cdots \\ a_1(n) & \cdots & a_u(n) & a_1(n)x_1(n) & \cdots & a_u(n)x_1(n) & \cdots & a_1(n)x_r(n) & \cdots & a_u(n)x_r(n) \end{bmatrix}^T \tag{3.29}$$

where $a_j(k)$ (same as $\psi_j$ above) is the normalized output from Layer 4, $j = 1,2,...,u$.

4. Repeat the process above.

In noise cancellation applications, the noise to be estimated, $d(n)$ in Figure 3.12, is usually embedded in the primary signal (the primary signal is composed of noise and useful

signals, and only the primary signal can be measured) and is not directly measurable. Therefore, the system error, which is defined as $e(n) = d(n) - \hat{d}(n)$, can *not* be used as a guide to dynamically generate RBF neurons as in many other applications. Consequently, the accommodation boundary is used as the only condition to determine the neuron generation process, as shown in Step 1 above. This in turn requires the threshold for the radius of accommodation boundary ($k_d$ above) to be properly chosen. However, in stator current-based bearing fault detection, it is difficult to set this threshold due to the complexity of the problem. Therefore, the performance of the system can not be assured when it is used to detect real bearing faults.

Another disadvantage of the FNN method in the sense of bearing fault detection is as follows: it is well known that the changes in the stator current that are caused by bearing faults are usually reflected in the *frequency domain*. Unlike a Wiener filter or other digital filters, which *fully* utilizes the frequency properties of signals (such as narrowband vs. broadband) to accomplish noise cancellation, the FNN algorithm does not *fully* take advantage of the particular frequency patterns that are injected by bearing faults.

### 3.3.7 THE DECONVOLUTION ALGORITHM

Deconvolution is performed to restore a true signal from convolutional distortion. For example, in image processing, blurring due to linear motion in a photograph may be modeled as a convolution problem. This can be formulated to recover (deblur) the true signal $d(n)$ from the observations $x(n)$, i.e., to solve $d(n)$ from

$$x(n) = d(n) * g(n) + w(n), \tag{3.30}$$

where $g(n)$ models the 'blurring' effect, and $w(n)$ is additive noise.

If $g(n)$, which is called the convolution kernel, is known, then this is the classical image restoration problem. In this case, several approaches can be used, such as inverse filtering and Wiener filtering. For example, an optimum Wiener filter for deconvolution may be in the following form [37] that is similar to Equations (3.9)-(3.10).

$$H(z) = \frac{P_{dx}(z)}{P_x(z)} = \frac{1}{G(z)}\left[\frac{P_d(z)}{P_d(z) + P_w(z)/\left|G(z)\right|^2}\right] \tag{3.31}$$

However, if the convolution kernel is not known, then this is a blind deconvolution problem. Several methods have been proposed for blind deconvolution, such as the independent component analysis method, the iterative blind deconvolution method, the higher order statistics method, and the annealing method. The details of those algorithms are beyond the scope of this research.

Research work on applying a deconvolution algorithm to noise cancellation problems has been done primarily in certain areas such as image processing and communication channel equalization [37, 55-57]. This is because in those areas, the observed signal can be *well* modeled as a convolution of signals. However, in stator current-based bearing fault detection, especially to the generalized-roughness bearing faults detection, it has *not* been established that the measured stator current is viable to be modeled as the convolution of signals. For example, it has been observed that at an incipient stage, generalized-roughness bearing faults are likely to cause subtle broadband changes, such as changes in the position of the noise floor, in the sampled stator current signal primarily consisting of sinusoidal components. Such changes are difficult to model as convolution effects. Therefore, a deconvolution formulation faces difficulties in practice for stator current-based bearing fault detection, at least at the present time.

## 3.4 SUMMARY

In this survey, different noise cancellation structures and algorithms have been reviewed. These structures and algorithms are summarized as follows, considering their potential applications in current-based bearing fault detection.

### 3.4.1 SUMMARY OF THE DIFFERENT STRUCTURES

Noise cancellation structures fall into different categories according to the inherent control strategy: feedforward structures, feedback structures, hybrid structures and other structures. Feedforward noise cancellation systems utilize the coherence between secondary signal and primary signal to estimate the noise. Feedback noise cancellation systems estimate the noise from the output of an error sensor. Hybrid noise cancellation systems can be built by combining feedback structures and feedforward structures. In a specific application, a proper structure should be chosen by considering factors such as the availability of a secondary signal. For example, if a secondary signal is not available, a feedback structure can be used, or a feedforward structure can be applied with a delayed version of the primary signal as secondary signal. Further more, a feedback system is equivalent to a feedforward system given that the secondary path can be well modeled.

*In stator current-based bearing fault detection*, a secondary signal is not available, and the secondary path modeling is not necessary since all the information is processed in the digital domain once the stator current is sampled by an Analog/Digital converter. Hence, a feedforward structure is appropriate and a delayed version of the primary signal should be used as a secondary signal for noise cancellation purposes.

If non-stationarity of the primary noise is significant, then an adaptive strategy may be

applied. For adaptive noise cancellation, an error signal is measured and used as a guide in filter weights adjustment. Further more, additional issues such as stability, convergence speed, and computation burden should be carefully considered during implementation.

*In current-based bearing fault detection*, non-stationarity is the property of *both* the fault-related and non-fault-related components of the stator current. However, the non-stationarity of the non-fault-related components of the stator current can be neglected under steady state at the same load condition. Furthermore, when the bearing fault characteristic frequencies are present in the stator current, an adaptive strategy will unavoidably filter out those frequencies, which is not desired. Therefore, from the above analysis, an adaptive noise cancellation does not obviously perform better than a non-adaptive strategy and it may mistakenly remove the non-stationary part of the fault-related components from the final output of the system. This is true especially if the bearing fault frequencies present in the stator current.

Some practical issues related to the structures of noise were also discussed, such as secondary path modeling, and feedback effects from anti-speaker. Though they are important issues in many applications, they do not apply to current-based bearing fault detection.

### 3.4.2 SUMMARY OF THE DIFFERENT ALGORITHMS

Different noise cancellation algorithms were reviewed in this chapter, including the FIR/IIR Wiener filtering, the steepest descent algorithm, the LMS algorithm, the RLS algorithm, the nonlinear filtering algorithms, the fuzzy-neural network algorithm, and the deconvolution algorithm.

*The Wiener filtering* is well developed and has numerous applications in practice. It has proven to be effective in most applications. Wiener filter-based noise cancellation is a classical noise cancellation algorithm. It can fully use the frequency characteristics, such as the broadband and narrowband properties, of signals to differentiate between noise and desired signal. Also, many adaptive filters converge to the Wiener solution, and Wiener filters can achieve deconvolution if the convolution kernel is known.

In current-based bearing fault detection, it has been observed that bearing faults, especially the generalized roughness faults, may cause broadband changes in the power spectra of the stator current. Therefore, the Wiener filtering is chosen as the tool for stator current-based bearing fault detection.

*The steepest descent algorithm* is an iterative algorithm that tries to search for optimum filter coefficients in the negative gradient direction of the error space. Therefore, it converges to an optimum Wiener filter solution for wide-sense stationary processes. However, it has little practical use because it requires the expectation $E\{e(n)\mathbf{x}^*\mathbf{(n)}\}$ to be known. By replacing this expectation with a simple estimate $e(n)\mathbf{x}^*\mathbf{(n)}$, the LMS algorithm and the normalized LMS algorithm were derived by whom. *The LMS algorithm and the normalized LMS algorithm* are widely used in practice, though it requires effort to choose a proper step size to ensure convergence. However, the LMS algorithm and the normalized LMS algorithm might experience slow convergence. To overcome this problem, *the RLS algorithm* can be used, which tries to find optimal solutions for given data, disregarding the statistics of the underlying processes. Different forms of the RLS algorithm exist, such as the exponentially weighted RLS, the growing window RLS, and the sliding window RLS.

In current-based bearing fault detection*, if* an adaptive filter has to be used to accommodate

the non-stationarity of the stator current, then the LMS algorithm or the normalized LMS algorithm can be used. The RLS algorithm does not have any advantage except fast convergence, which is obtained in the cost of an increased computation burden at each iteration cycle.

*Non-linear filtering approaches* for noise cancellation were also reviewed, including particle swarm optimization, the cellular neural networks approach, and the fuzzy-neural networks approach. The amount of the research work of applying those approaches to noise cancellation is limited in the literature. Since particle swarm optimization and cellular neural network are usually suitable for multi-dimensional problems and don't see obvious advantages in the noise cancellation for bearing fault diagnosis, only the dynamic fuzzy-neural network approach was further evaluated. *The dynamic fuzzy-neural network* approach developed for noise cancellation purposes can not use a system error as a guide to dynamically generate neurons, and its performance relies heavily on a proper choice of the inherent parameters.

A bigger disadvantage of the fuzzy-neural network approach in the sense of stator current bearing fault detection is as follows: it is well known that the changes in the stator current that are caused by bearing faults are usually reflected in the frequency domain. Unlike a Wiener filter or other digital filter, which fully utilizes the frequency properties of signals (such as narrowband vs. broadband) to accomplish the noise cancellation, the FNN algorithm does not take full advantage of the particular frequency patterns of the fault signatures that are injected by bearing faults.

*The deconvolution algorithm* has applications in the areas of image processing and communication channel equalization. A primary assumption of this algorithm is that the observed signal can be modeled successfully as a convolution of signals; its performance

relies heavily on the closeness of this assumption to the real situation. For stator current-based bearing fault detection, especially for generalized-roughness bearing faults detection, it has not been well established that the stator current can be correctly modeled as the convolution of bearing fault signal and other signals. For example, it has been observed that at an incipient stage, generalized-roughness bearing faults are likely to cause subtle broadband changes, such as changes in the position of the noise floor, in the sampled stator current signal primarily consisting of sinusoidal components. Such changes are difficult to model as convolution effects. Therefore, a deconvolution formulation faces difficulties in practice for stator current-based bearing fault detection, at least at the present time.

# CHAPTER 4

# BEARING FAULT DETECTION VIA STATOR CURRENT NOISE CANCELLATION (SCNC)

Since current monitoring offers significant economic savings and easy implementation, current monitoring is receiving more and more attention. Specifically, many studies show how single-point defects on bearings can be successfully detected via stator current. However, much work remains to be done on detecting generalized-roughness faults. The objective of this chapter is to introduce a new current monitoring technique that aims to detect generalized-roughness faults.

It is well known that bearing fault signatures are significantly less prominent in the stator current than in machine vibration. Additionally, for generalized roughness faults, the characteristic fault frequencies may not appear in the stator current. For these reasons, the current-based method proposed in this chapter does not attempt to identify the specific fault frequencies. Instead, the proposed method treats the detection problem as a low signal-to-noise ratio (SNR) problem, where all components in the stator current that are not related to the fault are considered to be *noise*, while the components injected by the fault are considered to be the signal. According to this notion, the noise could be $10^4$ times stronger than the signal (as tens of Amperes vs. mili-Amperes). For such a low SNR problem, a noise cancellation method is very useful. Therefore, in the proposed method, the noise components in the stator current are estimated by a Wiener filter and then cancelled by their estimates in a real-time fashion. A fault indicator is formed from the remaining components.

A theoretical analysis of the proposed method is presented in this chapter. It includes the noise cancellation concept, and the noise cancellation model for bearing fault detection, the design of the Wiener filter, and system performance analysis. Experimental verification of the proposed method is provided in the next two chapters.

## 4.1 NOISE CANCELLATION AND BEARING FAULT DETECTION

### 4.1.1 INTRODUCTION

Noise cancellation is an attractive means to achieve large amounts of noise reduction in a small package, particularly at low frequencies. As mentioned in the previous chapter, noise cancellation has been applied to a wide variety of problems in manufacturing, industrial operations and consumer products.

In the concept of noise cancellation, *noise* is defined as any kind of undesirable disturbance, whether it is borne by electrical, acoustic, vibration, or any other kind of medium. Noise cancellation algorithms usually involve a digital system that cancels the primary noise based on the principle of superposition; specifically, an estimated noise of equal amplitude and same (or opposite) phase is generated and subtracted from (or added to) the primary noise, thus resulting in the cancellation of both noises. Figure 4.1 shows a typical noise cancellation system. In this system, a corrupted observation that is recorded by the primary sensor includes a desired signal and unwanted noise. A secondary sensor is placed within the noise field. Then a digital signal processor generates an estimate of the primary noise from the noise (the reference signal) measured by the secondary sensor. After subtraction, the desired signal is recovered. Usually, the noise measured by the secondary sensor has the same source as the primary noise, or at least they should be correlated.

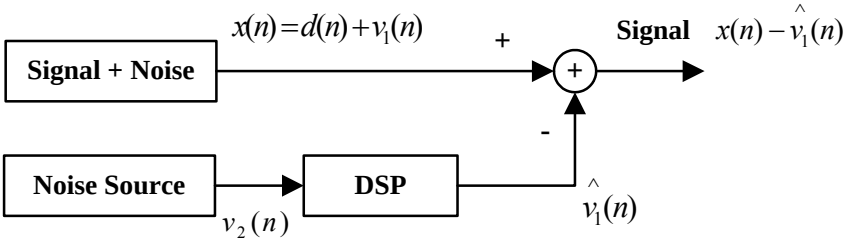


**Figure 4.1 Noise cancellation model using a secondary sensor to measure the additive noise.**

To better illustrate the use of such a system, consider situations in air-to-air communications between pilots in fighter aircraft or in air-to-ground communications between a pilot and the control tower [37]. In such situations, engine and wind noise within the cockpit of the fighter aircraft usually conceal the pilot's voice. However, if a secondary sensor (microphone) is placed within the cockpit, the noise that is transmitted when the pilot speaks into the microphone can be estimated. Subtracting this estimate from the transmitted signal significantly increases the signal-to-noise ratio.

When the digital signal processor in Figure 4.1 is a Wiener filter, the coefficients of the filter $\mathbf{w}$ can be solved from the Wiener-Hopf equation [refer to Section 3.3.1]:

$$\mathbf{R}_{v_2}\mathbf{w} = \mathbf{r}_{v_1 v_2} \tag{4.1}$$

where $\mathbf{R}_{v_2}$ is the autocorrelation matrix of the reference signal $v_2(n)$ and $\mathbf{r}_{v_1 v_2}$ is the vector of cross-correlation between the primary noise $v_1(n)$ and the reference signal $v_2(n)$.

As can be seen from Equation (4.1), to compute the coefficients of the Wiener filter, neither the autocorrelation nor the frequencies of the primary noise is required. This makes noise cancellation preferable to notch filtering in many applications. For example, though noise having known frequencies can be filtered by notch filters, such filtering process could make the desired signal un-recoverable if the desired signal and the noise have components at the same frequencies. This is the case in the bearing fault detection problem, where the

eccentricity components in the stator current exist before and after the presence of a generalized-roughness fault and therefore, are desired to be removed to uncover the faulted bearing signal. However, it is possible that the changes in the current, caused by the bearing fault, may simply be an increase in the amplitude of the eccentricity components [11]. If notch filters are used to remove these components, the useful information about the bearing fault is lost. Therefore, in this case, noise cancellation should be employed instead of notch filtering.

### 4.1.2 STATOR CURRENT NOISE CANCELLATION

Though the application of noise cancellation in aircraft communications is straightforward, its application in current-based bearing condition monitoring is not obvious. However, the basic idea is similar. Dominant components in the stator current of a typical induction motor are supply fundamental and harmonics, eccentricity harmonics, slot harmonics, saturation harmonics, and other components from unknown sources, including environmental noises [20]. Since these dominant components exist before and after the presence of a bearing fault, a large body of the information they contain is not related to the fault. In this sense, they are *basically* noise for the bearing fault detection problem. From this notion, an interesting analogy between aircraft communication (human voice) and motor condition monitoring (fault signal) can be found as illustrated in Table 4.1. (*Note: The noise here and hereafter refers to the components in stator current that are not related to bearing faults, unless where stated otherwise.*)

**Table 4.1 Analogy between aircraft (human voice) and motor (fault signal) in signal detection.**

| | Aircraft | | Motor | |
|---|---|---|---|---|
| | Source | Level | Source | Level |
| Signal | Human voice from the pilot | Low | Fault signal from the bearing | Low |
| Noise | Propeller, Engine, Wind, etc. | High | Supply, Load, Misalignment, etc. | High |
| | Measurement | Negligible | Measurement | Negligible |

To uncover the bearing fault signal in the stator current, it is desirable to remove the noise components mentioned above. Ideally, a secondary sensor should be used to provide a reference signal (a stator current without a fault signal) that can be used to estimate these noise components. However, this has difficulties, since it is not practical to have an additional machine identical to the testing machine to provide the reference signal. Even if an identical machine is available, noise components can still be injected by other factors besides the machine structure, such as reassembling actions and misalignments. For these reasons, the model with a secondary sensor shown in Figure 4.1 cannot be applied in the bearing fault detection problem. Instead, a model without a reference signal, as shown in Figure 4.2, should be considered. In this model, the noise components are estimated from previous samples of the stator current, rather than from a reference signal. Note that at constant loads, the dominant noise components (sinusoidal) essentially do not change, either in magnitude or in frequency; therefore, they can be predicted by using the most recent samples of the stator current.

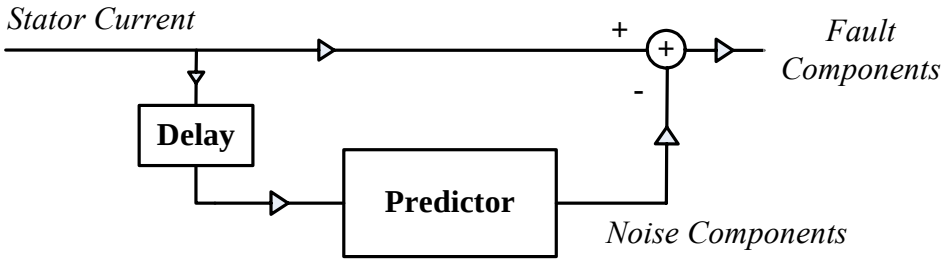


**Figure 4.2 Noise cancellation model for bearing fault detection.**

For the current-based bearing fault detection in this research, a Wiener filter has been chosen, based on the survey performed in Chapter 3. By using a Wiener filter, the noise can be optimally estimated in the Least Mean Square sense and the frequency properties of the noise (i.e. consisting of the sinusoidal components) can be fully utilized.

When the predictor is a Wiener filter, the model can be redrawn, as shown in Figure 4.3,

where

$x(n)$ is the stator current;

$y(n)$ is the remaining components in the stator current after noise cancellation;

$d_1(n)$ is the noise components;

$\hat{d}_1(n)$ is the estimated noise components;

$d(n)$ is the fault signal;

$v_1(n)$ is the measurement noise;

$\hat{v}_1(n)$ is the estimated measurement noise; and

$z^{-n_0}$ is a delay of $n_0$ data samples.

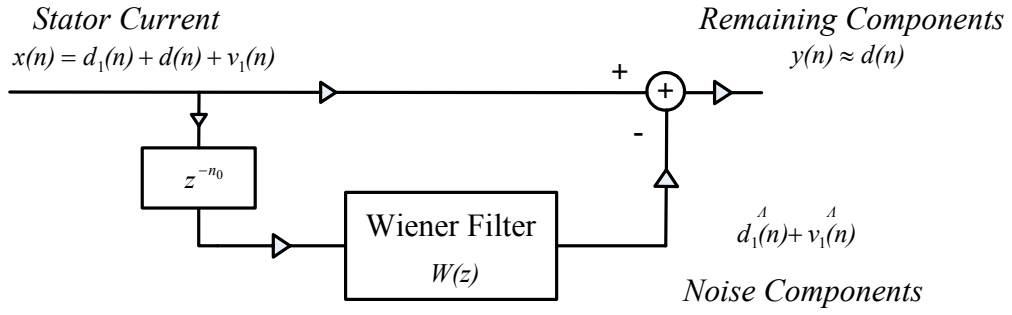


**Figure 4.3 Noise cancellation model with a Wiener filter as the predictor.**

From the model, it can be seen that if the Wiener filter $W(z)$ has a good performance, i.e., $\hat{d}_1(n)+\hat{v}_1(n)$ is close to $d_1(n)+v_1(n)$, the remaining part of the stator current after noise cancellation will be the fault signal $d(n)$. Usually, the measurement noise $v_1(n)$ is negligible, given today's advanced data acquisition techniques.

Another interpretation of the above model is that the remaining components in this model are the prediction error of the Wiener filter [37]; when the bearing fault develops and the

condition of the system changes, the prediction error increases. This interpretation is illustrated in an equivalent model in Figure 4.4.

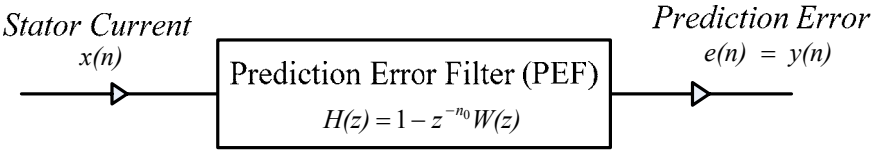


**Figure 4.4 Interpretation of the noise cancellation method from prediction error filtering.**

## 4.2 WIENER FILTER DESIGN

The Wiener filter should be designed such that (a) it can estimate most noise components in the stator current and (b) the fault signal should not be included in its output. Therefore, it is clear that the Wiener filter should be designed from *pure noise* data that does not include fault information. This can be achieved by designing the Weiner filter using the stator current data for a healthy bearing condition. Since all the components in the stator current at a healthy bearing condition are *noise*, no fault information is embedded into the coefficients of the Wiener filter. Therefore, when the fault develops, the Wiener filter predicts only the noise components and keeps the fault information intact during the noise canceling process. Consequently, the prediction error shown in Figure 4.4 gets larger when the system enters a bearing fault condition from a healthy bearing condition.

The design system for the Wiener filter is shown in Figure 4.5. The stator current $x(n)$ does not contain the fault signal $d(n)$ in the system since it is for a healthy bearing condition. In practice, it usually takes a long time (typically months or years) before a bearing starts to fail, and it is justified to assume such healthy bearing condition is available.

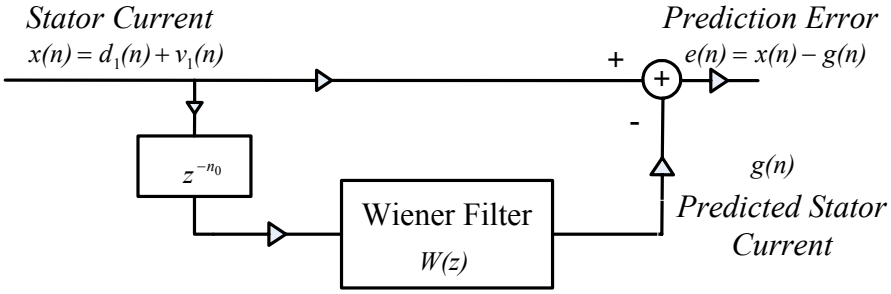


**Figure 4.5 Wiener filter design system.**

The objective of the design work is to minimize the prediction error in the mean-square sense. The coefficients of the Weiner filter are assigned by using the minimum mean-squared error (MMSE) method, which is formulated as follows.

Solve for $w(k), k = 0,1,...,p$ to minimize

$$\xi = E\left\{|e(n)|^2\right\} = E\left\{\left|x(n) - \sum_{k=0}^{p} w(k)x(n-n_0-k)\right|^2\right\} \qquad (4.2)$$

where $E\{\cdot\}$ is expected value, $n_0$ is the delay of the input $x(n)$, $w(k), k = 0,1,...,p$ are the coefficients of the Wiener filter, and $p$ is the order of the filter.

The coefficients are found by setting the partial derivatives of $\xi$ with respect to $w(k)$ equal to zero, as follows

$$\frac{\partial \xi}{\partial w(k)} = E\frac{\partial e^2(n)}{\partial w(k)} = E\left\{2e(n)\frac{\partial e(n)}{w(k)}\right\} = 0 \;;\quad k = 0,1,...,p \;. \qquad (4.3)$$

Substituting $\frac{\partial e(n)}{\partial w(k)} = -x(n-n_0-k)$ into Equation (4.3) yields

$$E\{e(n)x(n-n_0-k)\} = 0 \;;\quad k = 0,1,...,p \qquad (4.4)$$

which is known as the orthogonality principle or the projection theorem. Substituting $e(n) = x(n) - \sum_{j=0}^{p} w(j)x(n-n_0-j)$ into Equation (4.4) yields

$$E\left\{\left[x(n)-\sum_{j=0}^{p}w(j)x(n-n_0-j)\right]x(n-n_0-k)\right\}=0\ ;\ \ k=0,1,...,p \tag{4.5}$$

or equivalently,

$$\sum_{j=0}^{p}w(j)E\{x(n-n_0-j)x(n-n_0-k)\}=E\{x(n)x(n-n_0-k)\};\ \ k=0,1,...,p \tag{4.6}$$

By assuming that the signal $x(n)$ is wide-sense stationary (WSS), then

$$E\{x(n-j)x(n-k)\}=r_x(k-j) \tag{4.7}$$

Equation (4.6) is simplified to

$$\sum_{j=0}^{p}w(j)r_x(k-j)=r_x(n_0+k)\ ;\ \ k=0,1,...,p \tag{4.8}$$

In matrix form, Equation (4.8) can be written as

$$\begin{bmatrix} r_x(0) & r_x(1) & \cdots & r_x(p) \\ r_x(1) & r_x(0) & \cdots & r_x(p-1) \\ \vdots & \vdots & & \vdots \\ r_x(p) & r_x(p-1) & \cdots & r_x(0) \end{bmatrix}\begin{bmatrix} w(0) \\ w(1) \\ \vdots \\ w(p) \end{bmatrix}=\begin{bmatrix} r_x(n_0) \\ r_x(n_0+1) \\ \vdots \\ r_x(n_0+p) \end{bmatrix}, \tag{4.9}$$

or denoted by

$$\mathbf{R}_x\mathbf{w}=\mathbf{r}\,. \tag{4.10}$$

The autocorrelation sequences in Equation (4.9) can be estimated by time averages when implementing this method. For finite data records, $x(n)$, $0\le n\le N-1$, the autocorrelation sequences can be estimated by

$$\hat{r}_x(k)=\frac{1}{N}\sum_{n=0}^{N-1}x(n)x(n-k) \tag{4.11}$$

The matrix $\mathbf{R}_x$ is a symmetric Toeplitz matrix and can be solved efficiently by the Levinson-Durbin Recursion algorithm [37].

## 4.3 SYSTEM PERFORMANCE

If the noise cancellation model is viewed as a prediction error filter (PEF), as illustrated in Figure 4.4, then the system performance can be measured by the prediction error of the

filter. That is, to have good performance, the prediction error should be significantly larger for a faulted bearing condition than for a healthy bearing condition.

In this section, the performance of the system is examined. First, a general equation describing the prediction error is given, and then specific equations for the system performance for a healthy-bearing condition and a bearing-fault condition are derived, respectively. Finally, observations are made based on the equations.

By definition, a general equation for the mean-square prediction error of the system is

$$\xi = E\left\{\left|x(n)-\sum_{k=0}^{p} w(k)x(n-n_0-k)\right|^2\right\} \tag{4.12}$$

This is the same error as in Equation (4.2), which was minimized to find the coefficients of the Wiener filter. Upon expansion, the above equation can be rewritten as

$$\xi = \left[r_x(0)-\sum_{k=0}^{p} w(k)r_x(n_0+k)\right] + \sum_{k=0}^{p} w(k)\left[\sum_{j=0}^{p} w(j)r_x(k-j)-r_x(n_0+k)\right] \tag{4.13}$$

### 4.3.1 System Performance for a Healthy-Bearing Condition

Since the Wiener filter is designed to minimize the error in Equation (4.12) by using healthy bearing data, this prediction error is small for a healthy-bearing condition. In fact, for a healthy-bearing condition, since $w(k), k = 0,1,\ldots,p$, are solutions to Equation (4.8), the second term of the right hand side (RHS) of Equation (4.13) is zero. Therefore, the prediction error for a healthy-bearing condition is

$$\xi_{\min} = r_x(0)-\sum_{k=0}^{p} w(k)r_x(n_0+k)\,. \tag{4.14}$$

At such a condition, since $x(n) = d_1(n) + v_1(n)$, therefore, it follows that

$$\begin{aligned} r_x(k) &= E\{x(n)x(n+k)\} = E\{[d_1(n)+v_1(n)][d_1(n+k)+v_1(n+k)]\} \\ &= E\{d_1(n)d_1(n+k)\}+E\{d_1(n)v_1(n+k)\}+E\{v_1(n)d_1(n+k)\}+E\{v_1(n)v_1(n+k)\} \end{aligned} \tag{4.15}$$

Since $d_1(n)$ and $v_1(n)$ are jointly WSS, (4.15) becomes

$$r_x(k) = r_{d_1}(k) + 2r_{d_1 v_1}(k) + r_{v_1}(k) \tag{4.16}$$

Since the measurement noise $v_1(n)$ is random, its power spectrum is distributed over a broad frequency range; its autocorrelation is pulse-like and its cross-correlations with other signals are zero. (The autocorrelation sequences of a signal are the inverse Fourier transform of its power spectrum by definition.) It follows from Equation (4.16) that

$$r_x(0) = r_{d_1}(0) + r_{v_1}(0)\ ,\ r_x(k) = r_{d_1}(k), k \neq 0\ . \tag{4.17}$$

Substituting Equations (4.17) into Equation (4.14) yields

$$\xi_{\min} = r_{d_1}(0) + r_{v_1}(0) - \sum_{k=0}^{p} w(k) r_{d_1}(n_0 + k) \tag{4.18}$$

To further investigate the performance of the system, let the noise components (including the supply fundamental and harmonics, the eccentricity harmonics, the slot harmonics, etc.) be

$$d_1(n) = \sum_{m=1}^{M} A_m \sin(\omega_m n + \varphi_m)\ , \tag{4.19}$$

where $A_m$, $\omega_m$, $\varphi_m$, $m = 1,...,M$, are the amplitudes, the frequencies, and the angles of $M$ noise components in the stator current. It is desired to compute the autocorrelation sequences of the signal $d_1(n)$. By definition,

$$r_{d_1}(k) = E\{d_1(n) d_1(n+k)\} = E\left\{\left[\sum_{m=1}^{M} A_m \sin(\omega_m n + \varphi_m\right]\left[\sum_{j=1}^{M} A_j \sin\left[\omega_j (n+k) + \varphi_j\right]\right]\right\}$$

$$= E\left\{\sum_{m=1}^{M} {A_m}^2 \sin(\omega_m n + \varphi_m) \sin\left[\omega_m (n+k) + \varphi_m\right]\right\} + E\left\{\sum_{m=1}^{M} A_m \sum_{j=1, j\neq m}^{M} A_j \sin(\omega_m n + \varphi_m) \sin\left[\omega_j (n+k) + \varphi_j\right]\right\} \tag{4.20}$$

Equation (4.20) can be reduced by recognizing the following relationships:

$$E\left\{\sum_{m=1}^{M} {A_m}^2 \sin(\omega_m n + \varphi_m) \sin\left[\omega_m (n+k) + \varphi_m\right]\right\}$$

$$= \sum_{m=1}^{M} \frac{A_m^2}{2} E\{\cos(\omega_m k) - \cos(2\omega_m n + \omega_m k + 2\varphi_k)\} = \sum_{m=1}^{M} \frac{A_m^2}{2} \cos(\omega_m k) \tag{4.21}$$

$$E\left\{\sum_{m=1}^{M} A_m \sum_{j=1, j\neq m}^{M} A_j \sin(\omega_m n + \varphi_m) \sin\left[\omega_j (n+k) + \varphi_j\right]\right\}$$

$$= \frac{1}{2} \sum_{m=1}^{M} A_m \sum_{j=1, j\neq m}^{M} A_j \left\langle E\{\cos[(\omega_j - \omega_m)n + \omega_j k + (\varphi_j - \varphi_m)]\} - E\{\cos[(\omega_j + \omega_m)n + \omega_j k + (\varphi_j + \varphi_m)]\}\right\rangle = 0 \tag{4.22}$$

Therefore, the autocorrelation sequences of the signal $d_1(n)$ are simply

$$r_{d_1}(k) = \sum_{m=1}^{M} \frac{A_m^2}{2} \cos(\omega_m k) \tag{4.23}$$

(Equation (4.23) can also be derived from the inverse Fourier transform of the power spectrum of the signal $d_1(n)$, which is not shown here.)

Finally, substituting Equation (4.23) into Equation (4.18) yields the prediction error of the filter for a healthy-bearing condition as

$$\xi_{\min} = \sum_{m=1}^{M} \frac{A_m^2}{2} \left\{1 - \sum_{k=0}^{p} w(k) \cos[\omega_m (n_0 + k)]\right\} + r_{v_1}(0) \tag{4.24}$$

### 4.3.2 System Performance for a Faulty-Bearing Condition

For a faulty bearing condition, the mean square prediction error can still be calculated from the general equation (4.13). For convenience, Equation (4.13) is repeated here as

$$\xi = \left[r_x(0) - \sum_{k=0}^{p} w(k) r_x(n_0 + k)\right] + \sum_{k=0}^{p} w(k) \left[\sum_{j=0}^{p} w(j) r_x(k-j) - r_x(n_0 + k)\right]. \tag{4.25}$$

However, different from the situation of a healthy-bearing condition, the second term on the right hand side of (4.25) for a faulty-bearing condition is not zero, because of the presence of the fault signal $d(n)$ in the stator current, which is $x(n) = d_1(n) + d(n) + v_1(n)$. It follows that

$$r_x(k) = E\{x(n)x(n+k)\} = E\{[d_1(n) + d(n) + v_1(n)][d_1(n+k) + d(n+k) + v_1(n+k)]\} \quad (4.26)$$

Assuming $d_1(n)$, $d(n)$ and $v_1(n)$ are jointly WSS, then Equation (4.26) becomes

$$r_x(k) = r_{d_1}(k) + r_d(k) + r_{v_1}(k) + 2r_{d_1v_1}(k) + 2r_{d_1d}(k) + 2r_{dv_1}(k) \quad (4.27)$$

As for a healthy-bearing condition, assume now that the measurement noise $v_1(n)$ is a broadband signal and not correlated with $d_1(n)$ and $d(n)$. It then follows that

$$r_x(0) = r_{d_1}(0) + r_d(0) + r_{v_1}(0) + 2r_{d_1d}(0), \quad (4.28)$$

and that

$$r_x(k) = r_{d_1}(k) + r_d(k) + 2r_{d_1d}(k), k \neq 0. \quad (4.29)$$

Now, in addition to $d_1(n) = \sum_{m=1}^{M} A_m \sin(\omega_m n + \varphi_m)$ as in the previous subsection, let the fault components be

$$d(n) = \sum_{q=1}^{Q} B_q \sin(\omega_q n + \varphi_q) \quad (4.30)$$

where $B_q$, $\omega_q$, $\varphi_q$, $q = 1,...,Q$ are the amplitudes, the frequencies, and the angles of $Q$ fault components in the stator current injected by a bearing fault. The autocorrelation sequences of $d(n)$ can be calculated as in Equations (4.20)-(4.23). The result is

$$r_d(k) = \sum_{q=1}^{Q} \frac{B_q^2}{2} \cos(\omega_q k) \quad (4.31)$$

For $\omega_q \neq \omega_m$, $q = 1,2,...,Q$, $m = 1,2,...,M$, following the same steps as in Equations (4.20)-(4.23), the cross-correlation sequences between the noise components $d_1(n)$ and the fault components $d(n)$ become

$$r_{d_1d}(k) = 0, k : \text{integer} \quad (4.32)$$

Finally, combining equations (4.25)-(4.32), the prediction error for a faulty-bearing condition can be obtained as

$$\xi = \xi_{\min} + \sum_{q=1}^{Q} \frac{B_q^2}{2} \left\{ 1 - \sum_{k=0}^{p} w(k) \cos\left[\omega_q (n_0 + k)\right] \right\} + \sum_{q=1}^{Q} \frac{B_q^2}{2} \left\{ \sum_{k=0}^{p} w(k) \left[ \sum_{j=0}^{p} w(j) \cos\left(\omega_q (k-j) - \cos\left(\omega_q (n_0 + k)\right)\right) \right] \right\} \tag{4.33}$$

where $\xi_{\min}$ is the prediction error for a healthy-bearing condition expressed in Equation (4.24).

### 4.3.3 OBSERVATIONS

The following several observations can be made based on Equation (4.33).

(1) For a healthy-bearing condition, all $B_q$'s are zero, and Equation (4.33) is reduced to Equation (4.24), as expected.

(2) The prediction error increases as the bearing fault develops; the degree of the increase is related to the power of the fault signal. For this reason, the fault index is chosen to be the RMS value of the noise-cancelled stator current.

(3) For generalized-roughness faults, the frequencies of the fault signal, $\omega_q$'s, are difficult to locate and may spread out. Also, the magnitudes of the fault components, $B_q$'s, are small. These two facts make it difficult to detect a specific fault component. However, the method considers a collective effect of the fault components and thus facilitates the fault detection.

(4) If the fault signal, $d(n)$, is a broadband signal, then it has the same effect as the broadband measurement noise $v_1(n)$. Since the power of the broadband signal remains

in the prediction error (both for a healthy-bearing condition and for a faulty-bearing condition), the presence of the fault signal results in an increase of the prediction error.

(5) If $\omega_q = \omega_m$, there is a smaller increase in the prediction error, since the third term on the right hand side of Equation (4.33) is zero, while the second term is nonzero. This means that if the fault components and the noise components have common frequencies, (for example, when the bearing fault augments the dynamic eccentricity of the motor), the fault information is still conserved in the resulting predictor error.

## 4.4 SUMMARY

In this chapter, a new current-based technique has been proposed to detect generalized roughness bearing faults. The technique decomposes the stator current into noise components and bearing fault related components. The noise components are estimated by using a Wiener filter and then are cancelled to uncover the bearing fault signal.

The proposed noise cancellation method has been analyzed in detail from the signal processing theory. The analysis has shown that the bearing fault indicator developed can provide the information about bearing faults. To further validate the proposed method, several experiments have been done and they are presented in the next chapter.

# CHAPTER 5

# SCNC BEARING FAULT DETECTION UNDER CONSTANT-LOAD CONDITIONS

This chapter presents the experimental validation of the proposed method under constant-load conditions. In Section 5.1, experimental methods to generate bearing faults are discussed. In Section 5.2, a special experimental method used in this research, i.e. the shaft current method is described. In Section 5.3, the stator current noise cancellation results of several on-line experiments are presented. In Section 5.4, the noise cancellation results are compared to the results from the existing Mean Spectral Deviation method. In Section 5.5, the correlation between the noise cancellation results and vibration measurements is evaluated. In Section 5.6, the proposed noise cancellation method is applied to vibration measurements and the results are provided. A summary of this chapter is provided in Section 5.7.

## 5.1 EXPERIMENTAL METHODS TO GENERATE BEARING FAULTS

The life of a bearing can be affected by many factors, including load, speed, lubrication, clearance, temperature, misalignment, and steel compositions. Among these factors, the effect of the load on the lifetime of the bearing is the most fundamental, and research shows that bearing life is inversely proportional to the load cubed [2]. When a bearing fails, it causes extreme vibration, leading to catastrophic damage to the whole process in a plant.

Despite many ways in which a bearing could fail in real life, experimental methods to generate bearing faults play an important role in the bearing fault study. This is because the

expected lifetime of a typical bearing in industry is several years. Therefore, experimental methods are required to accelerate the bearing failure process for research purposes. It is also desired that the entire lifecycle of a bearing should be documented, studied, and used to test various condition monitoring schemes in a reasonable timeframe achieved via experimental methods.

Bearing faults can be generated off-line, as in most experimental methods reported in the literature. For example, bearing faults can be generated by drilling a hole in the bearing, scratching the bearing with diamonds or rotary tools, or by electric discharge machining (EDM). These faults can be located on any of the four parts of a bearing: the inner raceway, the outer raceway, the balls, and the cage. After a fault is introduced off-line, the bearing is then placed back in an electric machine. Though it is very convenient and time saving to generate bearing faults off-line, it has the following two major drawbacks.

a) Though such faults exist in real life, they can not represent most realistic faults. Most realistic bearing faults, especially at early stages, are generalized-roughness faults and often do not produce the characteristic fault frequencies. However, the faults generated off-line are single-point defects and produce the characteristic fault frequencies.
b) The act of disassembling, reassembling, remounting, and realigning the test machine, in itself causes significant additional changes to the spectrum of the stator current. This can potentially conceal fault signatures or contribute to misleading results [35].

Therefore, experimental methods to generate bearing faults on-line (*in situ*) are required. The faults generated on-line should have similar mode as realistic faults; that is, the faults are due to metal fatigue and are developed over time. It is also desirable to have information about the different development stages of the faults. The incipient stage of a fault is especially of interest, because bearings with incipient faults should be replaced as soon as possible (after all, bearings are cheap). By predicting a fault at an early stage,

potential catastrophic damage can be avoided.

An experimental method to generate bearing faults was proposed in [35]. This method utilizes shaft current to accelerate the bearing failure process. Experiments have shown that this method is successful to fail bearings in a reasonable time, and the resulting faults are generalized-roughness faults. Therefore, this method is employed in this research to generate bearing faults. It is described in detail in Section 5.2.

There is another method in the literature to generate generalized-roughness faults. It uses material from the floor of a machine shop to contaminate bearings [11]. The resulting faults are more representative of general bearing failures than machined faults. The study does not describe if the faults were generated on-line. However, it seems unlikely that the bearing could be contaminated without disassembling the machine even with a special test rig like the one used in that study. Also, the test bearing is at the non-drive end of the machine, while in practice the drive end bearings are more likely to fail because of stronger impact from load. Another disadvantage of this method is that the contamination cannot be quantified.

## 5.2 SHAFT CURRENT EXPERIMENTAL SETUP

Bearings can be damaged by shaft currents. For example, shaft currents cause electric discharge machining (EDM) inside a bearing when a film of lubricant is formed around the rotating bearing. The film of lubricant can be viewed as a capacitor, and if the voltage across it exceeds the dielectric strength of the grease, EDM current flows and pits are created on the bearing surfaces. The EDM current also generates heat inside the bearing which damages the lubricant and the bearing. For technical details on the mechanisms by

which shaft currents cause bearing failures, the reader is referred to [35] and other related materials.

A great deal of research has been performed to minimize shaft currents and prolong bearing life. However, the effects that shaft currents have on bearing life have been utilized in [35] to accelerate the bearing failure process for the bearing fault study. Successful experiments have been done on a 5-hp induction motor by using the shaft current method (shown in Figure 5.1) proposed in [35]. It was shown that by this method bearings can be failed within several days. Therefore, the experimental method and the experimental setup in this research are based on the work in [35]. However, two changes are made, as illustrated in Figure 5.2:

a) A 20-hp induction motor is now employed as the test machine. For this larger machine, more time is required to fail the bearings. Also the experiments show that bearing faults in the larger machine are more difficult to detect via current monitoring. This may be because, for larger machines, the bearing-to-machine size ratio is smaller and thus bearing fault signatures are less prominent. Random noises due to loads may be also larger for larger machines.
b) An isolation transformer is added in the shaft current circuit to prevent the shaft current from entering the measurement circuit. An accelerometer is attached to the motor frame and its transducer power module is supplied from the utility. Therefore, if the isolation transformer is not included, a branch of the shaft current could be formed through the vibration transducer path due to the same utility ground of the transducer voltage and the shaft voltage. This branch of the shaft current may interfere and even corrupt measured signals. The setup used in [35] with no isolation is shown in Figure 5.1; the improved setup used in this research with an isolation transformer added is shown in Figure 5.2. In both figures, the paths of the shaft current are marked with bold lines.

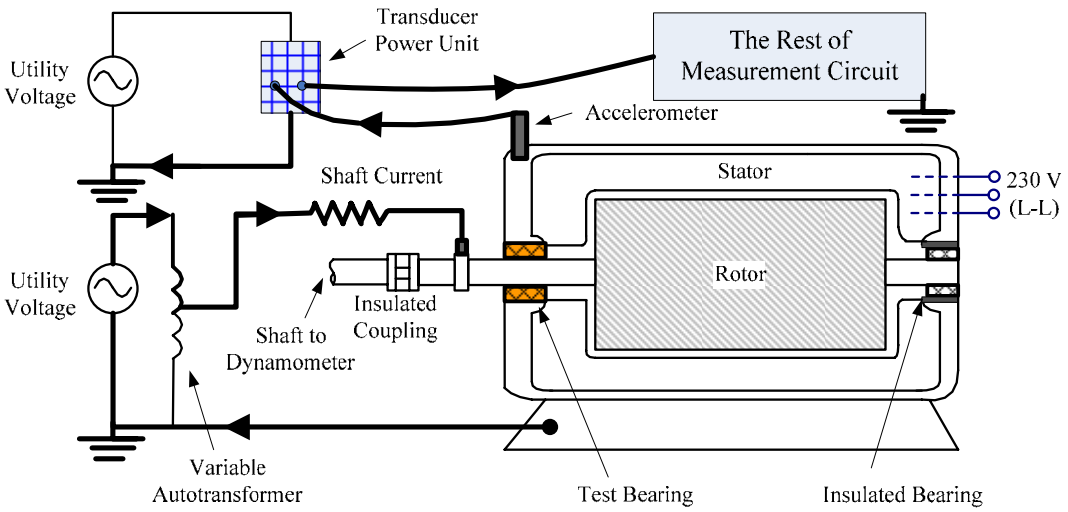


**Figure 5.1 Schematic diagram for the shaft current experimental setup without an isolator.**

The test machine is a 20 hp, 230 V, three phase, four pole, General Electric induction motor (model number 5KE256BC205B). This motor is supplied directly from the 230 V, three phase utility power. For convenience and availability, the shaft voltage is also taken from the utility power, and a variable autotransformer and an isolation transformer are employed to provide adjustability and isolation, respectively. The shaft current flows from the voltage source to the motor via a carbon brush. A 1 Ω, 200 W ballast resistor is placed in series with the voltage source to limit the shaft current. An aluminum disk is mounted on the shaft to provide a smooth contact surface for the brush. The part number for the test bearing (shaft-end) is SKF 6309 2Z or Koyo 6309 ZZ, and the part number for the rear bearing is SKF 6307 2Z. Since the rear bearing is electrically insulated from the stator, the shaft current is forced to flow from the shaft through the test bearing to reach the stator frame.

The adjustable load for the motor is provided by a dynamometer that is connected to the motor shaft via an electrically insulated Lovejoy coupling. The dynamometer is a 10 hp Westinghouse dc generator that supplies power to a resistor bank. The dynamometer is equipped with a speed sensor to record the operating speed. A photograph of the actual

setup is provided in Figure 5.3.

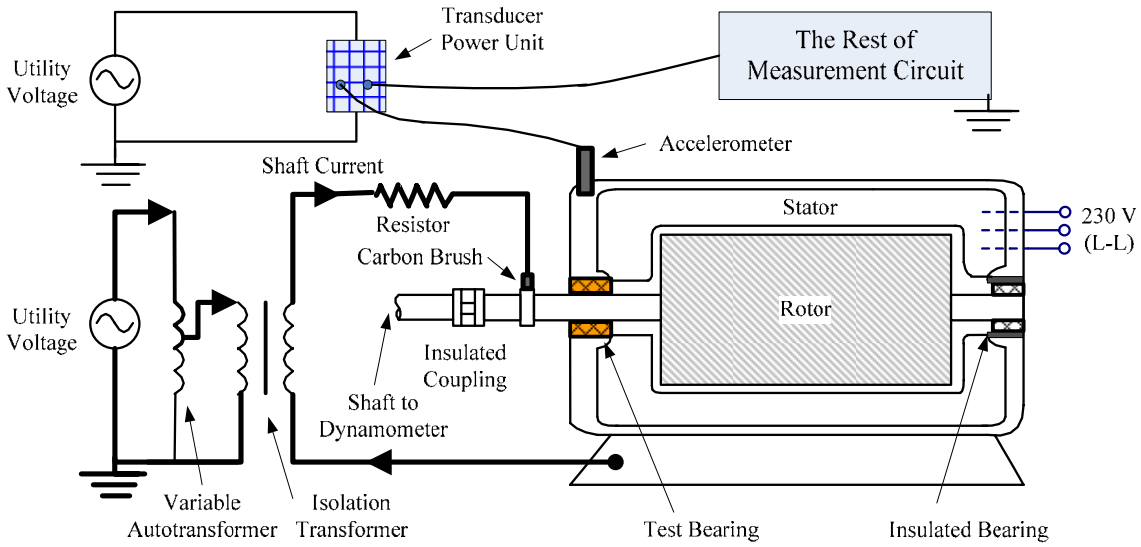


**Figure 5.2 Schematic diagram for the improved shaft current experimental setup with an isolation transformer included.**

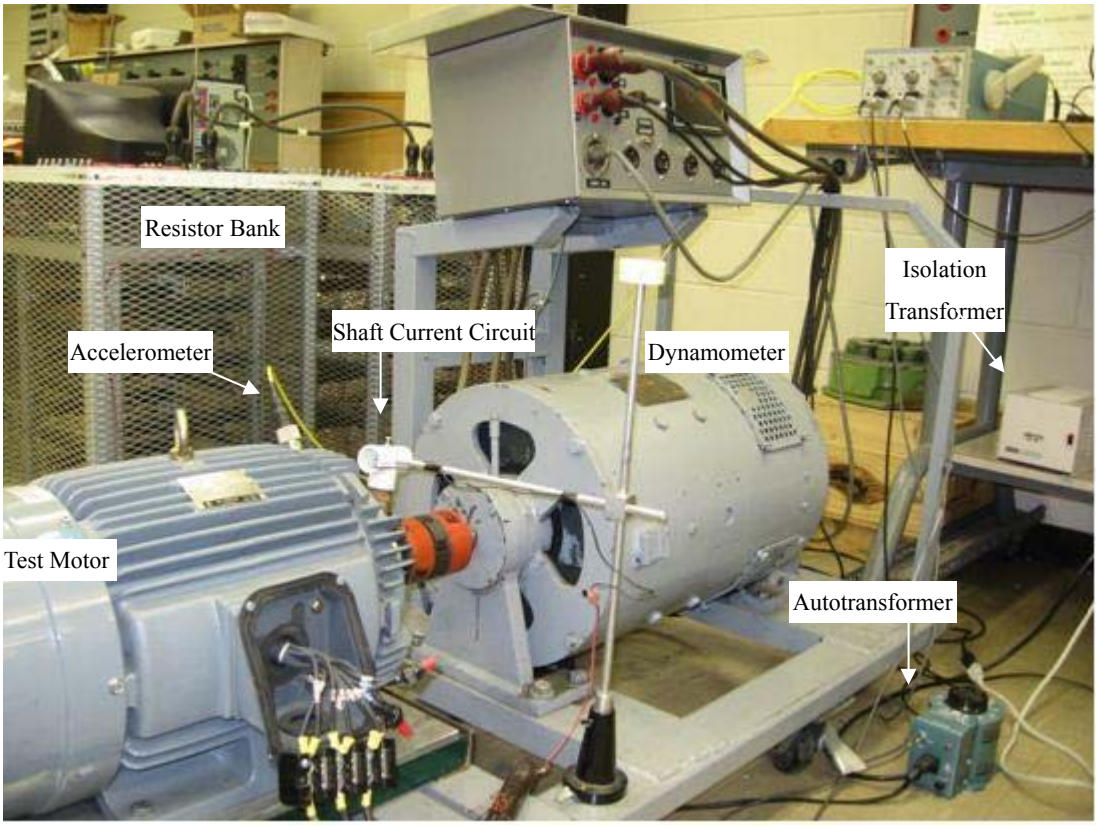


**Figure 5.3 A Photograph of the shaft current experimental setup.**

Three sensors are used to collect all the data as illustrated in Figure 5.4. One phase of stator current and the shaft current are each measured with Tektronix A6303 current probes and AM503 current probe amplifiers. A Wilcoxon model-P704B accelerometer (100mV/G) is mounted on the stator housing directly above the test bearing. The resonant frequency of the accelerometer is approximately 25 kHz. To implement current monitoring in practice, none of the above sensors would be needed, since a successful current monitoring scheme by itself could detect bearing faults and the stator current signal is readily available in the motor protection system. All measurements are collected by a National Instruments SCXI-1000 chassis. This chassis contains an SCXI-1141 programmable cutoff frequency, $8^{th}$ order elliptical anti-aliasing analog filter and an SCXI-1305 BNC connector block. Data from this chassis is then captured by a National Instruments (NI) PCI-6251M, 16-bit data acquisition card. This data is then acquired by LabView 7.1, which is running on a 1.7 GHz Pentium 4 computer with Windows Xp professional. All data is sampled at 6 kHz, and the cutoff frequency for the programmable anti-aliasing filter is automatically set by internal NI program, and is about 2 kHz. Since the working range of the PCI-6251M is set to ±5 V, an analog notch filter and several amplifying circuits are employed, as shown in Figure 5.4, to best utilize the dynamic range of this data acquisition system. The notch frequency of the analog notch filter is 60 Hz. The amplifying circuits were designed (by previous researchers) such that the output of each sensor is approximately ±5 V when the sensor is reading its maximum expected value. For the vibration measurement, since useful information also exists in high frequencies beyond the cutoff frequency of the anti-aliasing filter, an additional circuit is provided to compute the RMS value of the vibration sensor over its entire working frequency response ranges. The details about the preprocessing circuits are available in [38].

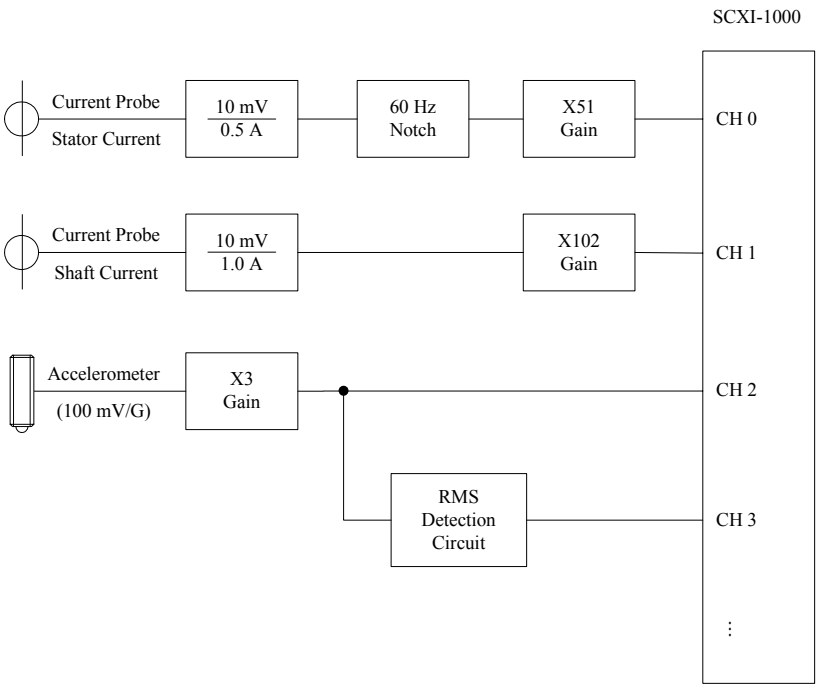


**Figure 5.4 Instrumentation setup used for all data acquisition in the shaft current experiment.**

The amount of time taken for a bearing to fail, by using this method, is variable and depends mainly on the shaft current level and the amount of grease in the bearing. The load and the environmental temperature also affect the bearing lifetime, to a lesser degree. The shaft current is adjusted between 6 A and 15 A (in RMS) in the experiments performed in this research. To control the amount of grease inside a bearing, the bearing is first soaked in a degreasing solution to remove all of the grease; then the bearing is repacked with a small amount of the original grease. Usually an amount of about 5% of the original grease is repacked. Then the bearing is placed in the motor, and an experiment starts. The experiment should be run continuously if possible, to minimize the amount of time it will take to fail the bearing.

## 5.3 EXPERIMENTAL RESULTS

Several tests have been done to evaluate the proposed bearing condition monitoring

scheme under constant-load conditions. For each test, a new bearing is cleaned and repacked with smaller amount of grease, before installing it into the test motor. After a few hours of steady operation, the machine reaches thermal steady state, and then the data acquisition process starts. (In real life, a run-in period should be considered when taking data for monitoring purposes.) The sampling frequency is 6 kHz. Every 15 minutes a 10 second window of data is sampled and stored in a new file each time. The data in the first file is used as the baseline data for the test. Since it usually takes several days for the bearing to fail, it is justified that the baseline data can be tagged as a healthy bearing condition. The coefficients of the Wiener filter are solved from the baseline data and are stored. Then the Wiener filter estimates the noise components in the real-time data from the recent data samples. Finally the estimated noise components are subtracted from the real-time data, and the RMS value of the resulting (noise-cancelled) data is calculated. The schematic diagram of this process is shown in Figure 5.5.

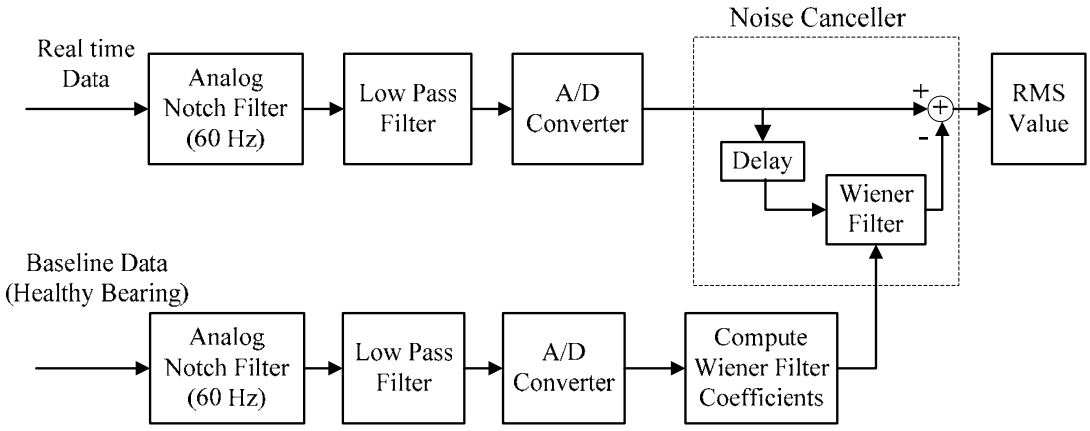


**Figure 5.5 Schematic diagram of the bearing condition monitoring via stator current noise cancellation.**

For each of the following tests, the length of the Wiener filter is chosen as 100 data samples, i.e., its order is 99 data samples. The delay of its input is one data sample. Therefore, for a 6 kHz sampling frequency, one cycle (of 60 Hz signal) of previous data samples is used to predict the next data sample. Different values of the length of the Wiener filter have also

been tried, including 200 data samples and 50 data samples, however, no significant differences have been found on the experimental results. Trials with different input delays yielded no significant differences either.

For the following tests, several vibration-based fault indices are calculated. They include the RMS value of the vibration acceleration from 0 to 1 kHz, the RMS value of the vibration velocity from 10 Hz to 1 kHz (the ISO 10816 measurement, see Section 2.3.1), and the RMS value of the vibration velocity from 1 kHz to 3 kHz. These indices are used to approximate the actual bearing health according to the ISO 10816 standard. The RMS value of vibration velocity from 1 kHz to 3 kHz is calculated, since a higher signal-to-noise ratio is expected in this range than the range from 10 Hz to 1 kHz especially when the fault is at its early stage. This is similar to the envelope method in Section 2.3.2 which tries to extract the characteristic fault frequencies in high-frequency regions.

Since only the vibration acceleration measurement is available in each test, the following formulas are used to calculate the vibration velocities from the vibration acceleration [12].

$$v_{rms} = \frac{10^3}{2\pi}\sqrt{\left(\frac{a_1}{f_1}\right)^2 + \left(\frac{a_2}{f_2}\right)^2 + \ldots + \left(\frac{a_n}{f_n}\right)^2} \tag{5.1}$$

where $a_1, a_2, \ldots, a_n$ are the RMS value acceleration values in meters per square second, $f_1, f_2, \ldots, f_n$ are frequencies in hertz, $v_{rms}$ is the associated RMS velocity in millimeters per second.

### 5.3.1 CONSTANT LOAD EXPERIMENT 1 (50% LOAD TEST)

Results from the 50% load test are shown in Figure 5.6. The top plot in this figure shows the RMS value of the noise-cancelled stator current minus the baseline value; the middle

shows the RMS value of the vibration acceleration; and the bottom plot shows the RMS value of the vibration velocities.

From Figure 5.6, one can see that both the noise-cancelled stator current RMS and the vibration RMS increase as the fault develops, though the increase is accompanied by several occasional decreases or dips. This is typical to all experiments performed in this research and other research as well [38]. Specifically, according to the vibration velocity from 1 kHz to 3 kHz, the incipient fault builds up between the $30^{th}$ and the $55^{th}$ hour. During this same time period, the noise cancellation method increases. From the $60^{th}$ hour to the end of the experiment, both the noise-cancelled current RMS and the vibration RMS remain at relatively high levels due to the bearing fault developed. Also from Figure 5.6, one can see that the ISO 10816 metric (the RMS of the vibration velocity from 10 Hz – 1 kHz) can be used to monitor the bearing health, as expected. It seems, however, that in this experiment and others done by the author that acceleration and velocity above 1 kHz are more sensitive to *incipient* bearing faults. This verifies that in many situations the fault signatures from incipient bearing faults are more salient in high frequencies [2, 14, and 18]. The linear correlation between the noise-cancelled stator current and the vibration acceleration is 0.69 (see Section 5.5 for details about the correlation between machine vibration and the noise-cancelled stator current).

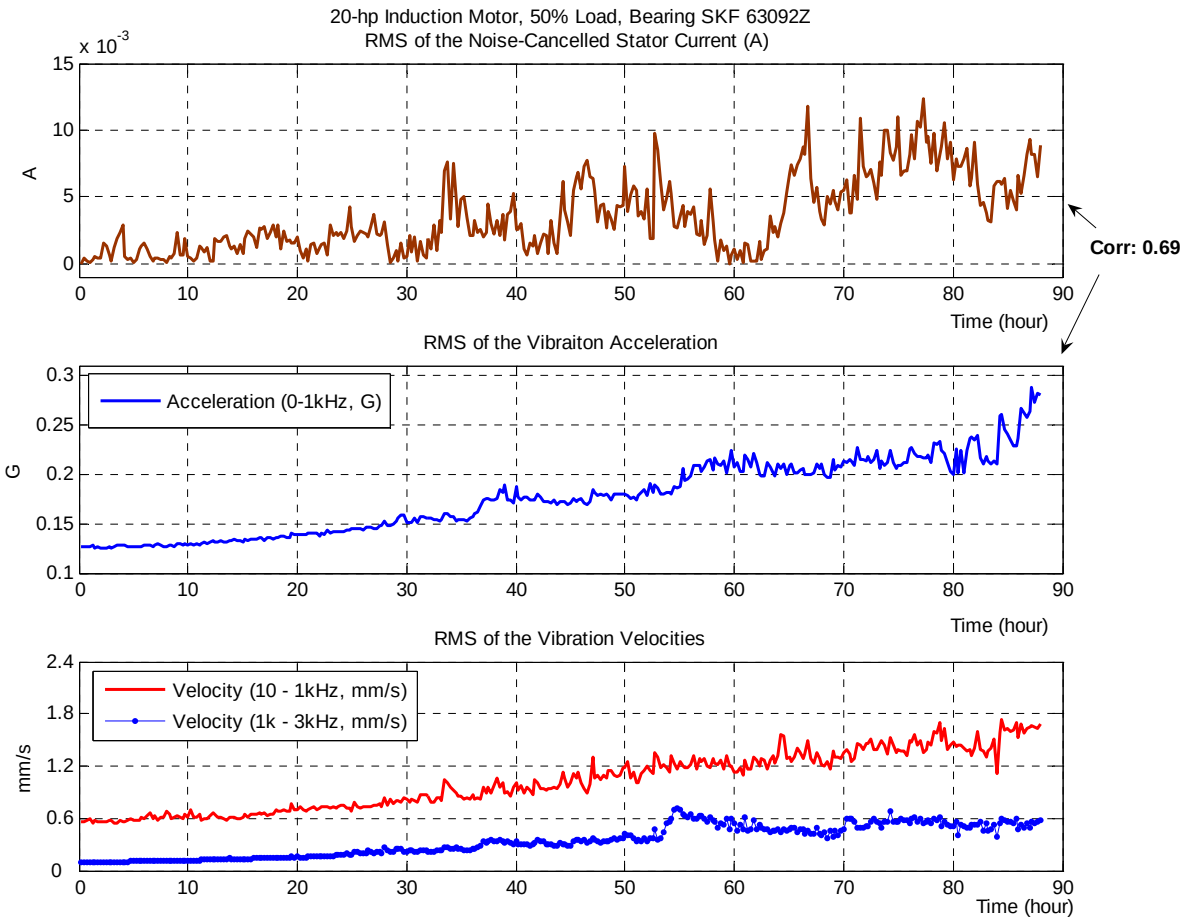


**Figure 5.6 Results for bearing type-6309 at a 50% load level. (top) The RMS value of the noise-cancelled stator current increases as the fault develops. (middle and bottom) The RMS values of the vibration acceleration and the vibration velocities also increase as the fault develops.**

### 5.3.2 CONSTANT LOAD EXPERIMENT 2 (33% LOAD TEST)

The results from the 33% load test are shown in Figure 5.7. As in Figure 5.6, the top plot shows the RMS value of the noise-cancelled stator current minus the baseline value; the middle and the bottom plots show the RMS of the vibration acceleration and the vibration velocities, respectively.

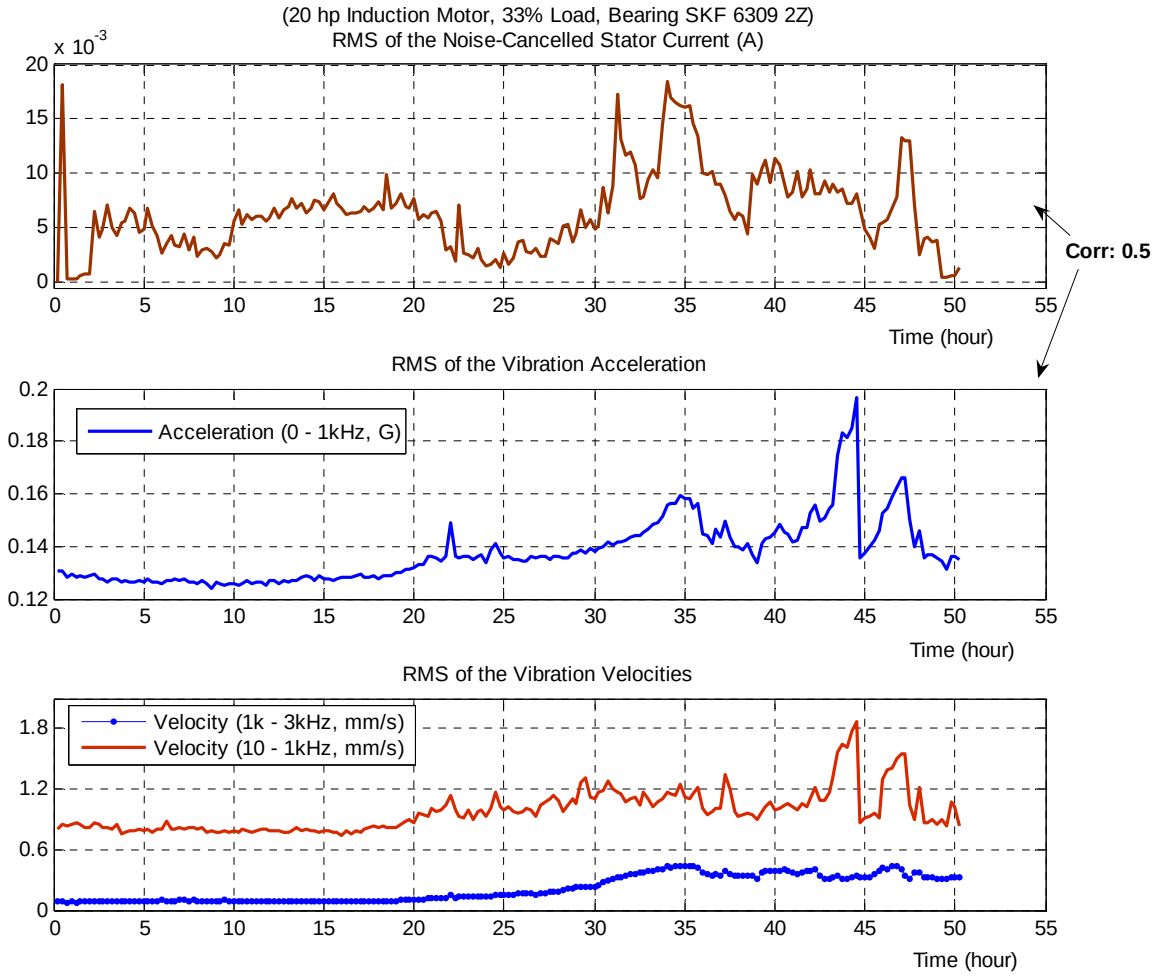


**Figure 5.7 Results for bearing type-6309 at a 33% load level. (top) The RMS value of the noise-cancelled stator current indicates the presence of the incipient bearing fault. (middle and bottom) The RMS values of the vibration acceleration and the vibration velocities indicate the presence of the incipient bearing fault.**

Figure 5.7 shows an abnormal peak in the top plot at the second data point (i.e., at the end of the first half hour). It is probable that this abnormality is due to bad data, since the points around it are still at a low level. With exception of this point, generally speaking, the noise cancellation curve (the top plot) mainly follows the vibration curves (the middle and the bottom plots). From the 25$^{th}$ to the 35$^{th}$ hour, the incipient fault builds up which can be seen from the 1k-3k Hz vibration velocity curve. Correspondingly, there is a substantial increase in the noise-cancelled current RMS during this time period. From the 40$^{th}$ hour to the end of

the experiment, the RMS value of both the vibration and the noise-cancelled current become unstable because of the deteriorated bearing condition. The bearing emits screeching sounds after 40 hours of operation; and the sound level increases until the experiment is ceased during the 50$^{th}$ hour. The linear correlation between the noise-cancelled stator current and the vibration acceleration is 0.5.

### 5.3.3 CONSTANT LOAD EXPERIMENT 3 (20% LOAD TEST)

The results from the 20% load test are shown in Figure 5.8. As in the previous figure, the top plot illustrates the RMS value of the noise-cancelled stator current; the middle and the bottom plots illustrate the RMS value of the vibration acceleration and the vibration velocity, respectively.

As seen from Figure 5.8, the RMS of the noise-cancelled stator current is at a relative high level from the 20$^{th}$ hour to the end of the experiment than the baseline level from the start to the 20$^{th}$ hour. Comparatively, from the 20$^{th}$ hour, the vibration becomes unstable due to the developing bearing fault. Again, as in the previous experiment, the bearing condition is reflected in changes in the RMS of both the machine vibration and the noise-cancelled stator current.

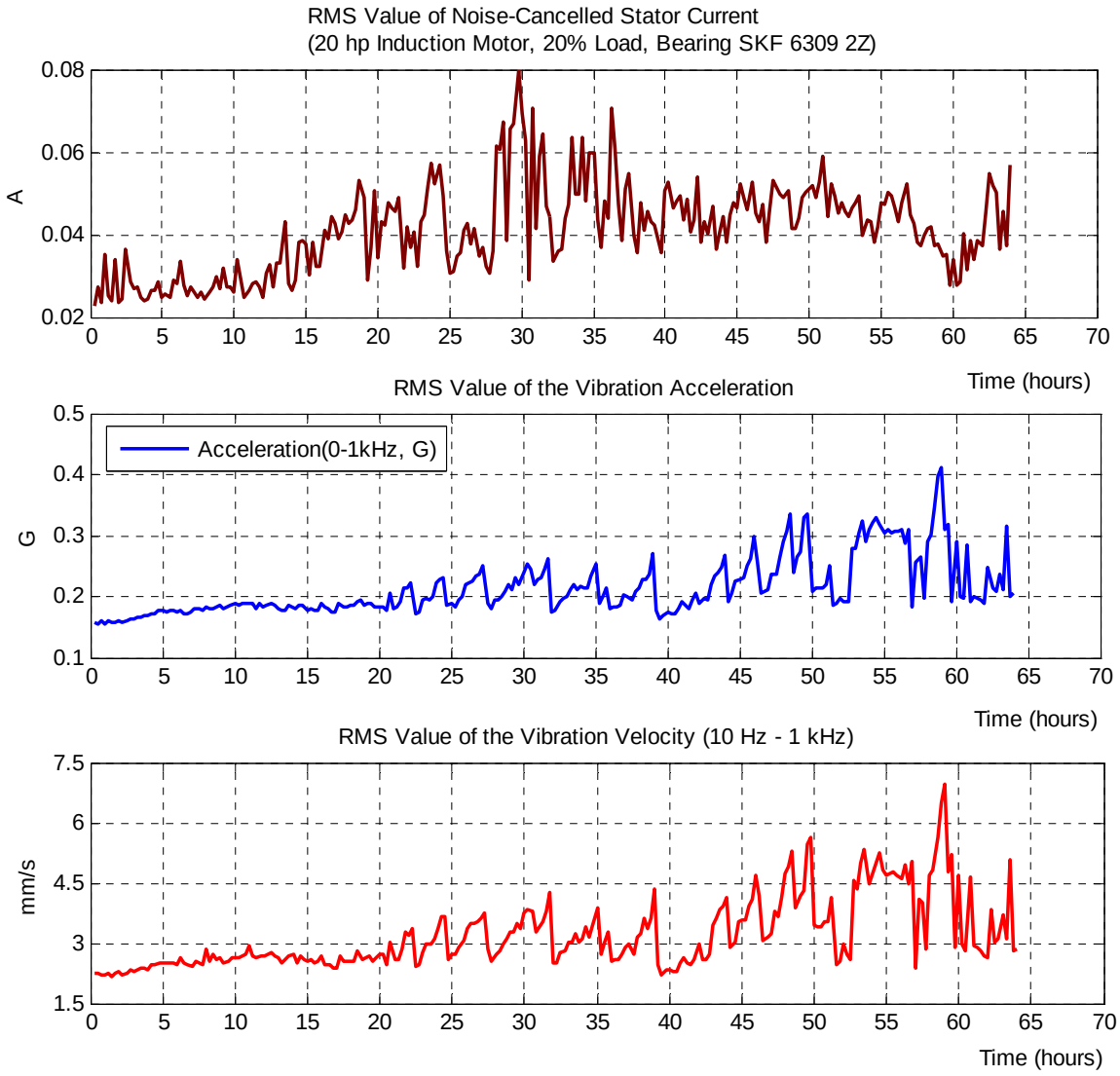


**Figure 5.8 Results for bearing type-6309 at a 20% load level. The RMS of the noise-cancelled stator current and the vibration becomes unstable because of degraded bearing condition.**

### 5.3.4 CONSTANT LOAD EXPERIMENT 4 (2% LOAD TEST)

The results for this near no-load experiment are shown in Figure 5.9. The top plot shows the RMS value of the noise-cancelled stator current minus the baseline value; the middle and the bottom plots illustrate the RMS value of the vibration acceleration of 0-1 kHz and the entire range (0-Infinite Hz), respectively.

As in the previous tests, there is variation in both the RMS of the noise-cancelled stator current and the RMS of the vibration as a result of the developing bearing fault. Specifically, the increases in those curves are accompanied by decreases in the fashion of increase-decrease-increase. For example, the machine vibration increases almost twice from the starting level around the 5$^{th}$ hour and remains at this level for 8 hours, and then it decreases back to the starting level. During the time, except the increase around the 5$^{th}$ hour, the noise-cancelled stator current remains at a relatively low level. Around the 25$^{th}$ hour, both the noise-cancelled stator current and the vibration increase again, After 30 hours' operation, a strange sound was emitted from the bearing and the machine was stopped. It is noted that in this experiment the shaft current is about 15 A, in the contrast to the level of 6-10 A in the previous experiments; consequently, it took only 5 hours for the machine vibration to increase substantially.

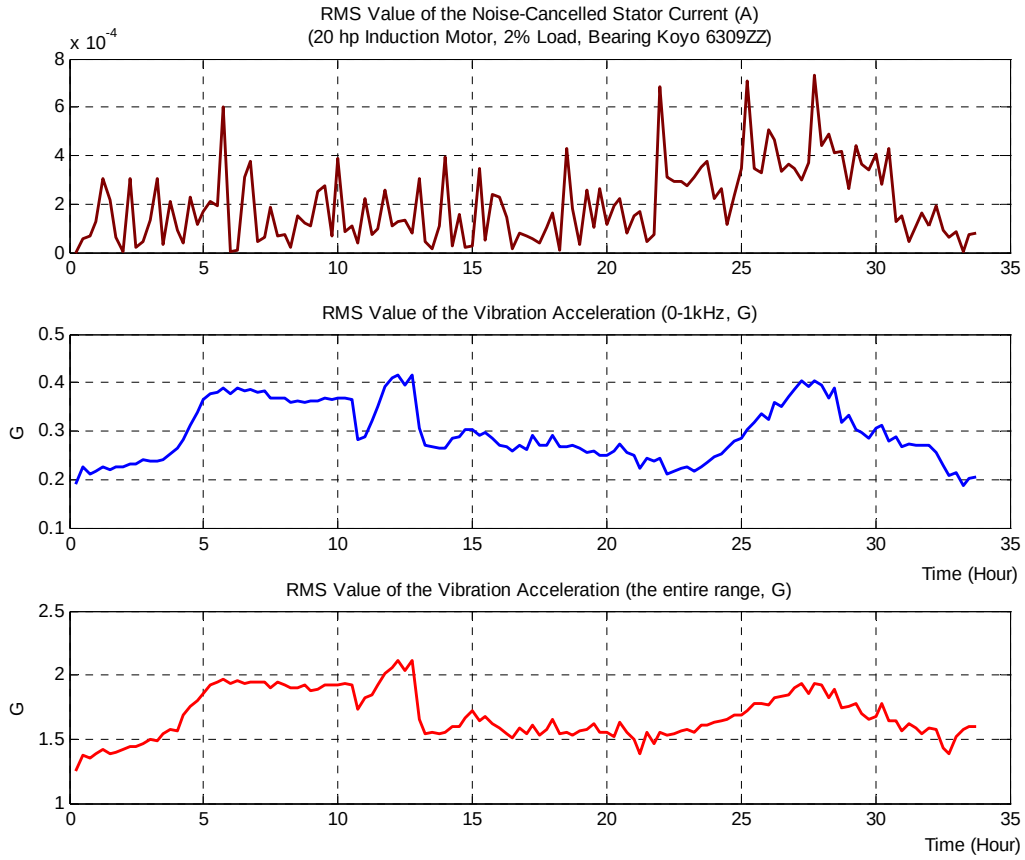


**Figure 5.9 Results for bearing type-6309 at a 2% load level. Variation in both the stator current and vibration measurements is observed as a result of the degraded bearing condition.**

### 5.3.5 CONSTANT LOAD EXPERIMENT 5 (10% LOAD TEST)

The results for this experiment are shown in Figure 5.10. This figure shows that the noise-cancelled stator current is closely correlated to the machine vibration in the sense of reaching peaks at the same time. Two peaks on the vibration curves around the 5$^{th}$ hour and the 8$^{th}$ hour, respectively, correspond to those on the current curve, indicating a degraded bearing health. Nearing the end of this experiment, a loud noise was emitted from the machine, which confirmed a degraded bearing condition because of the applied shaft current at about 15 A.

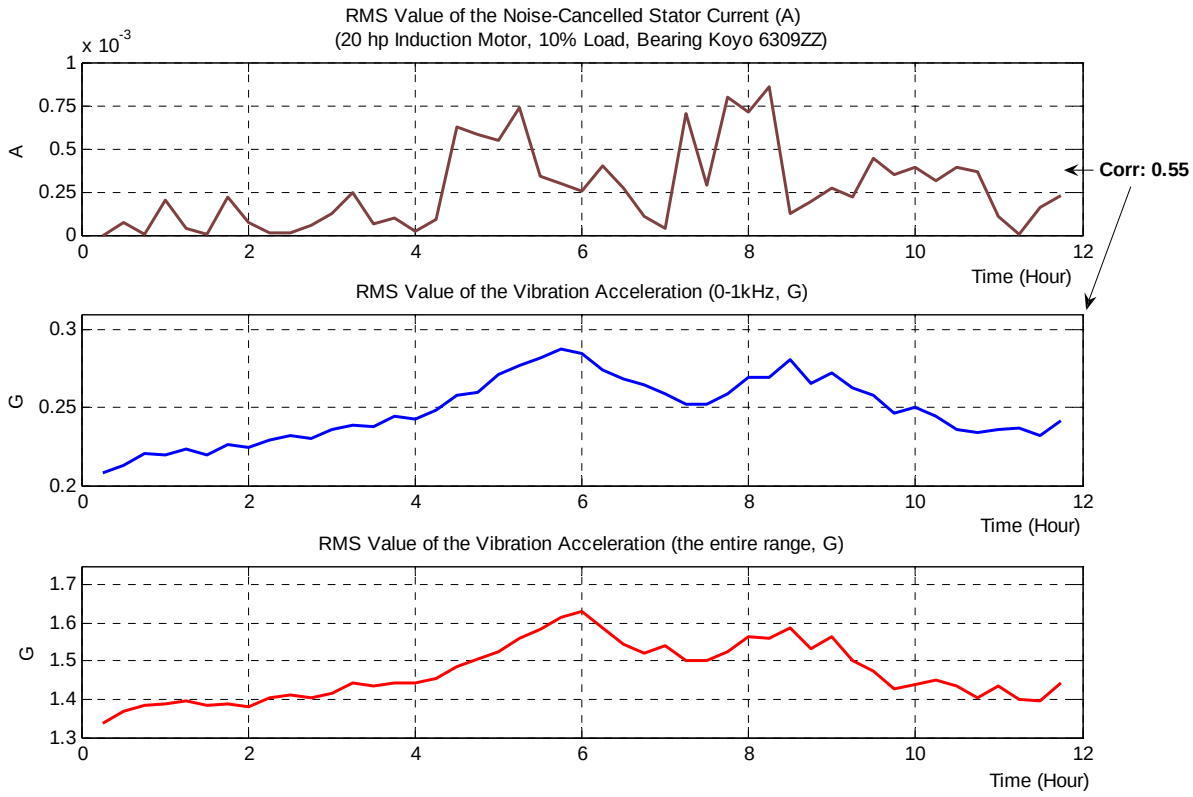


**Figure 5.10 Results for bearing type-6309 at a 10% load level. The noise-cancelled stator current and the machine vibration change in a similar fashion as the fault develops.**

### 5.3.6 CONSTANT LOAD EXPERIMENT 6 (15% LOAD TEST)

The results for this experiment are shown in Figure 5.11. As in the previous experiments,

the vibration increases during the experiment because of the degraded bearing condition, while the increase is accompanied by the dip around the 10$^{th}$ hour. The noise-cancelled stator current is correlated to the vibration and the linear correlation is 0.43. The experiment was stopped after one day's operation when a strange sound was emitted from the bearing.

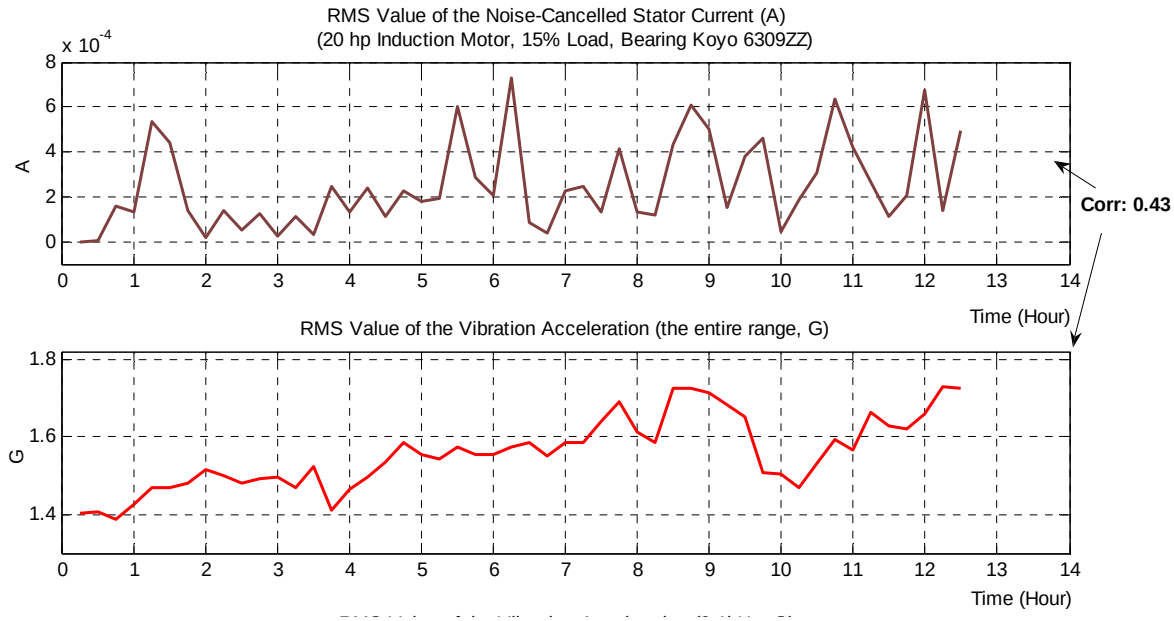


**Figure 5.11 Results for bearing type-6309 at a 15% load level. The noise-cancelled stator current and the vibration increase as the fault develops.**

## 5.4 COMPARISONS OF THE SCNC METHOD AND THE MSD METHOD

The Mean Spectral Deviation (MSD) method is the only algorithm available in the literature that was designed to detect generalized-roughness bearing faults via stator current (see Section 2.3 for details). Therefore, it will be interesting to compare the proposed Stator Current Noise Cancellation (SCNC) method to the MSD method.

First, it is noted that both methods are able to remove those dominant components in the stator current that are not related to bearing faults. In other words, the noise cancellation effects are significant in both methods, as shown in Figure 5.12. From the figure, it can be seen that the RMS curve of the stator current without noise cancellation (top plot) doesn't contain any bearing fault information, while the SCNC results ($2^{nd}$ plot) and the MSD results ($3^{rd}$ plot) contain valuable information about the fault. It can be clearly seen that there is no correlation between the stator current without noise cancellation and the machine vibration (bottom plot). The results shown in the figure are typical to all experiments performed in this research.

Secondly, it is noted that the two methods remove those dominant components in the stator current in quite different ways. In the MSD algorithm, the supply harmonics, eccentricity harmonics, and slot harmonics, etc. are filtered out from the sampled stator current by using traditional FIR/IIR digital filters. The spectral deviation of the remaining components is treated as the fault indicator. In the signal-noise point of view, the noise components are explicitly defined and then removed via the notch filtering operation. In the SCNC method developed in this research, the noise components in the stator current are estimated via a Wiener filter and are then removed via the noise cancellation technology. The RMS of the noise-cancelled stator current is the fault indicator.

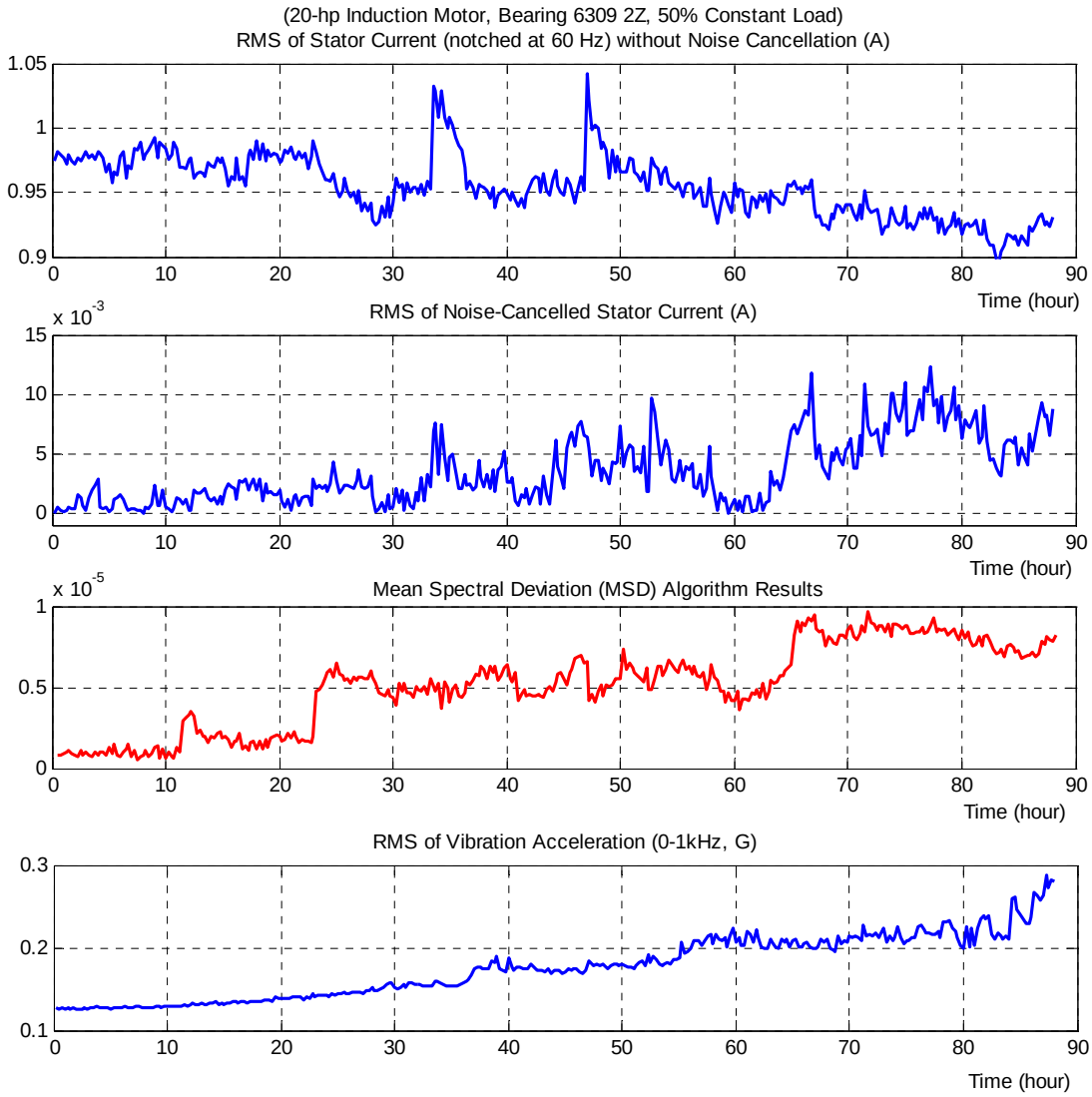


**Figure5.12 Illustration of the noise cancellation effects by the noise cancellation method and results of the MSD method.**

Thirdly, it is noted that the noise cancellation approach in the SCNC method is preferable to the notch filtering approach in the MSD method, because

1) In the noise cancellation approach, the frequencies of the noise components are not required, while in the notch filtering approach the frequencies of the noise components need to be calculated (from those equations as listed in Section 2.3). Further, the accuracy of the calculation is dependant upon the accuracy in rotor speed estimation and availability of machine parameters;

2) Unlike the noise cancellation process, the notch filtering operation can't separate a signal and noise having the same frequencies; this may be a problem of the MSD method, since the filtered components by the MSD method may actually contain bearing fault signatures [11]; and

3) The MSD method involves complicated calculations to obtain the fault indicator (i.e. computing the spectral deviation after notch filtering), while in the SCNC method only the RMS of the signal needs to be calculated once the noise components are removed.

Because of these reasons, the SCNC method outperforms the MSD method in many cases, as illustrated in Figure 5.13. It can be seen that the SCNC results contain useful information about the bearing health, while the MSD method failed in this test.

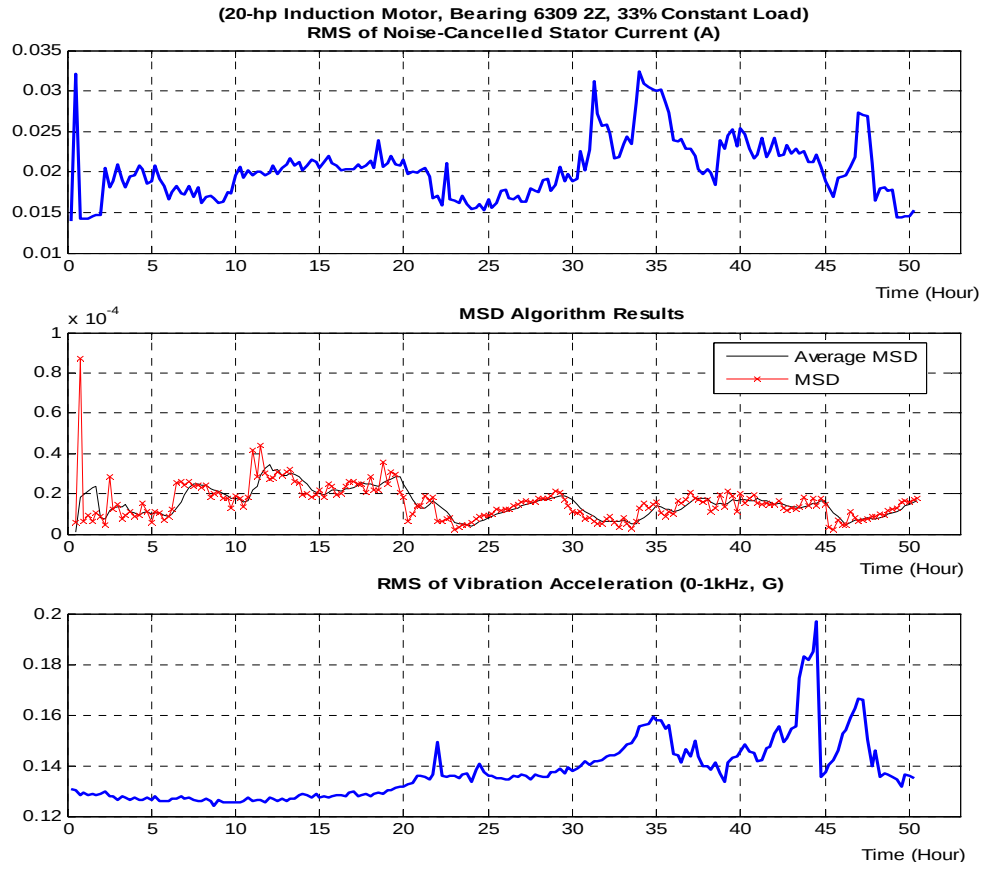


**Figure 5.13 The noise cancellation algorithm outperforms the MSD algorithm in some cases as verified by a real test on a 20-hp induction motor experiment at a 33% load.**

Lastly, it is noted that the MSD algorithm should provide similar results as the SCNC method if the noise components can be completely removed by notch filters while not affecting fault-related components. This is because the integration of the power spectrum of a signal, i.e. the fault indicator of the MSD method, is equal to the square of the RMS of that signal, i.e. the fault indicator of the SCNC method, according to Parseval's theorem which is stated by the following equations [47]:

$$\frac{1}{N}\sum_{n=0}^{N-1}\left|x[n]\right|^2 = \sum_{k=0}^{N-1}\frac{1}{N^2}\left|X[k]\right|^2 \tag{5.2}$$

where $X[k]$ is the discrete Fourier transform of the signal $x[n]$ of length $N$. This is verified by experiment results, as shown in Figure 5.12 above and Figure 5.14 below.

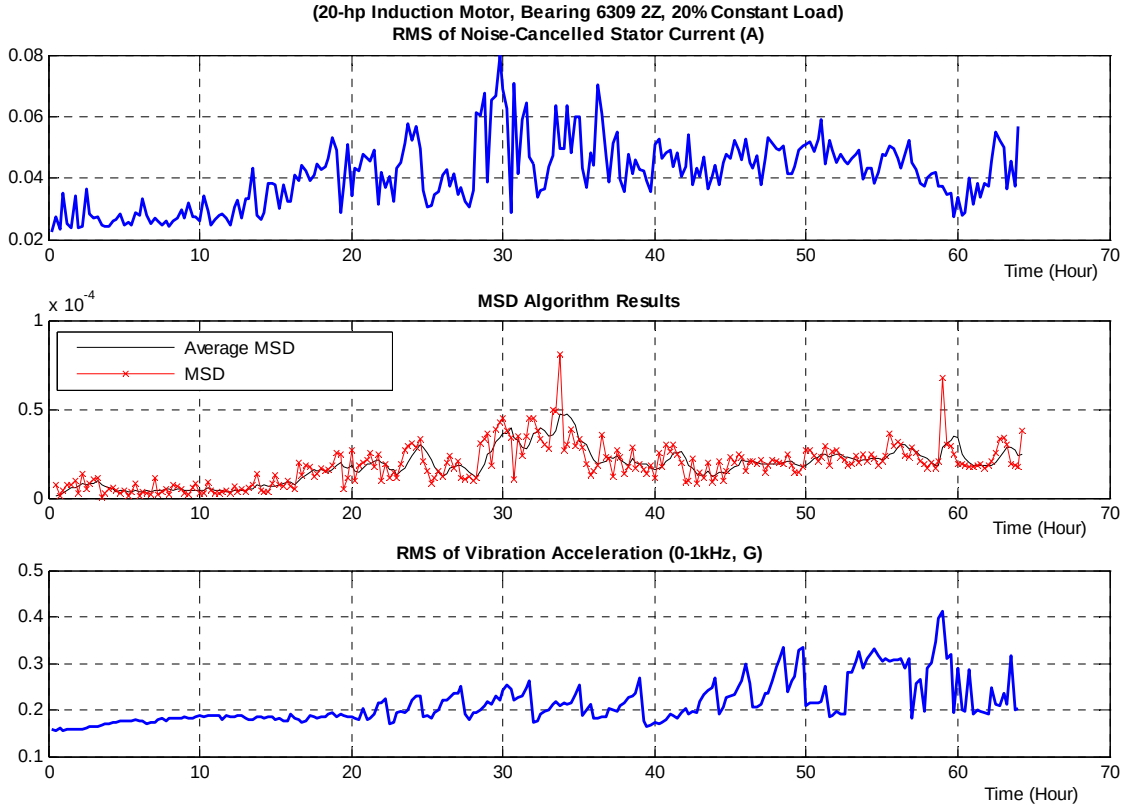


**Figure 5.14 Results from the MSD method and the SCNC method applied to the same data collected from a 20 hp motor at 20% load.**

## 5.5 Correlation Between Stator Current Noise Cancellation Results and Vibration Measurements

Vibration monitoring has been proved a reliable means for bearing fault detection. Therefore, it is of interest to evaluate the correlation between the SCNC results and vibration measurements. Typically, vibration measurements at different frequency bands have different sensitivities to bearing faults. For example, vibration in high-frequency ranges, especially around the mechanical resonance frequency, may be more sensitive to incipient bearing faults. Consequently, the correlation between SCNC results and vibration measurements of different frequency ranges may be different. In this research, the correlation between the noise cancelled stator current and the machine vibration over different frequency ranges (0-1kHz, 1kHz - 2kHz, 2kHz - 3kHz, 0-3kHz and 0-infinite Hz) is calculated.

Table 5.1 shows the correlation between the noise-cancelled stator current and the vibration measurements for the experiments performed in this research, including those under constant-load conditions and variable-load conditions. The details of the variable-load experiments are provided in the next chapter.

The p-Values for testing the hypothesis of no correlation are also given in Table 5.2. Each p-Value is the probability of getting a correlation as large as the observed value in Table 5.1 by random chance, when the true correlation is zero. Usually*, if the p-Value is less than 0.05, then the correlation is significant* [66]. The smaller the p-Value is, the higher the confidence in the correlation.

**Table 5.1 The correlation coefficients between the RMS of the noise-cancelled stator current and the RMS of the vibration acceleration** (The cells with coefficient larger than 0.4 are shadowed)

| *No. #* | *Noise-cancelled state current* | | *Vibration acceleration* | | | | |
|---|---|---|---|---|---|---|---|
| | | | *0-1kHz* | *1k-2kHz* | *2k-3kHz* | *0-3kHz* | *0-inf Hz* |
| 1 | Constant Load Experiment # | 1 | **0.69** | 0.64 | 0.68 | 0.68 | 0.66 |
| 2 | | 2 | 0.48 | 0.47 | 0.53 | 0.53 | **0.58** |
| 3 | | 3 | 0.34 | **0.46** | 0.44 | 0.45 | 0.42 |
| 4 | | 4 | **0.22** | 0.16 | 0.17 | 0.19 | 0.21 |
| 5 | | 5 | **0.55** | 0.41 | 0.53 | 0.53 | 0.53 |
| 6 | | 6 | 0.08 | 0.08 | 0.41 | 0.39 | **0.43** |
| 7 | Variable Load Experiment # | Exp. 1 Load 1 | **0.77** | -0.31 | 0.53 | 0.28 | 0.72 |
| 8 | | Exp. 1 Load 2 | 0.25 | 0.27 | **0.28** | 0.28 | 0.28 |
| 9 | | Exp. 2 Load 1 | 0.39 | 0.83 | **0.86** | 0.85 | 0.86 |
| 10 | | Exp. 2 Load 2 | **0.46** | 0.43 | 0.32 | 0.34 | 0.36 |
| 11 | | Exp. 2 Load 3 | **0.72** | 0.79 | 0.60 | 0.64 | 0.66 |

**Table 5.2 The p-Value between the rms of the noise-cancelled stator current and the rms of the vibration acceleration**

| *No. #* | *Noise-cancelled state current* | | *Vibration acceleration* | | | | |
|---|---|---|---|---|---|---|---|
| | | | *0-1kHz* | *1k-2kHz* | *2k-3kHz* | *0-3kHz* | *0-inf Hz* |
| 1 | Constant Load Experiment # | 1 | 4.7E-52 | 3.6E-42 | 2.4E-49 | 4.8E-49 | 2.7E-45 |
| 2 | | 2 | 6.6E-13 | 1.8E-12 | 5.6E-16 | 2.0E-16 | 2.2E-19 |
| 3 | | 3 | 2.5E-08 | 6.9E-15 | 9.1E-14 | 6.3E-14 | 2.8E-12 |
| 4 | | 4 | 1.0E-02 | 6.4E-02 | 5.6E-02 | 2.7E-02 | 1.5E-02 |
| 5 | | 5 | 6.8E-05 | 4.4E-03 | 1.2E-04 | 1.2E-04 | 1.4E-04 |
| 6 | | 6 | 6.0E-01 | 5.8E-01 | 3.2E-03 | 5.0E-03 | 1.9E-03 |
| 7 | Variable Load Experiment # | Exp. 1 Load 1 | 3.5E-20 | 2.3E-03 | 3.5E-08 | 6.2E-03 | 1.0E-16 |
| 8 | | Exp. 1 Load 2 | 3.4E-03 | 1.3E-03 | 8.7E-04 | 7.9E-04 | 9.8E-04 |
| 9 | | Exp. 2 Load 1 | 5.4E-03 | 7.5E-14 | 5.6E-16 | 4.1E-15 | 1.3E-15 |
| 10 | | Exp. 2 Load 2 | 5.3E-04 | 1.3E-03 | 1.7E-02 | 1.2E-02 | 6.8E-03 |
| 11 | | Exp. 2 Load 3 | 3.4E-08 | 1.9E-10 | 1.7E-05 | 3.4E-06 | 1.3E-06 |

From these results, it is clear that the correlation of the noise-cancelled stator current and the machine vibration is significant and *almost all p-Value's are much smaller than 0.05*. *The highest correlation coefficient is 0.86; and in 9 out of the 11 tests listed in Table 5.1, the correlation coefficient is greater than 0.43.* Also, in 4 out of the 11 tests, the correlation is greater than 0.69, and in 6 out of the 11 tests, the correlation greater than 0.55.

**Comments about those correlation coefficients:**

The following equation is used to calculate the correlation coefficients in Table 5.1

$$r_{xy} = \frac{\sum_{i=1}^{n}(x_i - \bar{x})(y_i - \bar{y})}{\sqrt{\sum_{i=1}^{n}(x_i - \bar{x})^2}\sqrt{\sum_{i=1}^{n}(y_i - \bar{y})^2}} \tag{5.3}$$

where $r_{xy}$ is the correlation coefficient of the variable $X$ and $Y$, $\bar{x}$ and $\bar{y}$ are the mean of $X$ and $Y$, $x_i$ and $y_i$ are samples of $X$ and $Y$. Specifically, the variable $X$ is the RMS value of noise-cancelled stator current and $Y$ is the RMS of the vibration measurement over one of the frequency ranges.

It is noted that the correlation coefficient calculated as above *only* measures the goodness of fitting the data to the model $Y = a + bX$, where $a$ and $b$ are the parameters to minimize the fitting error. In other words, the square of the above correlation coefficient is the coefficient of determination for this *first-order linear* polynomial model [67], i.e.,

$$r_{xy}^{\ 2} = 1 - \frac{\sum_{i=1}^{n}(y_i - a - bx_i)^2}{\sum_{i=1}^{n}(y_i - \bar{y})^2} \tag{5.4}$$

The correlation coefficient from Equation (5.3) may not be able to *fully* describe the relationship between the variables $X$ and $Y$ for practical problems. For example, suppose $X$ is uniformly distributed on the interval from -1 to 1 and $Y = X^2$. Then $Y$ is completely determined by $X$, but the correlation coefficient according to Equation (5.3) is zero.

Since the bearing-machine system is a complex system, both electrically and mechanically, the above model may not be able to *fully* describe the relationship between the noise-cancelled stator current and the vibration measurements. For example, Table 5.3 and Table 5.4 show the correlation coefficients (or the square root of the coefficient of determination of the fit) obtained based on third-order polynomial and nine-order polynomial fits, as described by the following expressions, respectively

$$Y = a_0 + a_1 x + a_2 x^2 + a_3 x^3 \tag{5.5}$$

$$Y = a_0 + \sum_{i=1}^{9} a_i x^i \tag{5.6}$$

It can be seen that the coefficients in Table 5.4 are larger than those in Table 5.3 and that the coefficient in both tables are larger than those in Table 5.1. Specifically, in 8 of the 11 tests, the correlation coefficient is equal to or larger than 0.7, and in 2 tests of the 11 tests, the correlation coefficient is close to 1.0, based on the nine-order polynomial fit according to Table 5.4. It is possible to obtain higher correlation coefficients by increasing the order of the polynomial or by using other models. The results here as shown in Tables 5.1 – 5.4 demonstrate that *the noise-cancelled stator current is closely correlated to the machine vibration*, but not limited to the first-order linearity. This provides a sound basis for bearing fault detection via the noise-cancelled stator current alone.

The relationship can also be explained by the following equation from *Ampere's Law*

$$\Phi R = NI \text{ and } R = \frac{g}{\mu A} \tag{5.7}$$

where $\Phi$ is the flux, $R$ is the reluctance of the magnetic path, $N$ is the stator winding turns, $I$ is the stator current, $g$ is the air gap length, $\mu$ is the permeability, and $A$ is the cross-section area. Anomalies in the air gap ($g$) caused by a degraded bearing condition produce radial magnetic force and increase the machine vibration; such anomalies also affect the (noise-cancelled) stator current according to Equation (5.7) [68-70].

**Table 5.3 The correlation coefficients between the RMS of the noise-cancelled stator current and the RMS of the vibration acceleration (based on a third-order polynomial fit)**

| *No. #* | *Noise-cancelled state current* | | *Vibration acceleration* | | | | |
|---|---|---|---|---|---|---|---|
| | | | *0-1kHz* | *1k-2kHz* | *2k-3kHz* | *0-3kHz* | *0-inf Hz* |
| 1 | Constant Load Experiment # | 1 | 0.71 | 0.71 | 0.71 | 0.71 | **0.72** |
| 2 | | 2 | 0.57 | 0.61 | 0.63 | 0.63 | **0.66** |
| 3 | | 3 | 0.55 | **0.64** | 0.62 | 0.61 | 0.63 |
| 4 | | 4 | 0.28 | 0.23 | 0.33 | 0.33 | **0.35** |
| 5 | | 5 | 0.53 | 0.71 | 0.48 | 0.53 | **0.53** |
| 6 | | 6 | **0.48** | 0.37 | 0.45 | 0.42 | 0.46 |
| 7 | Variable Load Experiment # | Exp. 1 Load 1 | **0.82** | 0.67 | 0.64 | 0.52 | 0.79 |
| 8 | | Exp. 1 Load 2 | 0.37 | **0.38** | 0.34 | 0.37 | 0.36 |
| 9 | | Exp. 2 Load 1 | 0.90 | 0.96 | **0.98** | 0.98 | 0.98 |
| 10 | | Exp. 2 Load 2 | 0.85 | **0.89** | 0.78 | 0.79 | 0.82 |
| 11 | | Exp. 2 Load 3 | 0.73 | **0.85** | 0.71 | 0.74 | 0.75 |

**Table 5.4 The correlation coefficients between the RMS of the noise-cancelled stator current and the RMS of the vibration acceleration (based on a nine-order polynomial fit)**

| *No. #* | *Noise-cancelled state current* | | *Vibration acceleration* | | | | |
|---|---|---|---|---|---|---|---|
| | | | *0-1kHz* | *1k-2kHz* | *2k-3kHz* | *0-3kHz* | *0-inf Hz* |
| 1 | Constant Load Experiment # | 1 | 0.74 | 0.74 | **0.77** | 0.76 | 0.75 |
| 2 | | 2 | 0.66 | 0.67 | 0.70 | 0.68 | **0.71** |
| 3 | | 3 | 0.57 | **0.69** | 0.66 | 0.66 | 0.67 |
| 4 | | 4 | 0.44 | 0.35 | **0.44** | 0.40 | 0.40 |
| 5 | | 5 | 0.70 | **0.78** | 0.70 | 0.71 | 0.71 |
| 6 | | 6 | 0.55 | 0.53 | 0.53 | **0.59** | 0.54 |
| 7 | Variable Load Experiment # | Exp. 1 Load 1 | **0.84** | 0.76 | 0.65 | 0.54 | 0.79 |
| 8 | | Exp. 1 Load 2 | 0.40 | 0.46 | 0.57 | 0.51 | **0.51** |
| 9 | | Exp. 2 Load 1 | 0.93 | 0.98 | **1.00** | 0.99 | 0.99 |
| 10 | | Exp. 2 Load 2 | 0.92 | **0.98** | 0.93 | 0.94 | 0.95 |
| 11 | | Exp. 2 Load 3 | 0.81 | **0.89** | 0.75 | 0.79 | 0.79 |

## 5.6 APPLYING THE NOISE CANCELLATION ALGORITHM TO VIBRATION SIGNAL

It is interesting to note that the proposed noise cancellation algorithm can also be applied to vibration measurements. Similar to the case for stator current, bearing fault-related components in vibration remain in the system output and the majority of non-fault-related components is removed during the noise cancellation process. This can be clearly seen in both Figure 5.15 and Figure 5.16. For example, in the beginning of the two tests, the RMS of the noise-cancelled vibration is around 0.02G (top plot in each figure) and the RMS of the original vibration around 0.06G (bottom plot in each figure). Therefore, nearly 2/3 of this 0.06G has been removed during the noise cancellation process.

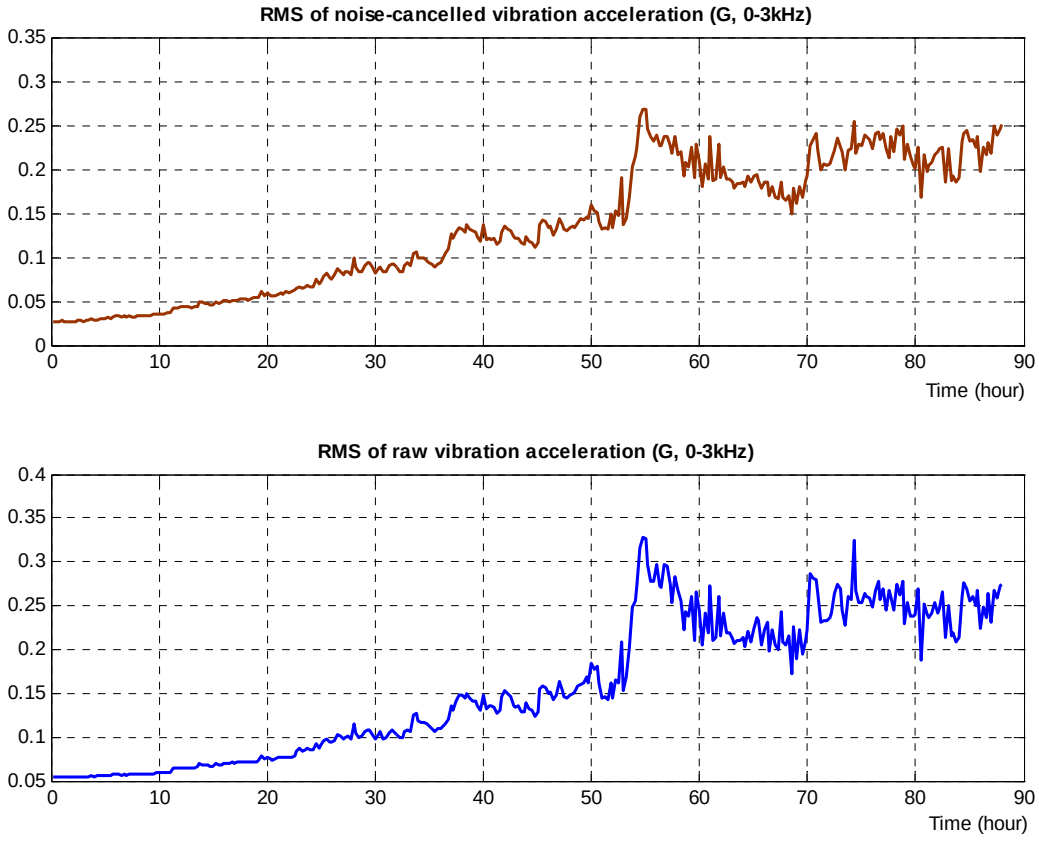


**Figure 5.15 Results attained by applying the noise cancellation algorithm to the machine vibration in Experiment - 1**

It is also clear that the trend of the vibration measurement doesn't change after the noise cancellation process. Since the change (the trend) in the vibration measurements is directly related to the development of the bearing fault in the tests, this indicates that *bearing fault-related components are not affected by the noise cancellation process*. The results here are typical to all experiments performed in this research.

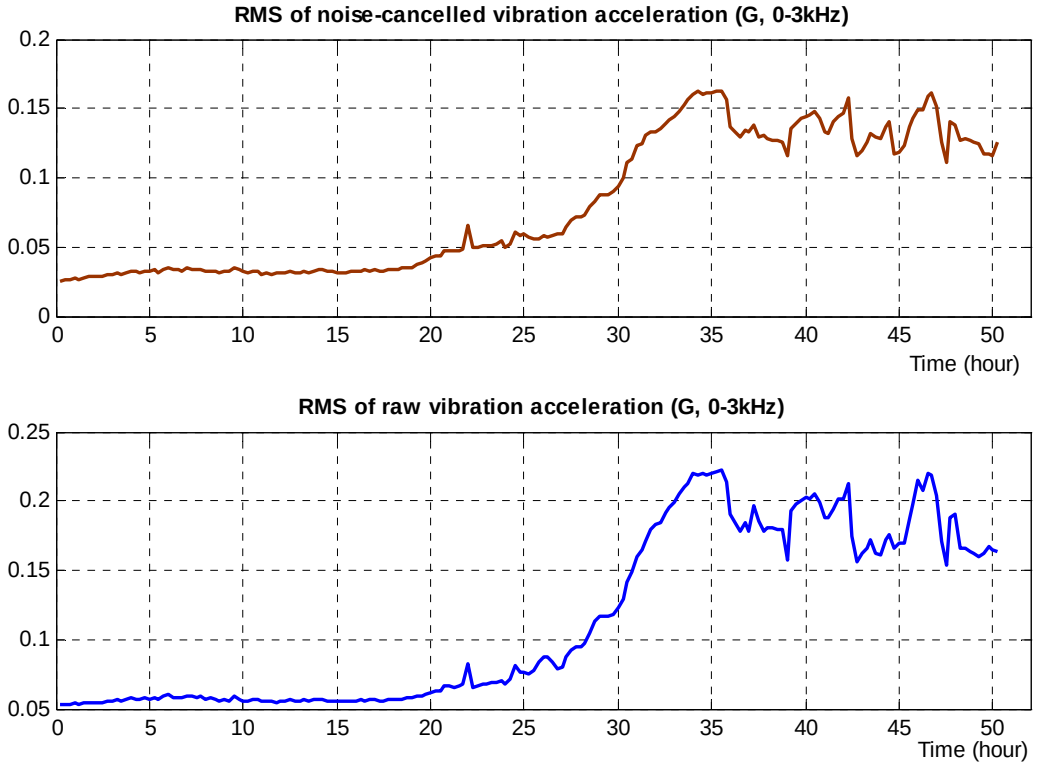


**Figure 5.16 Results attained by applying the noise cancellation algorithm to the machine vibration in experiment 2**

## 5.7 SUMMARY

In this chapter, the need of on-line generating bearing faults was discussed and the experimental setup used in this research to generate *in situ* bearing faults was described. By using the setup, several on-line experiments under constant-load conditions have been performed. The results attained by applying the proposed noise cancellation method to those experiments were presented. These results have confirmed the effectiveness of the proposed noise cancellation method in bearing fault detection. Further more, the performance of the proposed method was compared to the existing MSD method; theoretical analysis has shown that the noise cancellation method is preferable if the noise components and the fault-related components have similar frequencies. It was also shown that the noise-cancelled stator current is closely correlated to the vibration measurements. Finally, it is of special interest to note that the proposed method is applicable to processing vibration measurements and that bearing fault-related components are not affected by the noise cancellation process, as verified by experiment results.

# CHAPTER 6

# SCNC BEARING FAULT DETECTION UNDER VARIABLE-LOAD CONDITIONS

This chapter is broken into six sections as follows: Section 6.1, which discusses the effects of load on the stator current and the machine vibration regarding bearing fault detection; Section 6.2, proposing a bearing fault detection scheme considering the load effects; Section 6.3, which addresses the issue of current-based speed estimation – a key element of the detection scheme; Section 6.4, which presents the experiment results; and lastly Section 6.5 which summarizes the chapter.

## 6.1 BEARING FAULT DETECTION WITH VARYING LOAD

### 6.1.1 INTRODUCTION

Generally, it is more complicated to detect bearing faults under variable-load conditions than constant-load conditions. This is a result of the effects that variable loads may overwhelm bearing fault signatures, in addition to the dominant components in the signal.

When monitoring vibration with a varying load, vibration evaluation shall be made under all conditions at which the machine would be expected to operate for prolonged periods (ISO 10816). The maximum measured value under these conditions shall be considered representative of vibration severity. As a criterion for evaluating the severity of vibration, both the magnitude of observed broad-band vibration and changes in the magnitude need to

be considered [12-13].

For current monitoring with a variable load, the type of fault under detection plays an important role. For single-point defects, the detection usually relies on localizing the characteristic fault frequencies, which are determined by the supply frequency, the bearing dimensions, and the machine speed. A significant increase in the magnitude of the fault components indicates a bearing fault. Research studies have been published for single-point defects detection via stator current considering variable load conditions [5, 32]. For generalized roughness faults, the characteristic fault frequencies may not exist [9-11, 31], and therefore, little research in this area is available.

Given the current status of the research in the area, the purpose of this chapter is to extend the noise cancellation algorithm to the detection of generalized roughness faults under variable-load conditions.

### 6.1.2 Load Effects on Machine Vibration and Stator Current

Load has significant effects on the machine vibration and the stator current. Variable load can nonlinearly alter the level of machine vibration and distort the machine vibration monitoring results; thus caution should be taken when this occurs [38, 58]. The experiments performed in this research show that the vibration at a lower frequency range (i.e. below 1 kHz) is more sensitive to load changes than that at higher frequency range or the entire frequency range. Nevertheless, machine vibration is still effective for bearing fault detection for both constant-load and variable-load conditions.

In comparison, load effects on the stator current are more drastic in the sense of its influence on the bearing fault detection. This is due to the dominant components in stator

currents that are directly determined by the triplet: the load, the supply, and the machine itself. Even a slight change of the load may overwhelm the bearing fault signatures in the stator current. The load effects on the stator current regarding bearing fault detection are listed as follows:

1) When load changes, the sensitivity of the stator current to a bearing fault will change. For example, as the load increases, the magnitude of the dominant components may increase accordingly, as well as the level of the noise floor in the sampled signal, while the bearing fault signatures may remain essentially same. Consequently, the bearing fault signatures are likely to be pushed closer to the noise floor at a higher load level. In the noise-signal view, variable load essentially changes the signal-to-noise ratio (SNR). This is especially problematic because even at no-load the SNR is already low, i.e., the bearing fault signatures are already close to the noise floor in the sampled signal even at no-load.

2) When load changes, the load-related frequencies in the stator current will change. For example, the frequencies of the eccentricity harmonics, the slot harmonics and the broken bar harmonics will change as the load changes. This requires the noise cancellation algorithm to be able to change its frequency response to suppress those noise components accordingly.

3) Load changes can introduce transient processes, the pattern of which is usually unpredictable and random in nature. Therefore, when the pattern of the processes is similar to that of a bearing failure, it can be misinterpreted by a fault detection algorithm as the presence of a bearing fault.

The load effects on the stator current are illustrated in Figure 6.1, where the power spectra of the stator current at two load levels are plotted. The data for the plots were collected

from the same machine (4-pole, 20 hp) with healthy bearings at same conditions except the load level. As shown in the figure, the magnitude of the dominant components and the position of the noise floor changed significantly following the load change. The eccentricity-related components have also shifted in frequency.

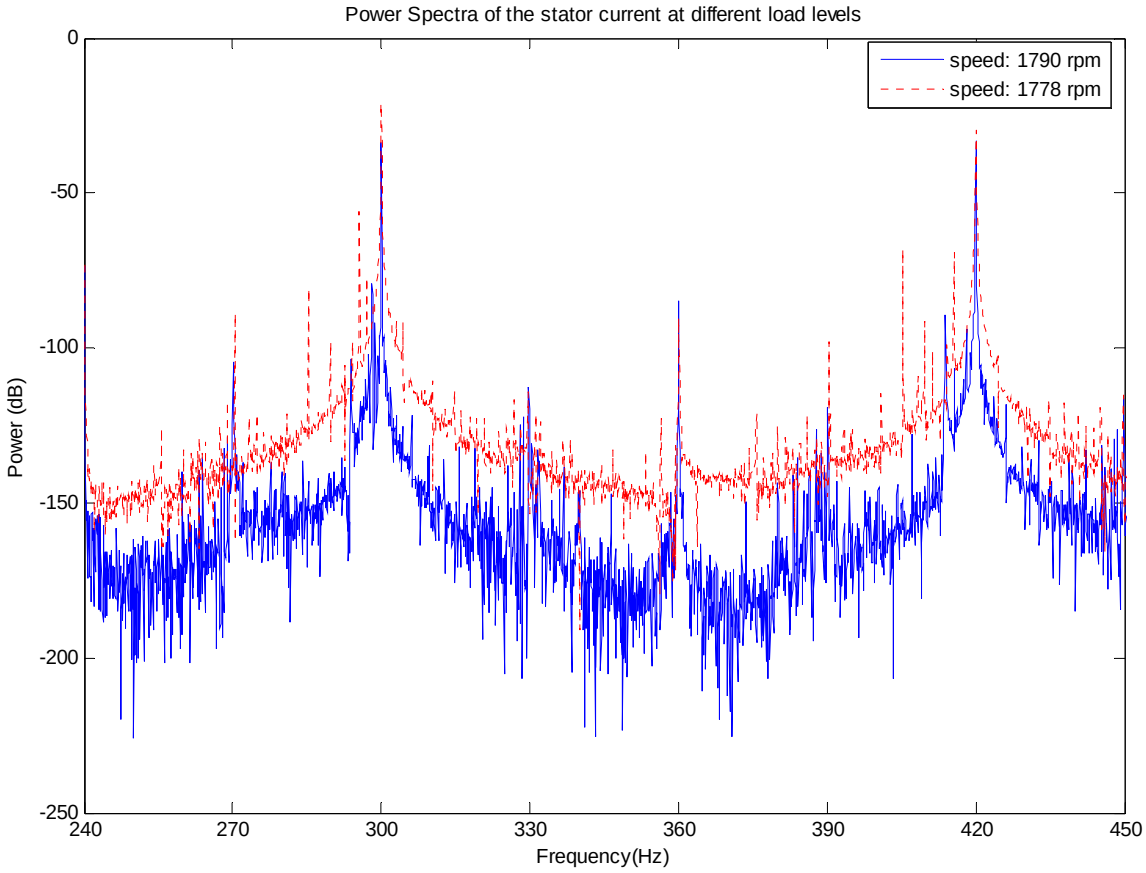


**Figure 6.1 Illustration of load effects on the power spectrum of the stator current.**

## 6.2 SCNC Bearing Fault Detection under Variable-Load Conditions

At different load conditions, the sensitivity of the stator current to bearing faults varies, as discussed in the previous section. Therefore, the RMS of the noise-cancelled stator current should be tracked over a same load level to provide meaningful results. In practice, the RMS of the noise-cancelled stator current should be compared to the baseline that is

obtained under the same load level, and this should be done for each load level under which the machine would be expected to operate for prolonged periods. Sometime, it is also appropriate to apply the noise cancellation algorithm when the machine reaches a steady state following a load change, to avoid the interference from the transient process associated with the load change.

To address the above issues, a bearing fault detection scheme for variable load conditions is introduced. This scheme is shown in Figure 6.2. The implementation procedure is as follows:

1) Obtain the speed (load level) from real time stator current data.

   A speed estimation algorithm may be involved to obtain the speed and thus the load level. For true non-intrusive fault diagnosis, the algorithm should be current-based – discussed in the next section.

2) Determine whether a load change has occurred.

   If a load change has been detected, then further determine whether the current load level is a new level (i.e. unseen before). If the current load level is new, a set of parameters of the noise canceller (i.e., the coefficients of the Wiener filter) should be computed after the machine reaches a steady state following the load change. Save those parameters, tagged with the load level, in a database. If the current load level is not new, then the parameters of the noise canceller are retrieved from the database.

3) Apply the noise cancellation algorithm to the sampled stator current data.

   With the parameters obtained in Step 2, apply the noise cancellation algorithm to the sampled stator current data if the machine is at a steady state. Calculate the

RMS of the noise-canceled stator current. If the current load level is new as determined in Step 2, save the RMS value as the baseline for this new load level. Therefore, each load level has a baseline value.

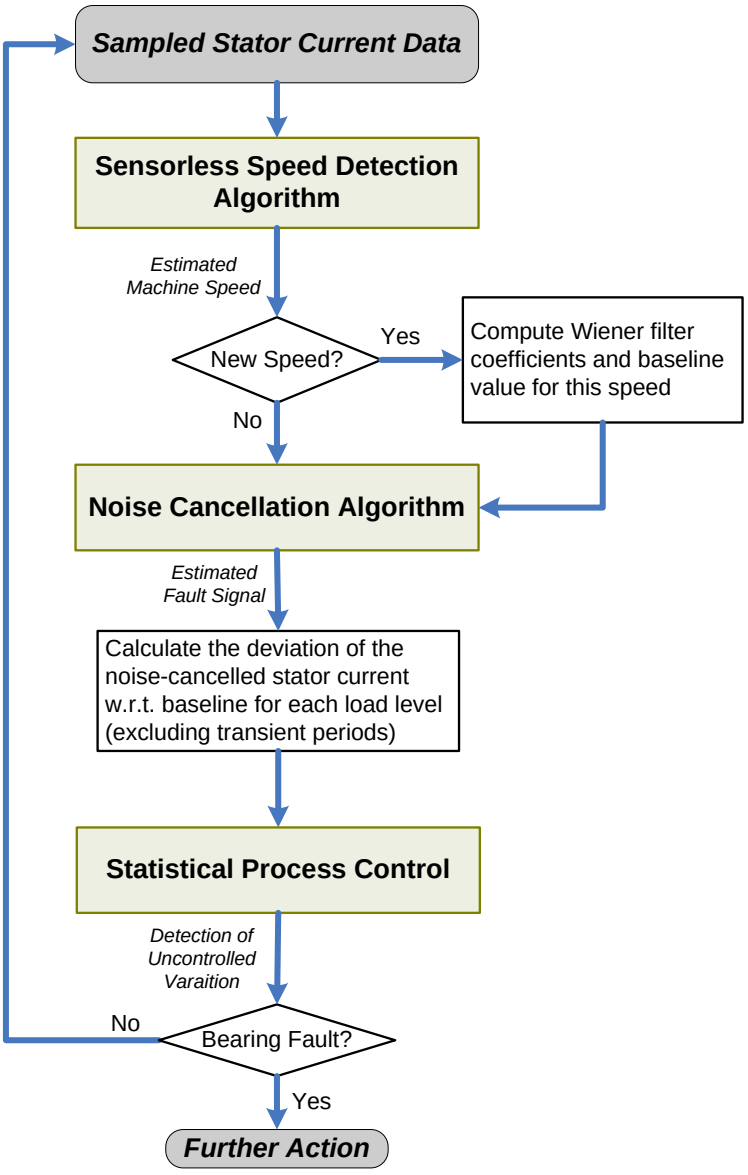


**Figure 6.2 Schematic diagram of bearing fault detection via stator current noise cancellation under variable load conditions.**

4) Make decisions about the bearing health from the noise cancellation results.

   For each load level, plot the deviation of the RMS of the noise-cancelled stator current from the baseline value along the time. A final decision about the bearing health condition should be made by considering the results obtained at all load levels under which the machine has been operating for prolonged periods. Usually a threshold is computed and drawn on these plots. The RMS value frequently falling outside the threshold indicates a deteriorated bearing condition. The determination of the threshold is achieved by using statistical methods such as the statistical process control, which is addressed in the next chapter.

For simplicity, in the experiments performed in this research, the induction machine with the speed varying within the extent of 5 rpm is regarded as operating under a same load level. For example, a machine is treated as running under the same load level for a speed of 1790 rpm, for a speed of 1795 rpm and for any speed in [1790, 1795] rpm. The range the speed is allowed to vary under a "same" load level can be different in practice. It is also possible to apply the procedure in [58] to divide the entire operation range into different load levels and the noise cancellation algorithm would be applied to those load levels separately.

## 6.3 CURRENT-BASED SPEED ESTIMATION FOR BEARING FAULT DETECTION

### 6.3.1 INTRODUCTION

As discussed in the previous section, speed estimation is required to differentiate load levels for current-based bearing fault detection. Usually, for bearing fault detection purposes, the fundamental component in the stator current at 60 Hz is notched by an analog filter. Advanced current-based *speed estimation* seems appropriate to estimate the load

level since the torque or the power can't be estimated from the notched stator current. In the detection of single-point-defect faults, speed information is also required to calculate those characteristic fault frequencies. In this research, current-based speed estimation is employed as a non-intrusive means to obtain load level information of induction machines.

The basic principle of current-based speed estimation is to calculate the machine speed from the speed-related frequencies in the stator current [59-60]. The speed-related frequencies include the eccentricity frequencies and the slot harmonic frequencies, as described by the following equation

$$f_{seh} = f_1\left[(kR + n_d)\frac{(1-s)}{P} + n_w\right]. \tag{6.1}$$

where $f_{seh}$ is the speed-related frequency, $f_1$ is the fundamental supply frequency, $k$ is an integer, $P$ is the number of pole pairs, $R$ is the number of rotor slots, $s$ is the slip, $n_d$ is the order of the rotating eccentricity (For a static eccentricity, $n_d = 0$; for a dynamic eccentricity, $n_d = 1$), $n_w$ is the order of the stator magneto motive force (MMF) harmonics.

In the above equation, when $k = 0$, $n_w = 1$, $n_d = \pm 1$, it follows

$$f_{seh} = f_1(1 \pm \frac{1-s}{P}) \tag{6.2}$$

This is known as the eccentricity frequency equation. The frequencies obtained from Equation (6.1) when $k \neq 0$ are known as the slot harmonic frequencies. The machine speed, denoted by $\omega_r$, is related to the slip by

$$\omega_r = \frac{60 f_1 (1-s)}{P}. \tag{6.3}$$

Therefore, the speed can be calculated from above equations, once the eccentricity

frequencies or the slot harmonic frequencies (along with the rotor number $R$) are known.

Since the slip, $s$, is usually close to zero under normal conditions, the eccentricity frequencies are low frequencies and often can be clearly identified on the power spectrum of the stator current, provided a high frequency resolution exists. Comparatively, the slot harmonics have high frequencies and usually are undistinguishable from noise. The accuracy of speed estimation via the slot harmonic frequencies can be high, which is $\frac{R}{P}$ times that of the estimation of slot harmonics.

For bearing fault detection, if time is not a critical factor and long data records are available, the speed estimation via the eccentricity frequencies is recommended due to its ease of use. However, in some applications, such as those in a wireless network environment, short data records are desired due to limited network throughput and speed should be estimated by using slot harmonics for a satisfactory accuracy.

### 6.3.2 SPEED ESTIMATION USING ECCENTRICITY HARMONICS

To effectively search the eccentricity harmonics in the stator current, the search region can be significantly narrowed down by using the proper range of the slip, $0 \le s \le 0.05$, which holds under normal conditions. For example, for a 4-pole machine ($P = 2$), it follows from Equation (6.2) that the search region for the lower and higher eccentricity harmonics can be narrowed down by using $0 \le s \le 0.05$ as

$$30 \le f_{eh1} \le 31.5,\ 88.5 \le f_{eh2} \le 90$$

rather than the region [30, 90] Hz by assuming $0 \le s \le 1$. This is shown in Figures 6.3 – 6.4.

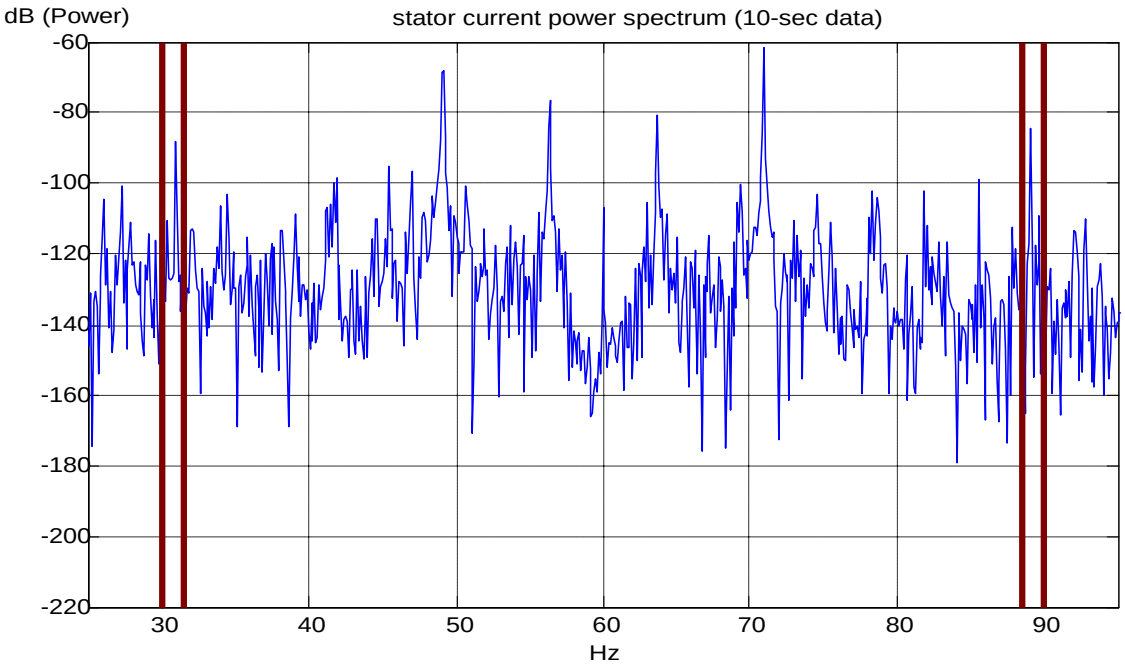


**Figure 6.3 The power spectrum of the stator current (notched at 60 Hz) from 10-second data**

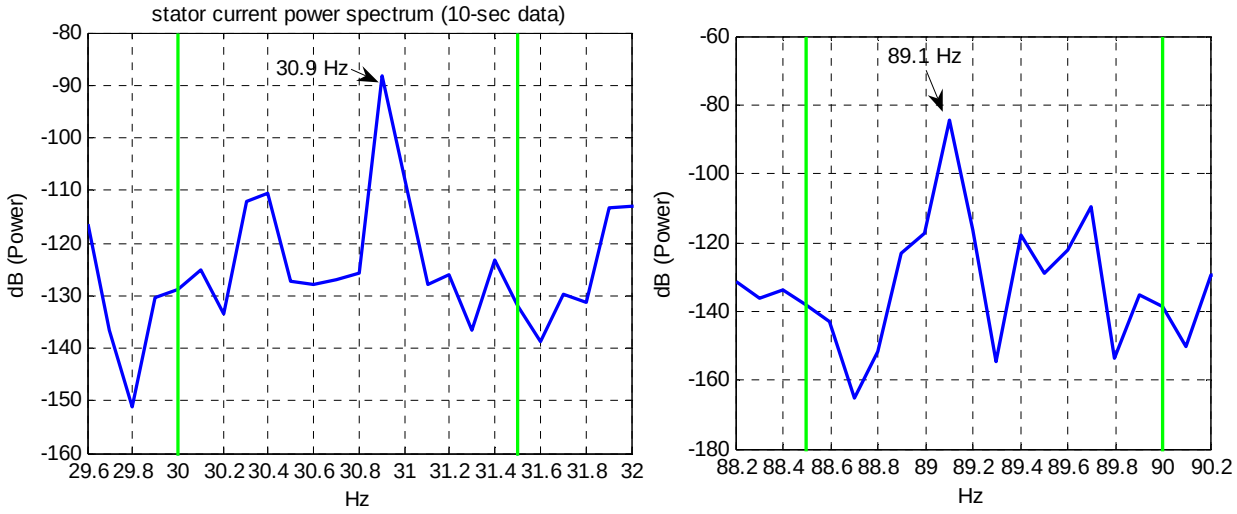


**Figure 6.4 the location of the lower eccentricity harmonic (left) and the higher eccentricity harmonic (right) on the frequency axis of the stator current for 10-second data**

The accuracy in the speed estimate shown in Figure 6.4 is determined by the frequency resolution, which is in turn determined by the length of the time window associated with

the sampled data. Specifically, the frequency resolution is given by [37]

$$\Delta f = \frac{1}{T_{samp}} \tag{6.4}$$

where $T_{samp}$ is the time window associated with the sampled data and $\Delta f$ is the frequency resolution. For example, for 10-second samples, the frequency resolution is 0.1 Hz; for a 4-pole motor, the error is less than 6 rpm, which can be calculated from Equations 6.2-6.3. As a test example, the machine speed obtained from the eccentricity harmonics shown in Figure 6.4 is 1746 rpm; this value compares to the reading of 1751 rpm from a tachometer amounted on the motor.

Shorter data records yield lower accuracy. For the same machine, the maximum error from a 2-second window of data for is as large as 30 rpm, due to the poor frequency resolution as shown in Figure 6.5. Such a large error is not acceptable for distinguishing load levels. In a scenario as such, sometimes the *estimation accuracy* can be improved by *zero padding*, as shown in Figure 6.6. As a test example, the speed is estimated as 1740 rpm according to Figure 6.5, and 1752 rpm according to Figure 6.6, compared to the tachometer reading 1751 rpm. It should be pointed out that the inherent frequency resolution thus the maximum error in the speed estimation can not be improved by the zero padding. Instead, the accuracy in the speed estimation can be improved by enlarging the sampling time window or by using slot harmonics.

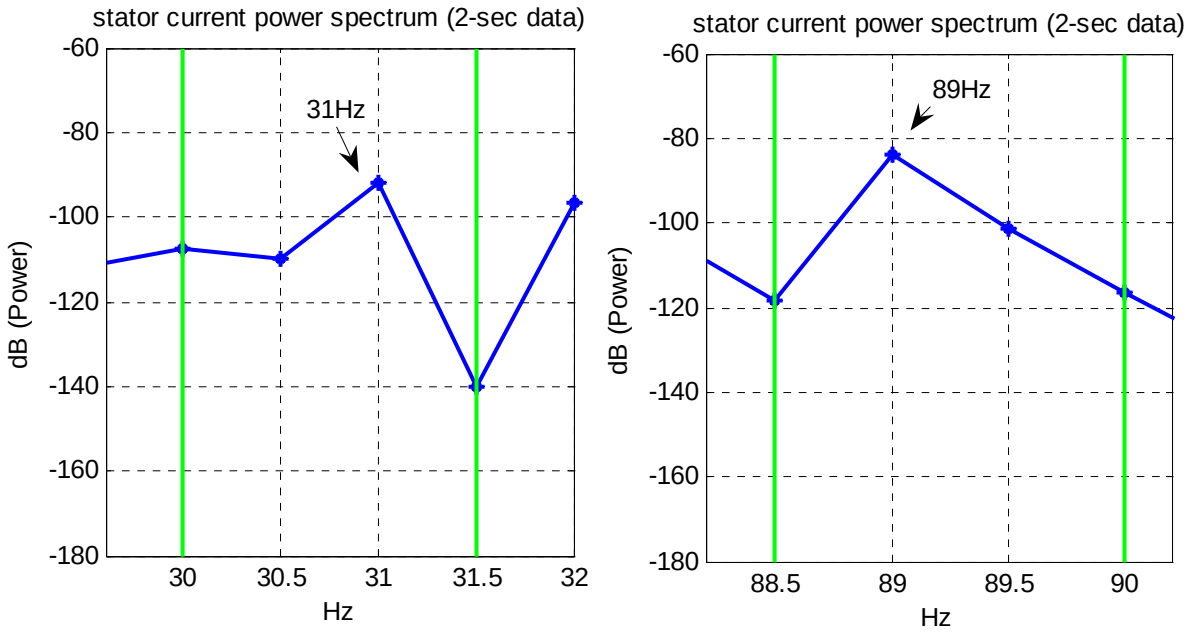


**Figure 6.5 Illustration of the frequency estimation of the lower eccentricity harmonic (left) and the higher eccentricity harmonic (right) for 2-second data**

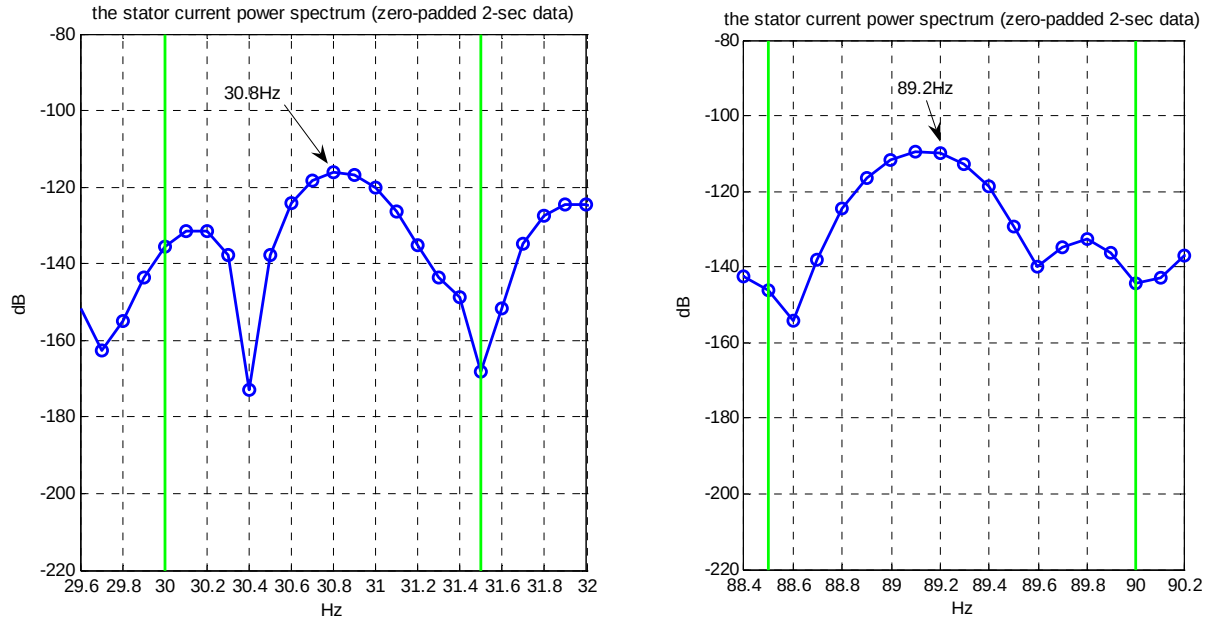


**Figure 6.6 Illustration of the frequency estimation of the lower eccentricity harmonic (left) and the higher eccentricity harmonic (right) for zero-padded 2-second data**

### 6.3.3 SPEED ESTIMATION USING SLOT HARMONICS

#### 6.3.3.1 Determining Rotor Number

As seen from Equation (6.1), for the speed estimation using slot harmonics, the slot number $R$ is required which is usually not shown on the name plate. However, by the following procedure, known as the initialization process in [59], it is possible and very often successful to determine the slot number $R$ solely from stator current measurements.

First substitute $n_w = \pm 1$, $n_d = 0$, $k = 1$ in Equation (6.1) to obtain the principle slot harmonic frequency as the function of the slot number *R*, as given by

$$f_{seh} = f_1 \left[ \frac{1-s}{P} R \pm 1 \right]. \tag{6.5}$$

where the slip $s$ is obtained from the eccentricity harmonics as shown in the previous subsection. The only unknown parameter in Equation (6.5) is $R$. Further more, it is known from the machine design theory that the possible values of R are $(14-26)\cdot P$ for most small- and medium-size motors [59]. Therefore, the second step is to find the best match between the possible values of *R* and the prominent peaks (not including MMF harmonics) on the power spectrum of the stator current and then determine the value of $R$. This is illustrated in Figure 6.7, where the data was collected from a 20-hp induction motor. It can be seen clearly that the prominent slot harmonics are located at 1103.45 Hz and 1223.45 Hz; with the slip *s* of 0.03 determined from the eccentricity harmonics, this leads to a rotor bar number of 40. (After disassembled the motor, it was found this is correct.)

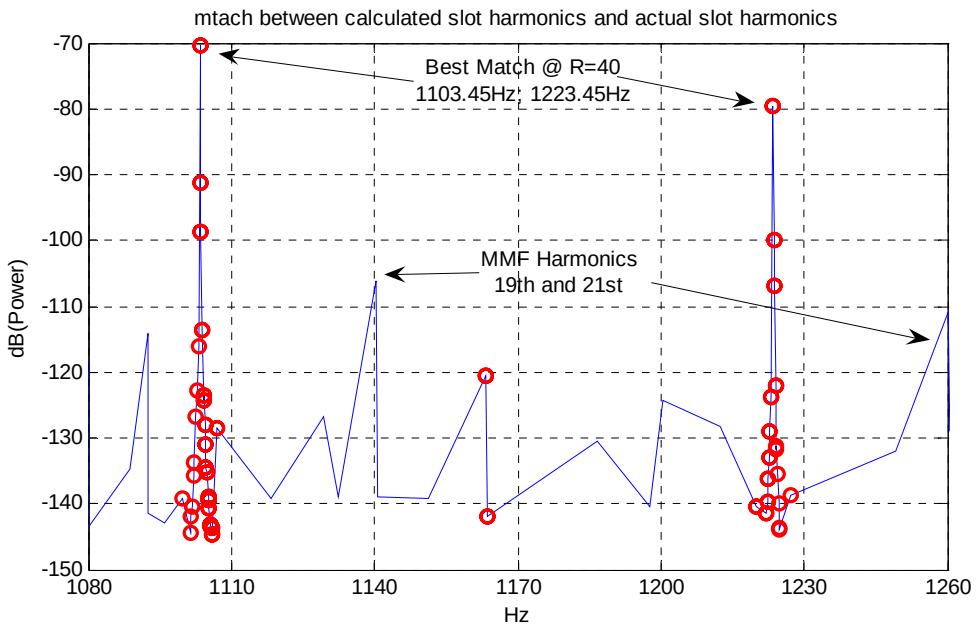


**Figure 6.7 The match between the calculated slot harmonics and the prominent slot harmonics on the frequency axis**

### 6.3.3.2 Estimating Speed from Short Data Records

Once the slot number $R$ is known, the speed can be obtained by using slot harmonics with short data records while meeting an acceptable accuracy. The equation to calculate the speed from slot harmonic frequencies is given by

$$f_{seh} = f_1\left[(kR + n_d)\frac{(1-s)}{P} + n_w\right] . \tag{6.6}$$

Since slot harmonics are small in magnitude, it is desired to reinforce these harmonics via aliasing on the frequency axis [59]. This is possible since they are separated exactly by $2 \cdot f_1$ on the frequency axis due to the multiple-value odd $n_w$ in the above equation [59]. To achieve this, band-pass filtering, down sampling, spectrum estimation, and frequency conversion are required.

Band-pass filtering is used to suppress low frequencies since the slot harmonics are at high frequency. The pass band of the band-pass filter should cover a proper region where slot harmonics are possibly located. In practice, by assuming $k=1$, $n_d=0$, $0 \le s \le 0.05$, and $n_w = \pm 1 \sim 7$, the pass band is set as

$$\left( f_1 \left[ R\frac{1-0.05}{P} - 7 \right], f_1 \left[ R\frac{1-0}{P} + 7 \right] \right). \tag{6.8}$$

To make the slot harmonics alias together and also the MMF harmonics alias together, the new sampling frequency should be $2 \cdot f_1$. If the raw data is sampled at another sampling frequency, interpolation and down-sampling (decimation) are required. For example, if the original sampling frequency is 4 kHz, it can be (digitally) resampled at $60 f_1$, and then decimated at $2 \cdot f_1$. The interpolation provides sufficient amount of data for down-sampling by an integer factor, for example, from $60 f_1$ to $2 \cdot f_1$. The interpolation is not necessary if the original sampling frequency is already integer times of $2 \cdot f_1$.

After the above operations, the slot harmonic frequency is salient on the normalized aliasing frequency axis due to the overlapping effect and the speed is calculated from this frequency. One way to calculate the speed that is possibly easier than the original method in [59] is to use the shift of the slot harmonic frequency on the aliased frequency axis, as derived below.

$$\Delta \frac{f_{seh}}{f_1} = (kR + n_d)\frac{\Delta s}{P} \tag{6.9}$$

$$\Delta s = \frac{P}{R}\Delta f_{sh,norm} \text{ (assume } k=1, n_d=0) \tag{6.10}$$

$$\Delta \omega_{rpm} = \Delta s \cdot \frac{60 \cdot f_1}{P} = \frac{60 \cdot f_1}{R} \cdot \Delta f_{sh,norm} \tag{6.11}$$

$$\omega_r = \omega_{base} + \Delta \omega_{rpm} \tag{6.12}$$

where $\Delta f_{sh,norm}$ is the shift of the slot harmonic frequency on the aliased normalized-frequency axis, $\omega_r$ is the actual speed, and $\omega_{base}$ is the baseline speed obtained from the eccentricity harmonics.

In the above derivation, the shift of the slot harmonic frequency on the normalized aliasing frequency axis was assumed to be less than 1, which is true in most cases. In some cases, the shift, $\Delta\frac{f_{seh}}{f_1}$, can be larger than 1, for example, when $R\frac{\Delta s}{P}>1$ (e.g., $P=1,\Delta s=0.05,R>20$). Then the conversion from the aliased frequency to the actual frequency is not unique. This problem can be solved by adjusting the sampling frequency of the aliased signal to $4\cdot f_1$ in addition to that of $2\cdot f_1$, which would limit the shift not crossing the boundaries of the normalized frequency axis, and the speed is obtained by considering the results under the both sampling frequencies. Another solution to this problem is to apply the technique described in [59], which uses an estimate of the eccentricity frequency or an indication of the load to help to find the precise location of the slot harmonic frequency on the actual frequency axis.

To calculate the shift of the aliased normalized-frequency, $\Delta f_{sh,norm}$, different spectral estimation algorithms can be used. Here the MUSIC (MUltiple SIgnal Classifier) algorithm is applied for an example. The aliased spectra estimated by the MUSIC algorithm for a real test are given in Figure 6.8. The solid line is from baseline data (of 10-second time window), collected at 50% load level, and the corresponding speed is 1751 rpm. The dash line is from test data of 10 cycles of a 60Hz signal (of 0.167-second time window). The shift in the slot harmonic frequency can be clearly seen on the aliased spectra in the picture, based on which the new speed was calculated as 1783 rpm, compared to the reading of a tachometer of 1784 rpm, which indicates a 20% load level.

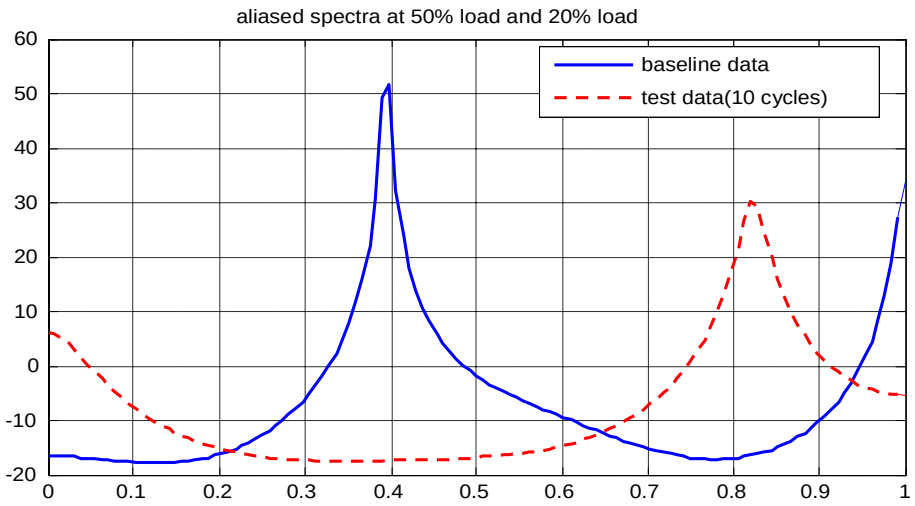


**Figure 6.8 The shift of the saliency slot harmonic frequency on the aliased normalized-frequency axis is used to obtain the machine speed**

## 6.4 VARIABLE LOAD EXPERIMENTAL RESULTS

Both constant and variable-load tests have been performed to validate the proposed algorithm. The constant-load test results, as well as the details regarding the experimental setup and the data acquisition instrument, are presented in Chapter 5. The results of the variable-load tests are presented in this section.

For all variable-load tests, a dynamometer (a DC generator connected to the 20-hp induction machine) serves as the load. By switching the resistors on the resistor banks that are connected to the dynamometer on and off, the output power of the dynamometer, thus the load of the induction machine, can be adjusted to a desired level. For each variable-load test, after a new bearing is refilled with a reduced amount of grease, it is installed and the experiment starts. After a few hours of operation, the machine reaches a thermal steady state and the data acquisition process starts. During each test, the load is adjusted to

different levels, while the bearing fault develops. At the same time, the proposed bearing condition monitoring scheme is applied. Specifically, the sensorless speed algorithm is applied to estimate the load level and the noise cancellation algorithm is applied to obtain the bearing fault signature. A final decision on the condition of the bearing is made by considering results obtained at all load levels at which the machine has been operated for prolonged periods.

### 6.4.1 VARIABLE LOAD EXPERIMENT 1

The results of this experiment are shown in Figures 6.9-6.11. Figure 6.9 shows that the RMS of the machine vibration, both of the entire range and of the 0 - 1 kHz range, increases significantly as the bearing health condition degrades due to the added shaft current. At the $24^{th}$ hour, the load is increased to a new level, resulting in a speed change from 1790 rpm to 1778 rpm. The load change has minimal effects on the magnitude of the vibration of the entire range (theoretically from 0 Hz – infinity). In contrast, it has noticeable effects on the magnitude of the vibration from 0 – 1 kHz and causes a big drop as shown in the figure (middle plot). During the remainder of the experiment, because of the continuous deterioration of the bearing condition, the vibration over the 0 – 1 kHz frequency range, as well as that of the entire range, increases substantially. Overall, it seems that the vibration of the entire frequency range serves as the reference of the bearing condition better than that of the range 0 – 1 kHz.

Since the machine experiences two load levels, the noise cancellation algorithm should be applied to the two load levels separately. Following the load change at the $24^{th}$ hour, the bearing detection algorithm recalculates the Wiener filter coefficients and the baseline for the new load level. Figure 6.10 and Figure 6.11 show the results for the two load levels.

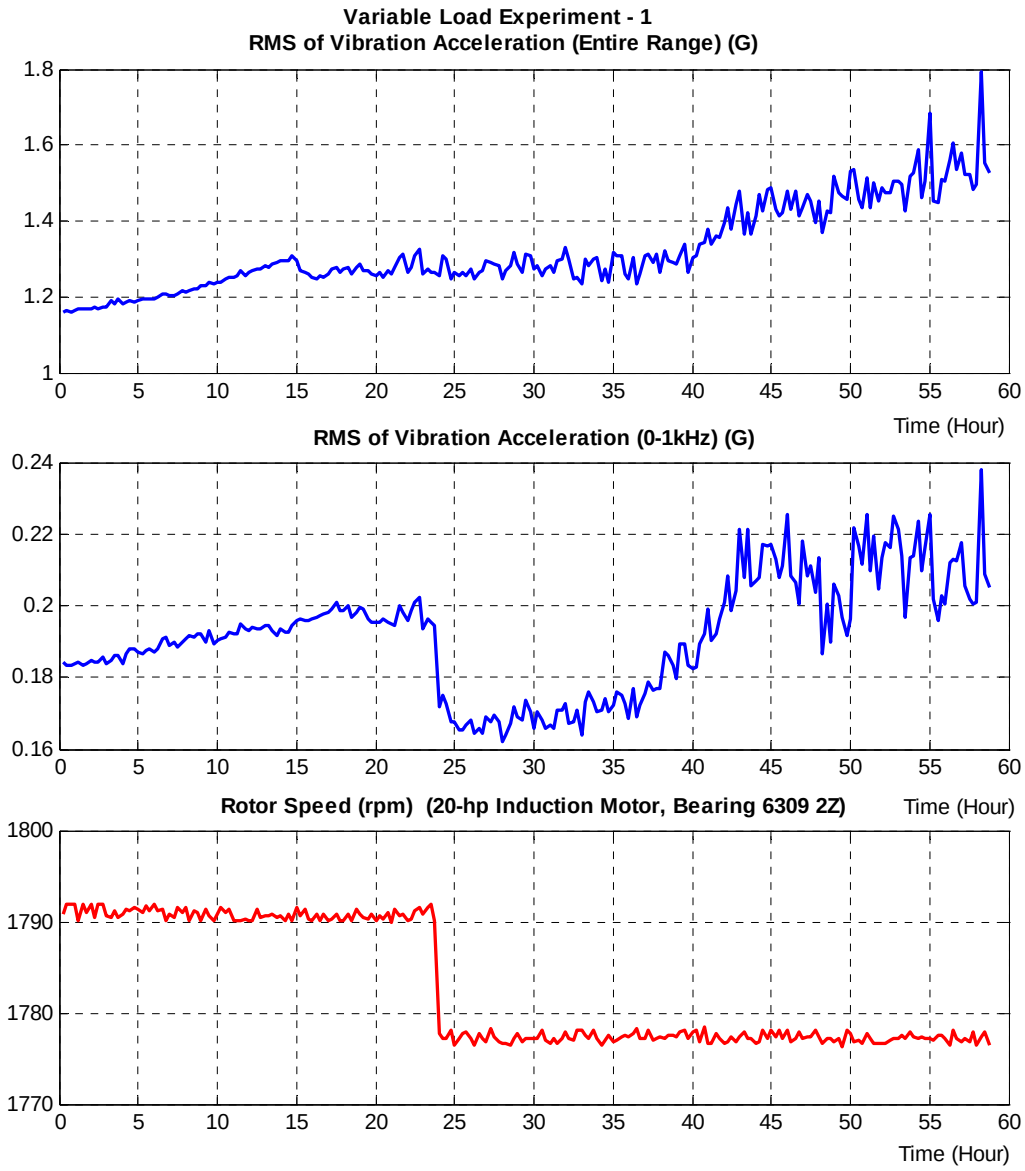


**Figure 6.9 Variable load experiment -1: the RMS of vibration increases significantly indicating a deteriorating bearing condition during the 2-speed test.**

From Figure 6.10, the noise-cancelled stator current increases substantially during the first load level section due to the degraded bearing condition and is closely correlated to the machine vibration.

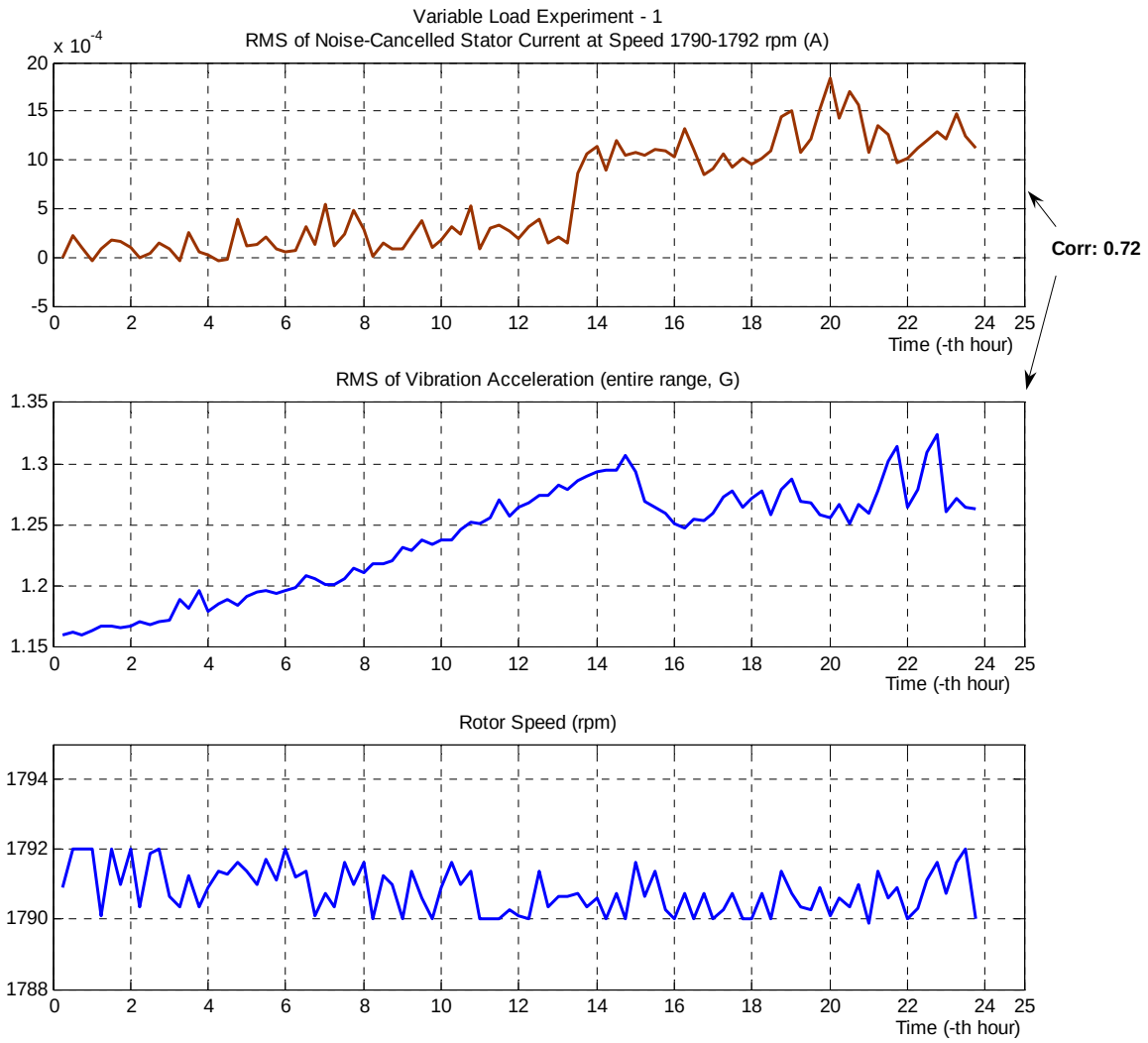


**Figure 6.10 The noise-cancelled stator current and the vibration increase substantially during the first speed section (1790-1792 rpm).**

Figure 6.11 shows the results for the second load level. From this figure, it can be seen that there is an increase in both the noise-cancelled stator current and the vibration at this load level.

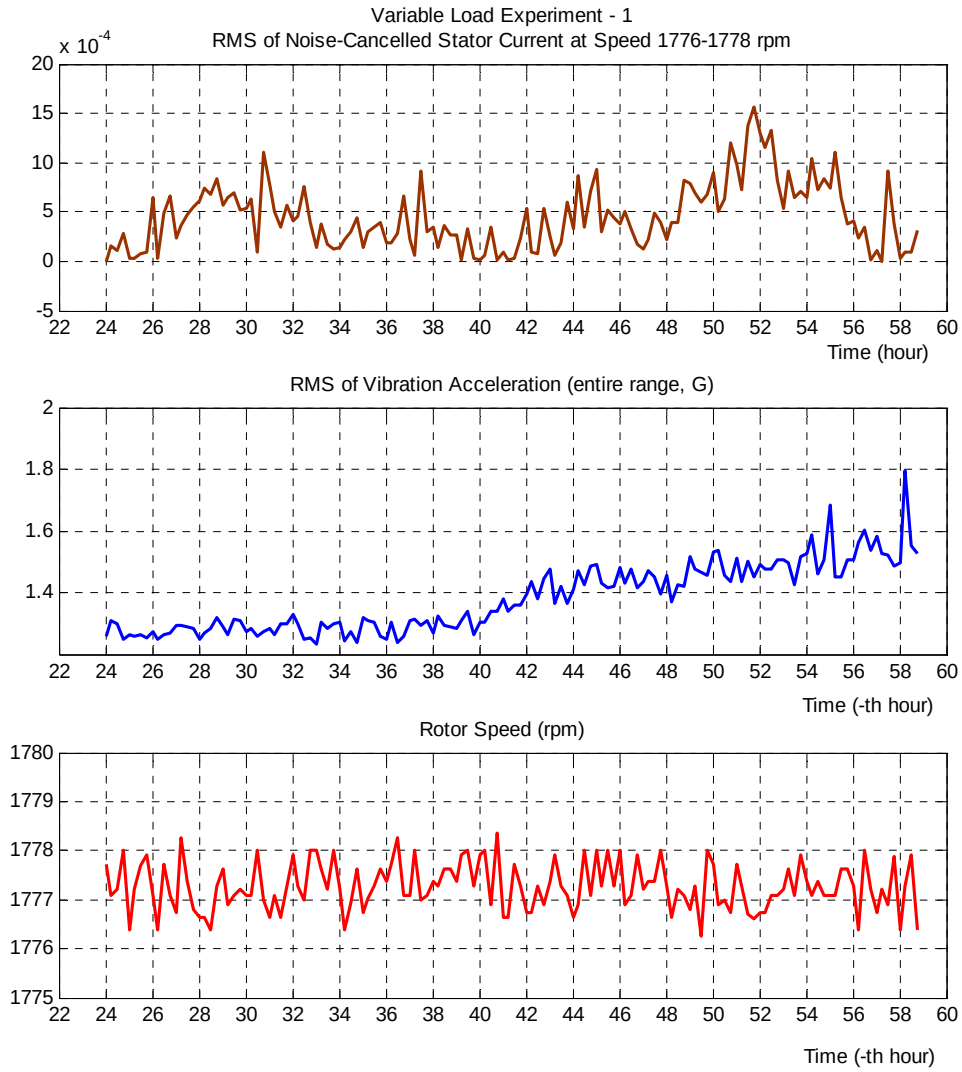


**Figure 6.11 There is increase in both the noise-cancelled stator current and the machine vibration during the second speed section (1776-1778 rpm).**

### 6.4.2 VARIABLE LOAD EXPERIMENT 2

The results of this experiment are shown in Figures 6.12 – 6.15. As shown in the top plot of Figure 6.12, three different load levels are involved in this experiment. The first load level is at the speed around 1790 rpm; the operation time is from the beginning to the 12$^{th}$ hour

and from the 36th hour to the 36.5th hour near the end of the experiment. The second load level is at the speed around 1750 rpm; the operation time is from the 12th hour to the 25th hour and from the 36.5th hour to at the end (i.e. the 37th hour). The third load level is at the speed around 1777 rpm; the operation time is from the 25th hour to the 36th hour. The bottom plot shows that the machine vibration of the entire frequency range increases significantly as the fault develops.

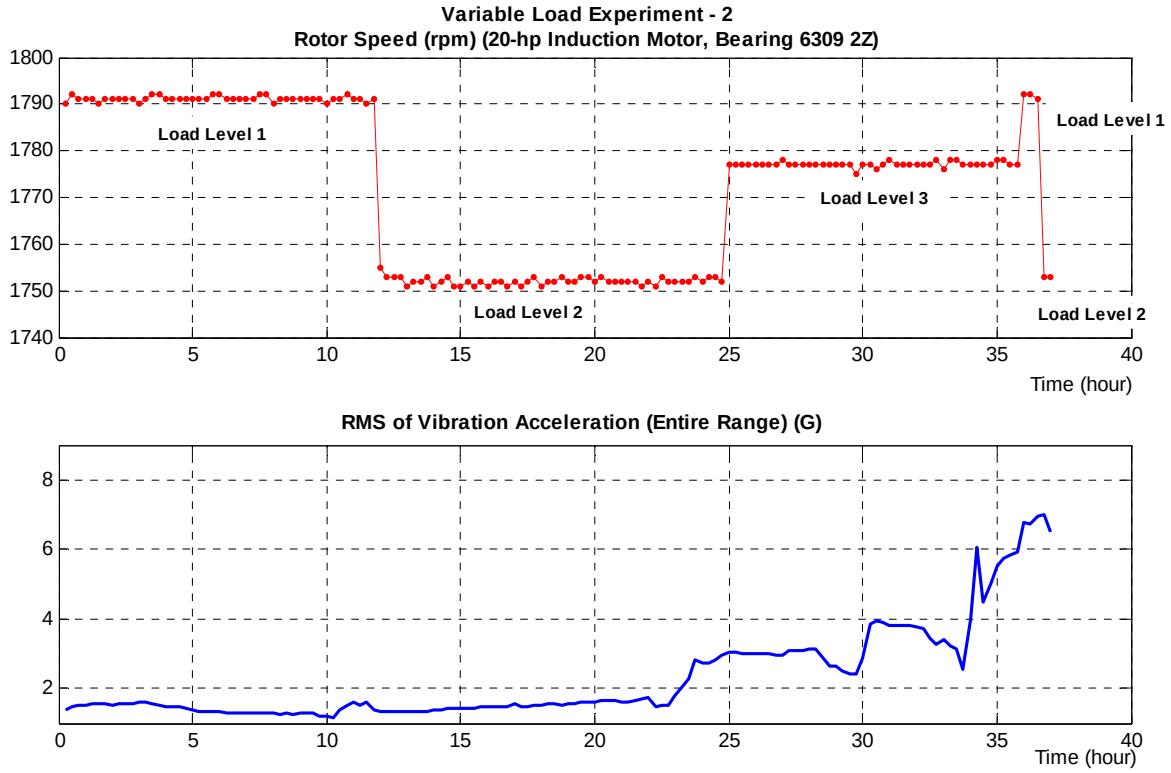


**Figure 6.12 Variable load experiment -2: the RMS of vibration increases significantly indicating a deteriorating bearing condition during the 3-speed test**

The results of the noise-cancelled stator current under the first load level are shown in the top plot in Figure 6.13. It can be seen that from the beginning to the 12th hour, the RMS of the noise-cancelled stator current remains at a low level; during the half hour following the 36th hour, the RMS of the noise-cancelled stator current is much higher due to the degraded bearing health. Again, the noise-cancelled stator current is closely correlated to the machine vibration.

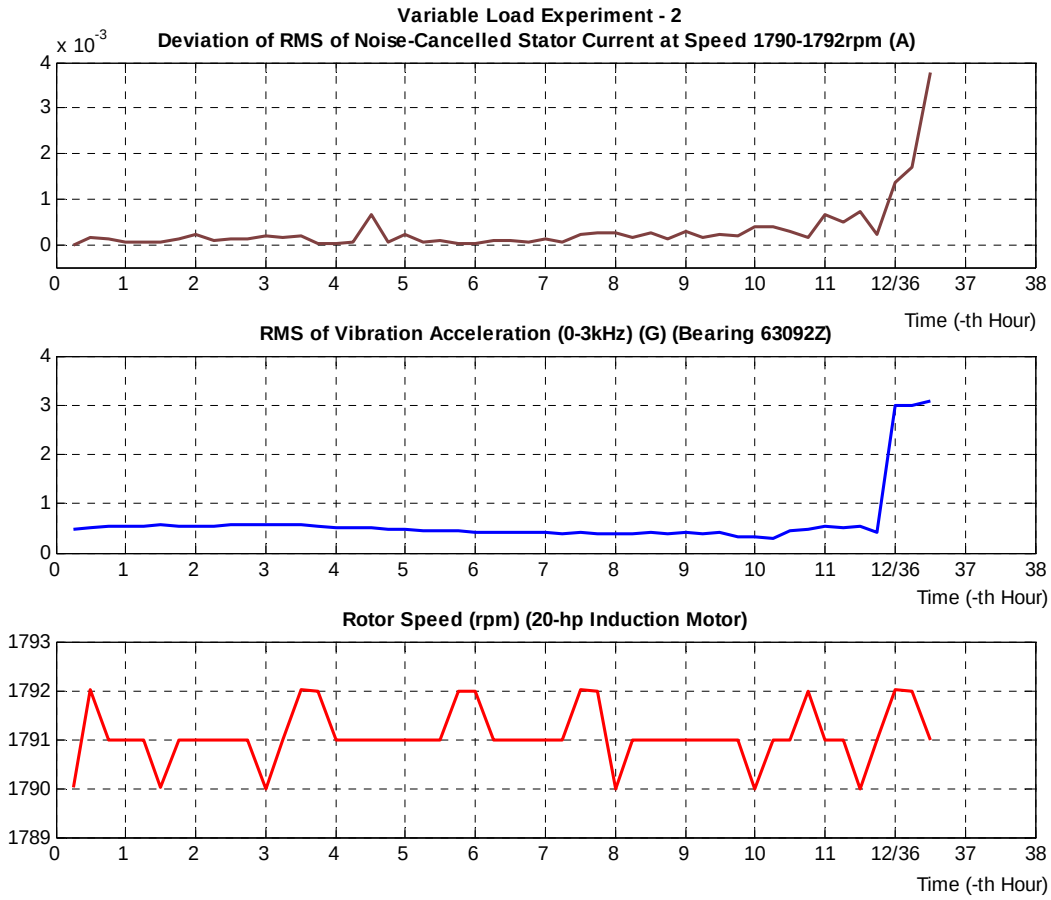


**Figure 6.13 RMS value of the noise-cancelled stator current and the machine vibration during the first speed section (1790-1792 rpm)**

The results for the second load level are shown in Figure 6.14. Only near the end of the experiment, the noise-cancelled stator current and the vibration display a significant increase due to the deteriorated bearing condition; and from the 12$^{th}$ hour to 35$^{th}$ hour, there is no substantial change in the both measurements.

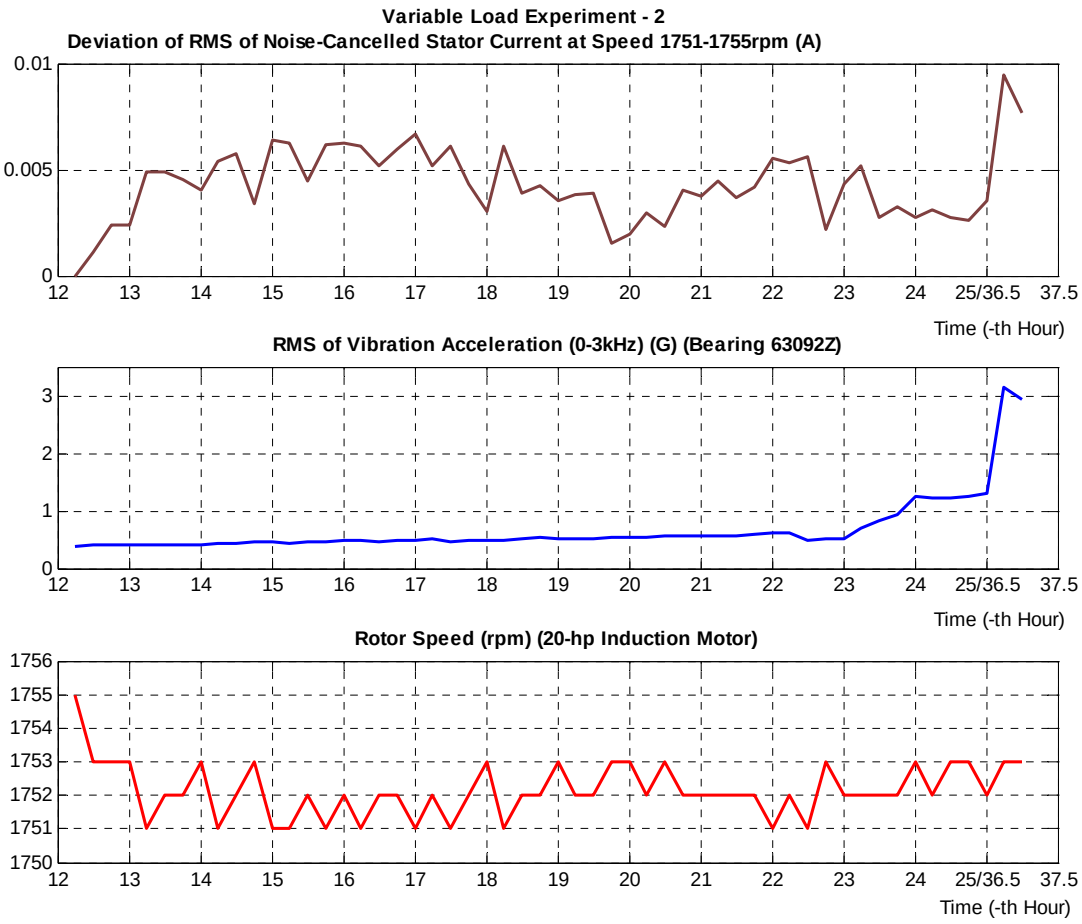


**Figure 6.14 RMS value of the noise-cancelled stator current and the machine vibration during the second speed section (1751-1755 rpm).**

The results of the third load level are shown in the top plot in Figure 6.15. From this figure, it can clearly be seen that both the vibration and the noise-cancelled stator current increase substantially from the 28$^{th}$ hour to the 36$^{th}$ hour, which indicates that the bearing fault is developing rapidly during this period. The correlation between the noise-cancelled stator current and the vibration is about 0.72 (refer to Table 5.1 on Page 96).

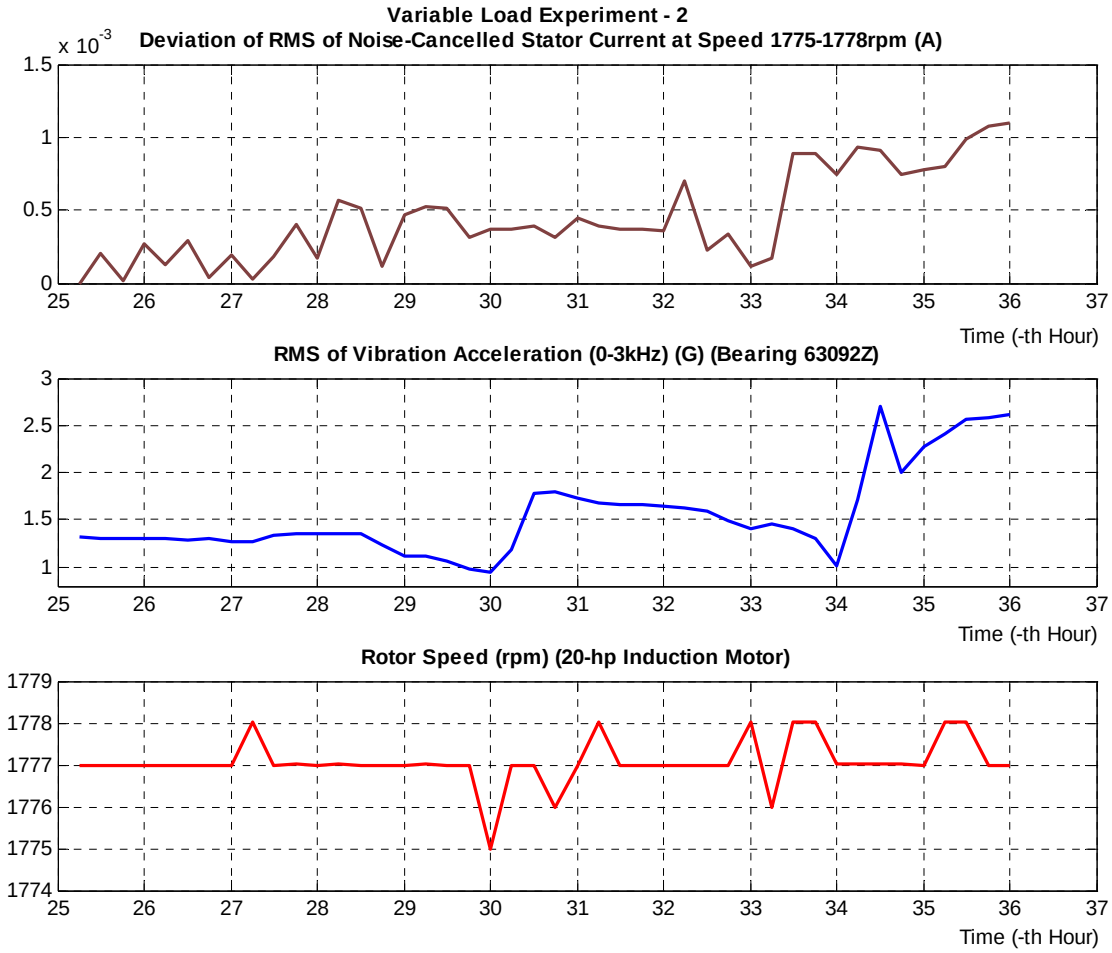


**Figure 6.15 The RMS of the noise-cancelled stator current increases significantly for the third speed section (1775-1778 rpm)**

## 6.5 SUMMARY

In this chapter, the stator current noise cancellation method has been extended to variable load conditions. First discussed were the load effects on the stator current and thus on the performance of current-based bearing fault detection. Secondly, to minimize the negative effects of load changes, a strategy was introduced for variable-load applications – using a current-based speed estimation algorithm to differentiate load levels. The speed estimation

algorithm by using eccentricity and slot harmonics was then illustrated with results from real tests. This speed estimation algorithm was originally from Reference [59] but was modified for bearing fault detection purposes in this research. Finally, the current-based bearing fault detection strategy was applied to the on-line variable load experiments. In those experiments, the noise cancellation method successfully detected the *in situ* bearing faults.

# CHAPTER 7

# DETERMINATION OF SCNC WARNING THRESHOLD

The RMS of noise-cancelled stator current has been established as the fault indicator. It has been shown that the fault indicator changes significantly as bearing faults develop. A remaining issue then is to evaluate a deteriorated bearing condition based on the value of the fault indicator in real time. This issue is addressed in this chapter. First, an introduction is presented in Section 7.1, where the difficulties in determining the threshold on the fault indicator are discussed. To minimize those difficulties, it is then proposed that statistical methods such as the Statistical Process Control (SPC) should be applied. In Section 7.2, the Statistical Process Control theory is introduced. The principle of calculating the statistical control limits is discussed in Section 7.3. The process of determining a warning threshold for bearing fault detection purposes is described in Section 7.4. Experimental verification is presented in Section 7.5. And finally, the chapter is summarized in Section 7.6.

## 7.1 INTRODUCTION

It has been verified that the noise cancellation method is effective in removing noise components in the stator current. It is also noted the noise-cancelled stator current is closely correlated to machine vibration. This makes it possible to monitor the bearing condition in an electric machine solely based on its stator current signal.

Based solely on the stator current results, a critical issue then is how to decide when a bearing condition is degraded such that maintenance care is required. Essentially, this is a fault severity assessment problem. Difficulties in solving the problem are significant. First,

it is difficult to relate fault signatures in stator current to the bearing fault severity. This difficulty comes from the fact that no physics equations are available to describe fault signatures in stator current injected by most realistic bearing faults. Second, this is an underdeveloped research area, and there is no industry standard. Limited experience exists in dealing with the problem. Third, given the subtleness of bearing fault signatures in stator current, it is difficult to predefine severity levels that are useful in practice. For different applications, the magnitude of the fault signatures varies. This adds another aspect of difficulty to the approach of predefining severity thresholds.

Therefore, it seems appropriate to establish a warning threshold based on the statistics of the signal of an application, rather than to preset a universal limit for all applications. This can be achieved by using a statistical method that can distinguish *abnormal* changes in the noise-cancelled stator current that are caused by a bearing fault, from ambient changes. In this research, a statistical method known as the Statistical Process Control (SPC) is applied. The details of the SPC and its application in this research are presented the following sections.

## 7.2 STATISTICAL PROCESS CONTROL

Statistical Process Control is a statistical tool for monitoring and improving a process. The essence of SPC is that there is variability in any process and that variation can be classified as controlled and uncontrolled. Controlled variation is characterized by a stable and consistent pattern of variation over time, usually driven by random factors in the process [61]. For example, a bearing production line may be designed to produce bearings with the diameter of 210.0 mm. However, the diameter of some bearings will be slightly larger than 210.0 mm (e.g., 210.005mm) and some smaller (e.g., 209.995mm), in accordance with some distribution. Such variation is controlled variation. Uncontrolled variation, on the

other hand, is characterized by a pattern of variation that changes over time, and the changes are caused by assignable causes rather than random factors. For example, as one or two components of the production line wear out, the diameter of the bearings no longer follow the distribution and may become unacceptably large (e.g., 210.9mm). Such variation is uncontrolled variation caused by the assignable cause (the wearing out of the components).

By the notion of controlled and uncontrolled variation, there are two ways to improve any process:

1) "When a process displays controlled variation, the process is stable and consistent and the variation consists only of that which is inherent in the process itself. The only way to improve the process is to change the process itself" [61], for example, by adopting new technologies or new materials.
2) "When a process displays uncontrolled variation, the process is both inconsistent and unstable" [61]. The variation in the process is caused by some assignable cause. To improve the process, the assignable cause needs to be identified and if detrimental, removed from the process.

The SPC theory was published by Dr. Walter A. Shewhart in the 1920's [65]. It was expanded by Dr. W. Edwards Deming and later by Dr. Donald J. Wheeler, Dr. John S. Oakland, and others. It gained extensive use in the manufacture of war materials during World War II in the United States and led to spectacular reductions in both scrap and rework. The SPC methods were successfully introduced in Japan around 1950 and the world after that. So far the SPC methods have been widely used in numerous areas, and have seen increasing interest in practice. Some examples of the application areas of the SPC methods include:

- Process monitoring and improvement in manufacture,

- Enterprise business and management improvement,
- Software development,
- Orbiter processing activities at space centers,
- Biomedical engineering,
- Fault diagnosis.

## 7.3 STANDARD DEVIATION AND CONTROL LIMITS

Standard deviation is a measure of the extent of variation in process data. Therefore, most control limits in SPC are built on the standard deviation of the process data. The meaning of standard deviation is perhaps most easily explained in terms of *normal* distribution. If measurements from a stable process are normally distributed, then 68.3% of the measurements will fall within one-*sigma* (standard deviation denoted as *sigma*) distance of the central (mean), 95.4% within two-sigma, and 99.7% within three-sigma, as illustrated in Figure 7.1. Therefore, one may be confident that almost all measurements will lie between the values of $\mu \pm 3\sigma$ if the process is stable, where $\mu$ is the mean and $\sigma$ is the standard deviation. In other words, if new measurements of the process *frequently* fall outside the three-sigma region, then the process is no longer stable and uncontrolled variation occurs.

If the measurements from the stable process are not distributed normally, according to the *central limit theorem*, the distribution of *sample means* will approach a normal distribution with a mean $\mu$ and a standard error of the means of $\sigma / \sqrt{n}$ as the sample size $n$ increases. *Therefore, even if the individual measurements are not normally distributed, the distribution of the means will tend to have a normal distribution*; the larger the sample size the greater this tendency will be. For practical engineering problems, it can be assumed that

the distribution of the sample means will be very nearly normal, even if the parent population is not normally distributed [62]. This provides a sound basis for the Shewhart's Control Charts which will be discussed later.

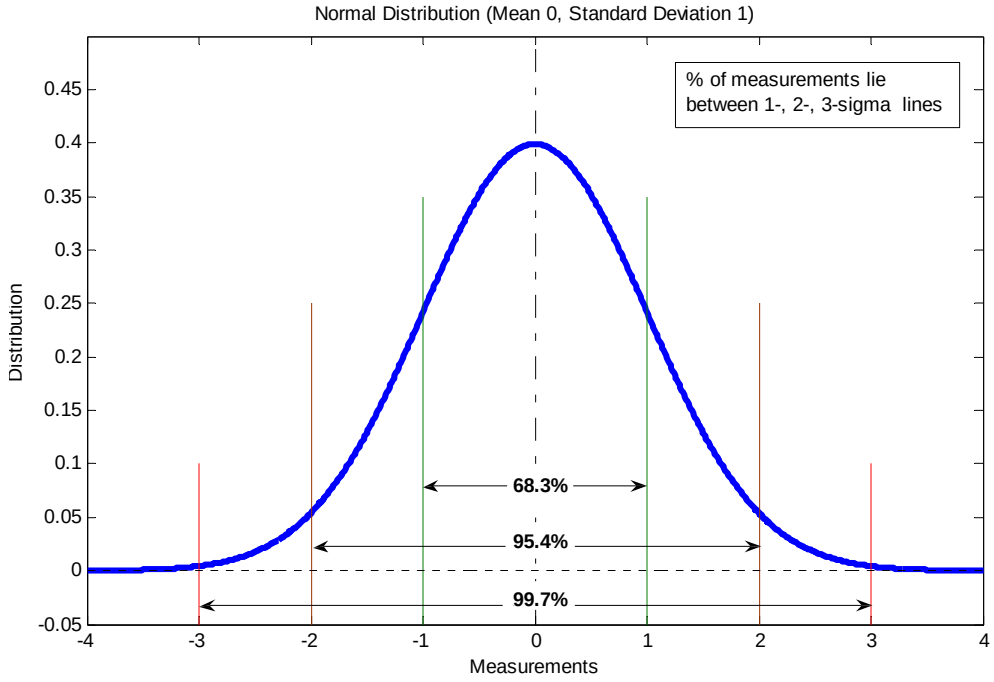


**Figure 7.1 The bell curve of the standard normal distribution (with mean 0, standard deviation 1)**

For convenience, the central limit theorem is given as follows, while the mathematical proof is referred to mathematical textbooks.

> Let $X_1, X_2, X_3, \ldots$ be a sequence of random variables which are defined on the same probability space, share the same probability distribution $D$ and are independent. Assume that both the expected value $\mu$ and the standard deviation $\sigma$ of $D$ exist and are finite.
>
> Consider the sum $S_n = X_1 + \ldots + X_n$. Then the expected value of $S_n$ is $n\mu$ and its standard error is $\sigma\sqrt{n}$. Furthermore, informally speaking, the distribution of $S_n$ approaches the normal distribution $N(n\mu, \sigma^2 n)$ as $n$ approaches $\infty$.

According to this theorem, the distribution of the sample means $\overline{X}_n = \frac{S_n}{n}$ approaches $N(\mu, \sigma^2 / n)$ as $n$ increases.

Therefore, the standard deviation can be used to establish thresholds to distinguish samples of an unstable process from those of a stable process. For different applications, different criteria can be applied to set those thresholds. For example, the 3-sigma lines can be used as warning/action thresholds and 6-sigma lines as severe danger thresholds. Also it is a common practice to monitor both the means and the ranges of the samples, by drawing so-called $\overline{X}$, and *R* charts. For simplicity, *the 3-sigma criterion is applied in this research*. Determination of the standard deviation of both sample means and sample ranges is discussed below.

Suppose the process measurements are assumed to come from a Normal $(\mu, \sigma^2)$ population. If the parameters $\mu$ and $\sigma$ are known, then in the usage of the $\overline{X}$ chart, one has

$$UCL = \mu + \frac{3\sigma}{\sqrt{n}} \qquad \text{and} \qquad LCL = \mu - \frac{3\sigma}{\sqrt{n}} \tag{7.1}$$

as the upper and lower $3\sigma$ control limits, respectively, for the sample means with sample size *n*. In above equations, $\frac{\sigma}{\sqrt{n}}$ is the standard distribution of the sample means. If the parameters $\mu$ and $\sigma$ are unknown, on the other hand, and if one has $k$ preliminary samples each of size $n$, the following quantities

$$\overline{\overline{X}} = \frac{1}{k}\sum_{i=1}^{k} \overline{X}_i \qquad \text{and} \qquad \overline{R} = \frac{1}{k}\sum_{i=1}^{k} R_i \tag{7.2}$$

can be calculated to construct the $\overline{X}$ chart. Usually, measurements that are obtained at a

given point in time constitute one sample, or called one subgroup, and the size of the subgroup/sample is the number of individual measurements in that subgroup. In above equations, $\overline{X}_i$ and $R_i$ are the mean and range obtained from the *i*th sample for $i = 1, 2, \ldots, k$; $\overline{\overline{X}}$ is called the grand average, which is the center of the $\overline{X}$ chart, and $\overline{R}$ is known as the average range, which is the center of the *R* chart. Generic $\overline{X}$, and *R* charts are shown in Figure 7.2.

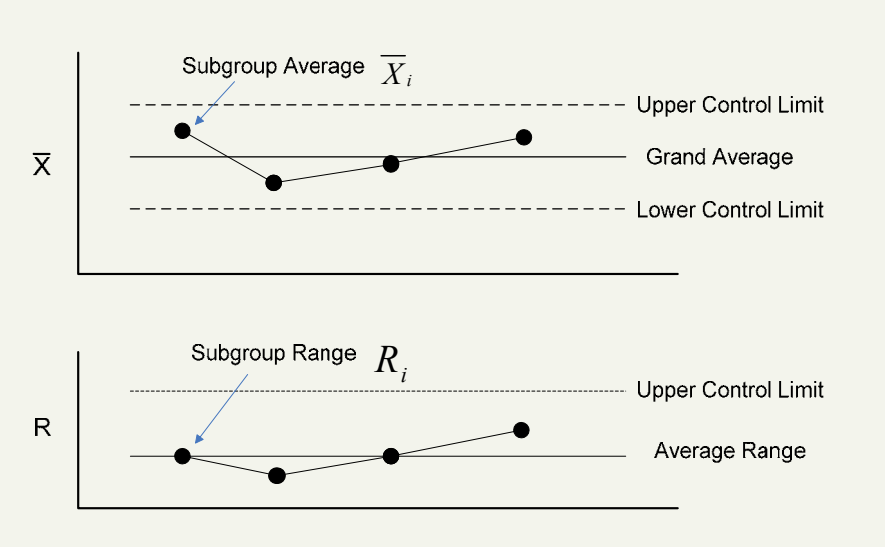


**Figure 7.2 Generic Shewhart's control charts based on subgroups**

While $\overline{\overline{X}}$ can be used as a pooled unbiased estimate of $\mu$, one has to consider

$$\hat{\sigma} = \frac{1}{k}\sum_{i=1}^{k}\frac{R_i}{d_2} = \frac{\overline{R}}{d_2} \tag{7.3}$$

as a pooled unbiased estimate of $\sigma$ [64]. In the above equation, $d_2$ is the expected value of the sample range in a sample of size *n* from the standard normal distribution. *The values of $d_2$ can be computed mathematically and they are tabulated in many statistics handbooks* [61-64]. The computation of $d_2$ is beyond the scope of this research and interested readers are referred to [64]. The derivation of $d_2$ is given below [63].

Assuming $Y \sim Normal(\mu, \sigma^2)$

$$E(R) = \int_{-\infty}^{\infty} Rf(R)dR = d_2\sigma_y \tag{7.4}$$

where $R = (y_{\max} - y_{\min})$ with $y_{\max}$ the largest value in a sample of size *n* and $y_{\min}$ the smallest value, *f(R)* represents the probability density function for the range, *E(R)* is the expected value of the range, and $d_2$ depends upon *n*. Therefore, it follows that one would estimate $\sigma_y$ as

$$\hat{\sigma}_y = \frac{\hat{\mu}_y}{d_2} = \frac{\overline{R}}{d_2} \tag{7.5}$$

where $\overline{R}$ is the average of the ranges for a set of subgroups.

By using these pooled unbiased estimates, in the implementation of the $\overline{X}$ chart, the upper and lower control limits can be calculated as

$$UCL = \overline{\overline{X}} + A_2\overline{R} \qquad \text{and} \qquad LCL = \overline{\overline{X}} - A_2\overline{R} \tag{7.6}$$

where $A_2 = \frac{3}{d_2\sqrt{n}}$ is constant as calculated from the value of $d_2$ and the sample size.

The constant needed for the construction of the range chart can be determined similarly. As mentioned before, the center line of the R chart is at $\overline{R}$. For the determination of the lower and upper control limits of this chart, one first writes the variable of the sample range *R* as

$$R = W\sigma \tag{7.7}$$

where *W* is the sample range (also a variable) in a sample of size *n* from the standard normal distribution. Then the standard deviation of *R* can be written as

$$\sigma_R = \sigma_W\sigma \tag{7.8}$$

where $\sigma_W$ denotes the standard deviation of the sample range in a sample of size *n* from

the standard normal distribution. The values of $\sigma_W$ can be computed mathematically and be found in many statistics handbooks [61-64]. Since $\sigma$ is unknown, by using its estimate $\frac{\overline{R}}{d_2}$ (Equation 7.3), one can estimate $\sigma_R$ by

$$\hat{\sigma}_R = \sigma_W \frac{\overline{R}}{d_2} \tag{7.9}$$

Finally, one can obtain the lower and upper control limits on the range chart as

$$LCL = \overline{R} - \frac{3\sigma_W}{d_2}\overline{R} = D_3\overline{R} \qquad \text{and} \qquad UCL = \overline{R} + \frac{3\sigma_W}{d_2}\overline{R} = D_4\overline{R}\,. \tag{7.10}$$

In the above equations, $D_3 = 1 - \frac{3\sigma_W}{d_2}$ and $D_4 = 1 + \frac{3\sigma_W}{d_2}$. Note that for some values of *n*, $D_3$ may turn out to be negative in which case it may be taken to be 0 for obvious reasons. For convenience, the values of $A_2$, $d_2$, $D_3$, and $D_4$ for *n* = (2-10) are provided in Table 7.1.

**Table 7.1 Constants for Average and Range Charts Based on the Average Range [61]**

| $n$ | 2 | 3 | 4 | 5 | 6 | 7 | 8 | 9 | 10 |
|---|---|---|---|---|---|---|---|---|---|
| $A_2$ | 1.880 | 1.023 | 0.729 | 0.577 | 0.483 | 0.419 | 0.373 | 0.337 | 0.308 |
| $d_2$ | 1.128 | 1.693 | 2.059 | 2.326 | 2.534 | 2.704 | 2.847 | 2.970 | 3.078 |
| $D_3$ | -- | -- | -- | -- | -- | 0.076 | 0.136 | 0.184 | 0.223 |
| $D_4$ | 3.268 | 2.574 | 2.282 | 2.114 | 2.004 | 1.924 | 1.864 | 1.816 | 1.777 |

## 7.4 WARNING THRESHOLD FOR DETERIORATED BEARING CONDITION

In the case of bearing fault detection in this research, the RMS of noise-cancelled stator current can be treated as an output measurement of the complicated machine-bearing process. The variation in the RMS of noise-cancelled stator current can be attributed to a) random factors, if the variation is in control, and b) assignable causes, if the variation is out-of-control. Since dominant non-bearing fault components are already removed in the RMS of noise-cancelled stator current, the uncontrolled variation is most likely caused by bearing faults. The controlled variation driven by random factors, on the other hand, is normal and no actions are required to 'correct.' Theoretically, any statistical method that can detect the uncontrolled change caused by a bearing fault will work for the bearing fault detection purpose. In this research, the three-sigma control limits calculated by using the SPC as described above serve as warning threshold regarding a deteriorated bearing condition.

In current-based bearing fault detection, data of one phase of stator current usually is collected for further processing. Therefore, at a given point in time, one measurement is obtained. Consequently, the subgroup size is one and the subgroup range does not exist. To accommodate this, the procedure described in Section 7.3 can be slightly modified; the so-called *X* chart and *mR* (the acronym for "moving Range") chart can be applied to monitor the process [61]. The generic *X* chart and *mR* chart are illustrated in Figure 7.3. The center of the *X* chart is $\overline{X}$, i.e., the mean of the individual samples, in which case $\overline{X}$ is the same as $\overline{\overline{X}}$. The center of the *mR* chart is the mean of differences of adjacent individual measurements. The individual measurements are plotted on the *X* chart and the differences (i.e., moving range) are plotted on the *mR* chart.

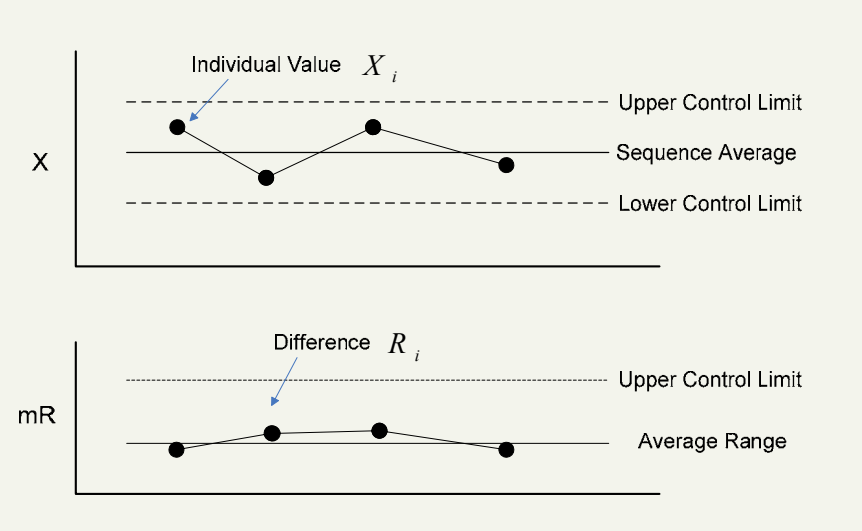


**Figure 7.3 Generic Shewhart's control charts for Subgroup Size One**

Since individual values are plotted on the *X* chart, the control limits for individual values (rather than the sample means), sometimes called Natural Process Limits (NPL), should be applied, which are [61]

$$UNPL_X = \overline{X} + 3\frac{\overline{R}}{d_2} \qquad \text{and} \qquad UNPL_X = \overline{\overline{X}} - 3\frac{\overline{R}}{d_2} \tag{7.11}$$

Further more, $\overline{R}$ is substituted by *mR*, by using $d_2 = 1.128$ ($n = 2$), one has

$$UNPL_X = \overline{X} + 2.660\overline{mR} \qquad \text{and} \qquad LNPL_X = \overline{X} - 2.660\overline{mR} \tag{7.12}$$

which are the upper control limit and lower control limit for the *X* chart. For bearing fault detection in this research, since the SPC is applied to noise-cancelled stator current, a sample falling below a lower control limit means a better bearing condition and therefore, is not of concern. In the following discussions, only upper control limits are of interest.

The upper control limit for the *mR* chart is

$$UCL_R = 3.268\overline{mR} \tag{7.13}$$

where $D_4 = 3.268$ ($n = 2$) has been used. (In above equations, the equivalent subgroup

size $n = 2$ is applied, indicating that the moving range of the individual values is taken as a second measurement at each given point in time [61].) The lower control limit for the *mR* chart is zero, as can be seen in Table 7.1.

Alternatively, one can group the measurements that are obtained over a short interval as one subgroup. In bearing fault detection, since bearing faults develop over a prolonged period, it may be reasonable to subgroup several adjacent measurements in time as one subgroup. By doing so, the control limits for sample means and sample ranges discussed in the previous section would apply.

The above two sets of control charts, i.e. the set (of the $\overline{X}$, and *R* charts with the limits determined by Equations 7.6 & 7.10) and the set (of the *X*, and *mR* charts with the limits determined by Equations 7.11 & 7.12) both can be applied. It should be noted that no matter which set of control charts is applied, the key is *the detection of uncontrolled variation in the noise-cancelled stator current is helpful to detect a deteriorated bearing condition*. Specifically, the sample *frequently* falling outside the control limits indicates a deteriorated bearing condition. The idea of combining the stator current noise cancellation method and the statistical process control for bearing fault detection is illustrated in Figure 7.4.

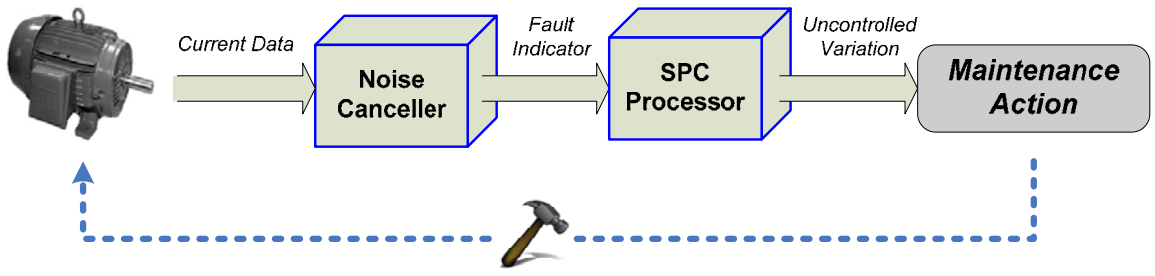


**Figure 7.4 Illustration of current-based bearing condition monitoring by combining SPC and SCNC**

A block diagram of the Noise Canceller in Figure 7.4 is shown in Figure 5.5 in Chapter 5 for constant-load conditions and Figure 6.2 in Chapter 6 for variable-load conditions. A block diagram of the SPC Processor is shown in Figure 7.5.

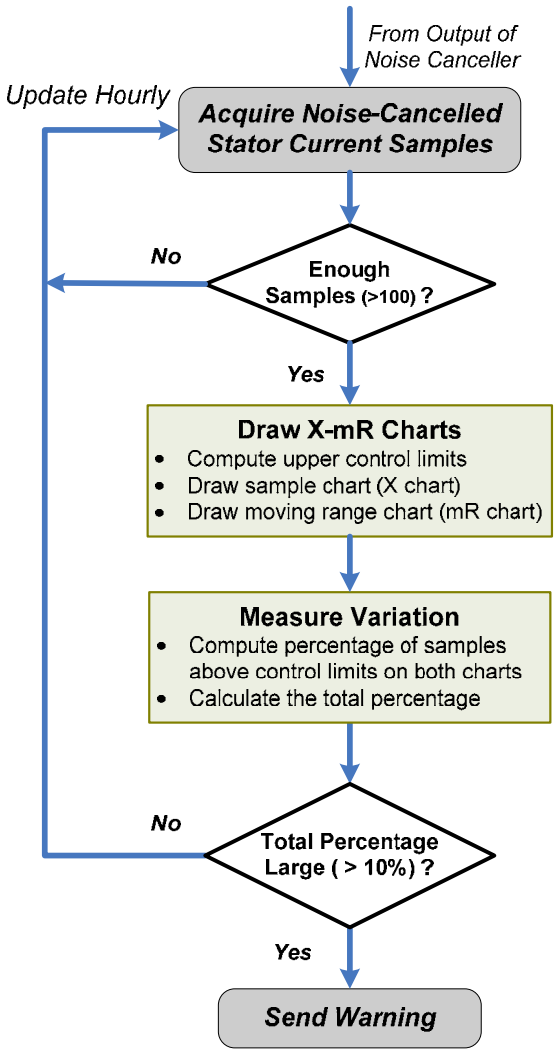


**Figure 7.5 A block diagram of the statistical processor for bearing fault detection.**

To avoid misjudgment due to insufficient data, the Processor starts after receiving enough samples of noise-cancelled stator current, say, after receiving over 100 samples as recommended in the references [61, 65]. The control charts are updated periodically, such as each hour as shown in the figure. In each period, *first*, the control limits are computed based on all the previous samples acquired prior to that period; therefore, the calculated

limits would apply to all the previous samples prior to that period. *Then*, the variation of the process is measured by calculating the percentage of the samples outside the updated control limits among all the previous samples prior to that period. Samples that fall outside a control limit are also called *out-of-control* samples. If there are many samples, e.g. over 10%, outside the control limits (i.e., over 10% *out-of-control* samples), a warning message about the bearing condition will be sent.

## 7.5 EXPERIMENT RESULTS ANALYSES

The scheme based on the combination of the SPC technique and the SCNC method has been applied to the experiment data collected in this research. The results show that at the beginning of those tests, no obvious uncontrolled variation was observed, and after the machine was running for a while in each test, some degree of uncontrolled variation was observed because of the deteriorated bearing conditions. Therefore, by detecting uncontrolled variation in the SCNC results, information about a deteriorated bearing condition can be generated.

The data collection system, the experiment setup, and the detailed stator current noise cancellation results for those experiments are provided in previous chapters. The SPC results for those experiments are shown in this section.

### 7.5.1 CONSTANT LOAD EXPERIMENT TEST 1

The SPC procedure described in the previous section is illustrated in details by using the data from this experiment – Constant-Load Experiment 1. The same procedure is also

applied to the other tests and the results are presented in the next subsections without details for conciseness.

The *X-mR* charts for this experiment are shown in Figure 7.6. Each point in the top plot stands for one RMS value of the noise-cancelled stator current and the x-axis is the time. The middle plot illustrates the moving range (i.e. the difference between two adjacent RMS values) of the noise-cancelled stator current along the time. The bottom plot records the RMS of the machine vibration, which indicates that a bearing fault is developing in this test.

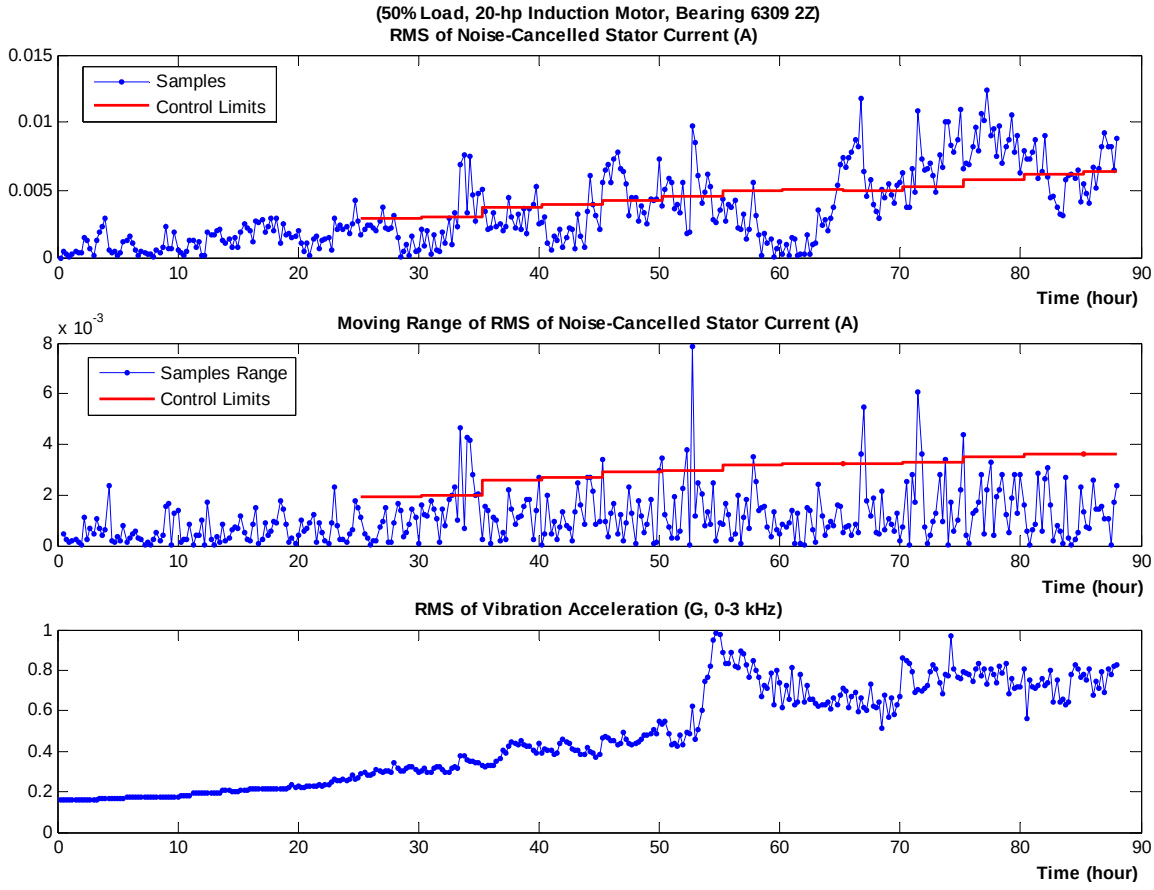


**Figure7.6 The *X-mR* Charts with updated control limits clearly show uncontrolled variation in the SCNC results as the bearing fault develops**

Figure 7.6 also shows the level of the control limits calculated in each processing period

(five hours in this case), where the control limits are calculated based on all previous samples acquired prior to that period. It can be seen clearly that uncontrolled variation takes place on both the charts as the bearing condition degrades.

It should be pointed out that the stator current measurement *frequently* falling outside the control limits means a deteriorated bearing condition. It should *not* be expected that the measurement should *always* fall outside those limits after a bearing fault has occurred. This is because the assignable cause of uncontrolled variation may come and go [61]. This is also reflected in the vibration measurement; as shown in the figure, the vibration decreases around the $60^{th}$ hour following the increase around the $55^{th}$ hour.

To quantify the degree of uncontrolled variation in the process along the time, the percentage of the out-of-control (OOC) samples was calculated, following the procedure depicted in Figure 7.5. Specifically, the percentage of the OOC samples on the *X* chart and the *mR* chart, as well as the total percentage, was calculated; the results are drawn in Figure 7.7. The control charts and the calculation were updated hourly. The percentage at each hour is the ratio of the number of OOC samples prior to that hour vs. the number of total samples acquired prior to that hour, and the OOC samples are those fall outside the control limits calculated based on all samples acquired prior to that hour. The calculation started at the $25^{th}$ hour, in order to avoid possible misjudgment due to insufficient data at the beginning. Around the $46^{th}$ hour, the total percentage of the OOC samples exceeded 10% and a warning message was sent. As seen from the figure, the total percentage of OOC samples increases from 3% to 23%, and the percentage of OOC samples on the *X* chart increases from 2% to 19%.

The percentage of OOC samples on the *mR* chart relates to the change rate in adjacent sample values. A relative large value indicates a relatively fast-changing process regardless

of a large or small sample value. The bottom plot in Figure 7.7 indicates that the process changes relatively fast from the 53rd hour to the 80th hour. This is verified by the vibration measurement as shown in Figure 7.6.

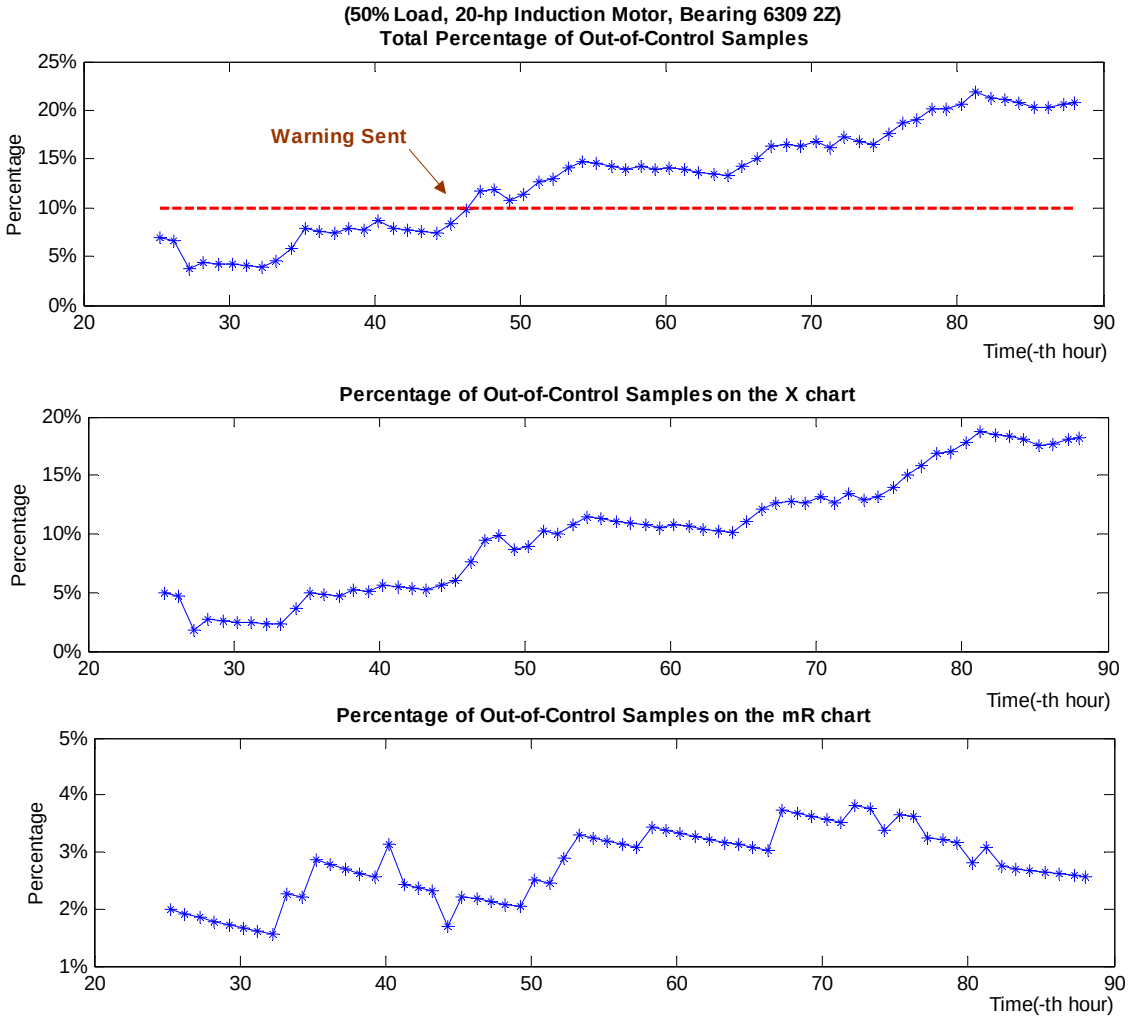


**Figure 7.7 The Percentage of the Out-of-Control Samples along the time for Constant-Load Experiment 1**

It is also noted that $\overline{X}$-$R$ charts would deliver similar information as $X$-$mR$ charts for the same process. For example, the $\overline{X}$-$R$ charts shown in Figure 7.8 were drawn by grouping the four adjacent values of the RMS of the noise-cancelled stator current in time as one

subgroup. I.e., four adjacent samples on the $X$ chart in the top plot of Figure 7.6 were grouped as one subgroup on the $\overline{X}$ chart in the top plot of Figure 7.8. It can be seen that Figure 7.8 shows similar results as Figure 7.6.

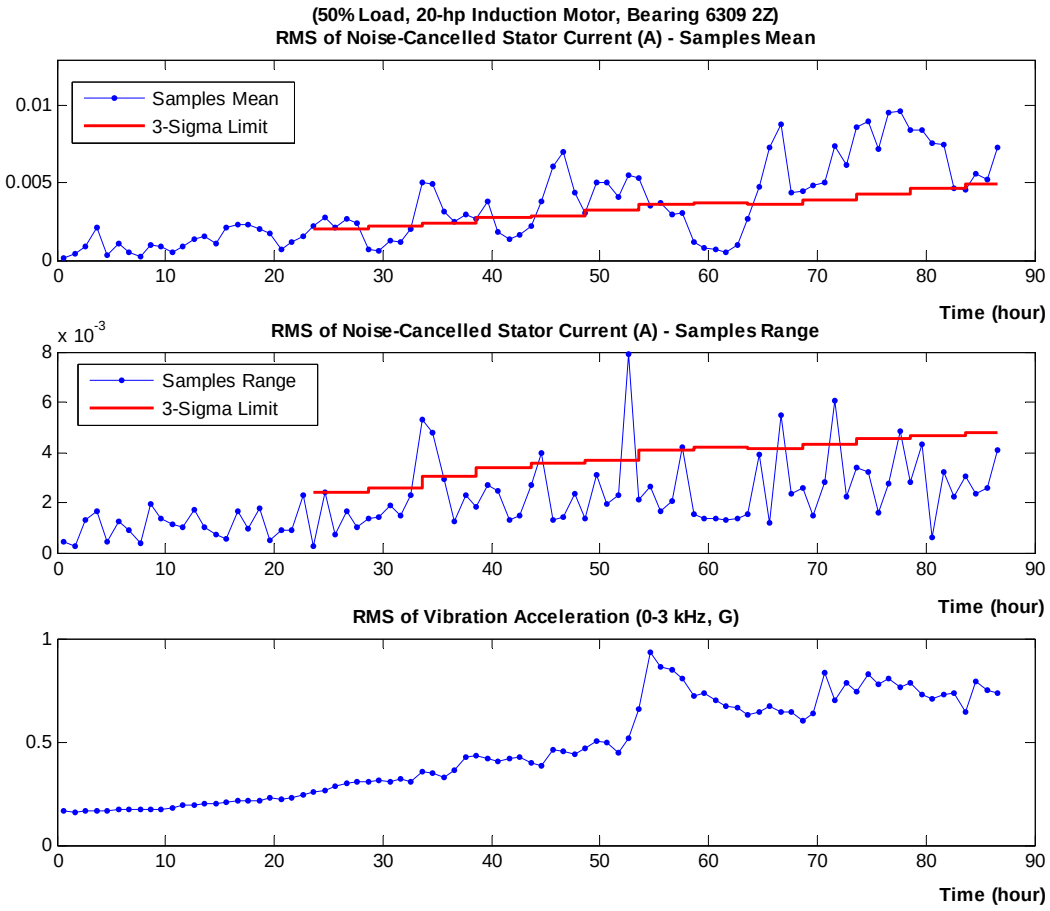


**Figure 7.8 Similar results to the *X*-*mR* charts observed on the $\overline{X}$ -*R* Charts (subgroup size 4)**

### 7.5.2 CONSTANT LOAD EXPERIMENT TEST 2

Similar results to those of Constant-Load Experiment Test 1 are obtained for this experiment (Constant-Load Test 2). Figure 7.9 shows the percentage of OOC samples by applying the SPC to this experiment. One can see that uncontrolled variation occurs as the result of the deteriorated bearing condition and the uncontrolled variation is significant after the 33rd hour. Specifically, the percentage of the out-of-control samples increased from 6% to over 20% during the experiment.

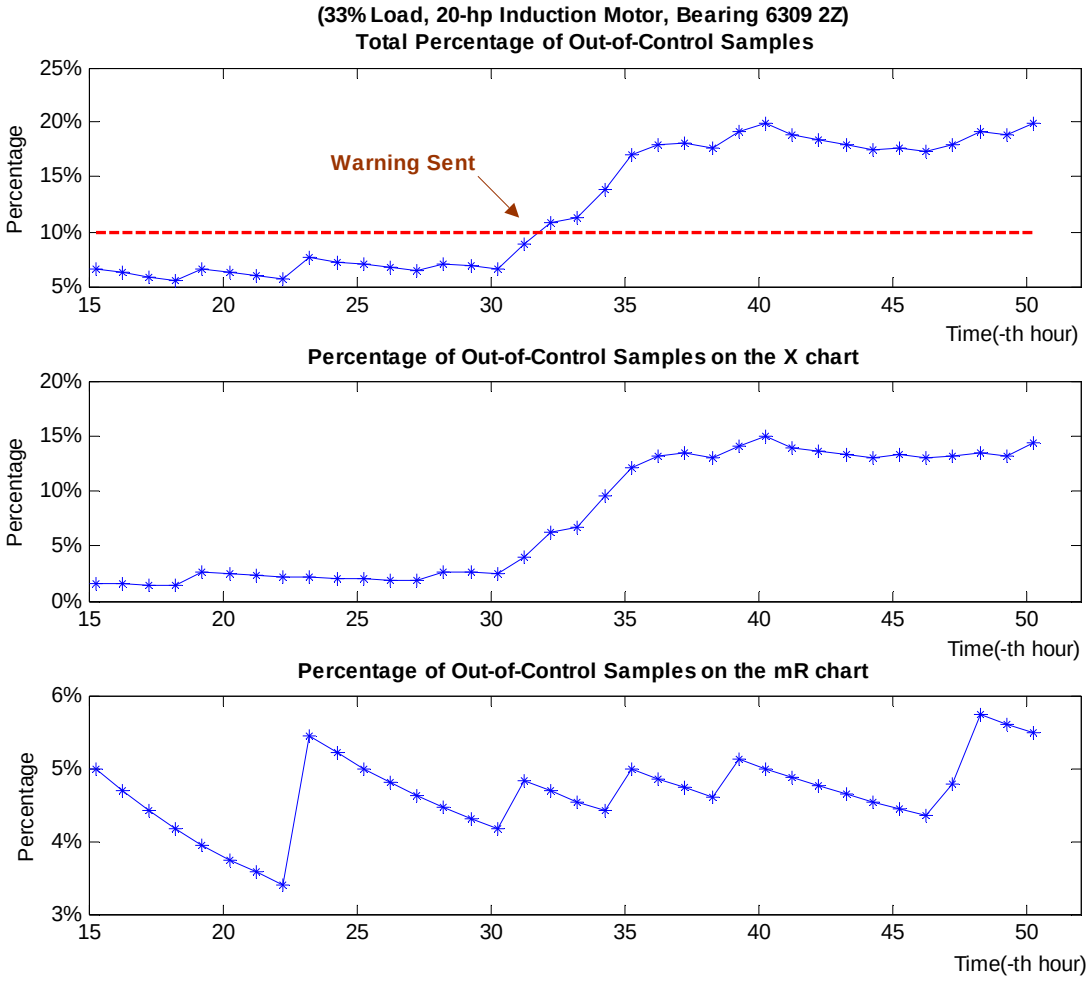


**Figure 7.9 The Percentage of Out-of-Control Samples along the time for Constant-Load Experiment 2**

### 7.5.3 VARIABLE LOAD EXPERIMENT TEST 1

Variable-load Experiment 1 involves two load levels. The vibration at the two load levels is shown in Figure 7.10, which indicates that the bearing condition is degraded along the time during the experiment.

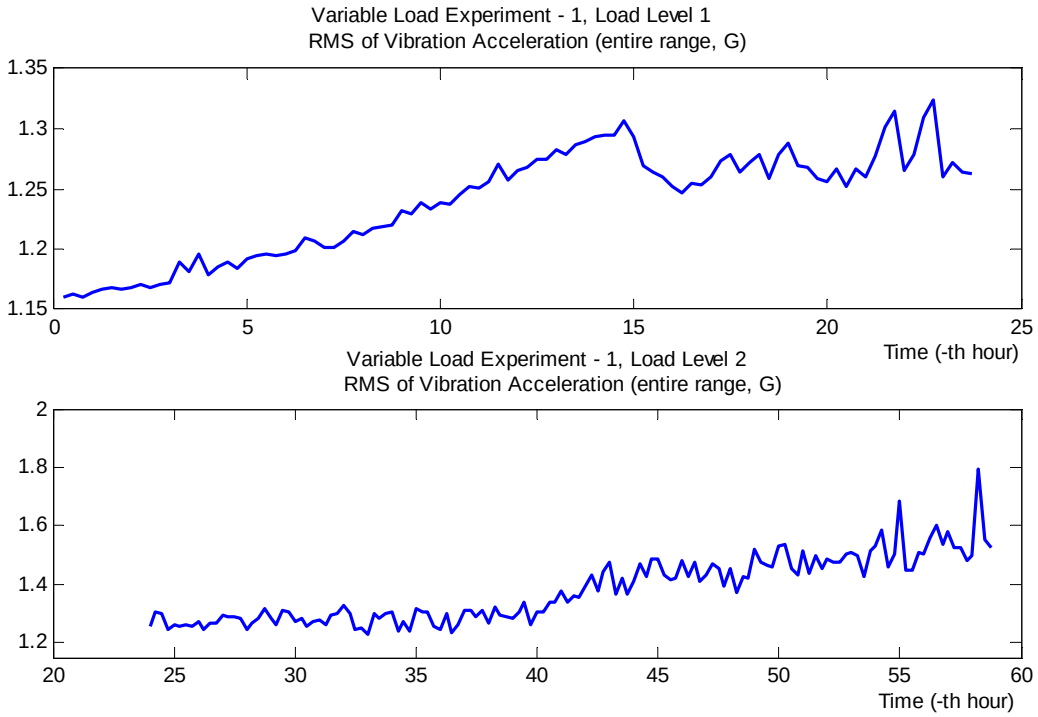


**Figure 7.10 The RMS value of the vibration at the two load levels during Variable-Load Experiment 1**

By applying the SPC to the noise-cancelled stator current, a warning message about the bearing condition was generated around the 15$^{th}$ hour during Load Level 1. The percentage of out-of-control samples for the load level is shown in Figure 7.11. It can be clearly seen that the total percentage of out-of-control samples increases from 0% to 32% for this load level.

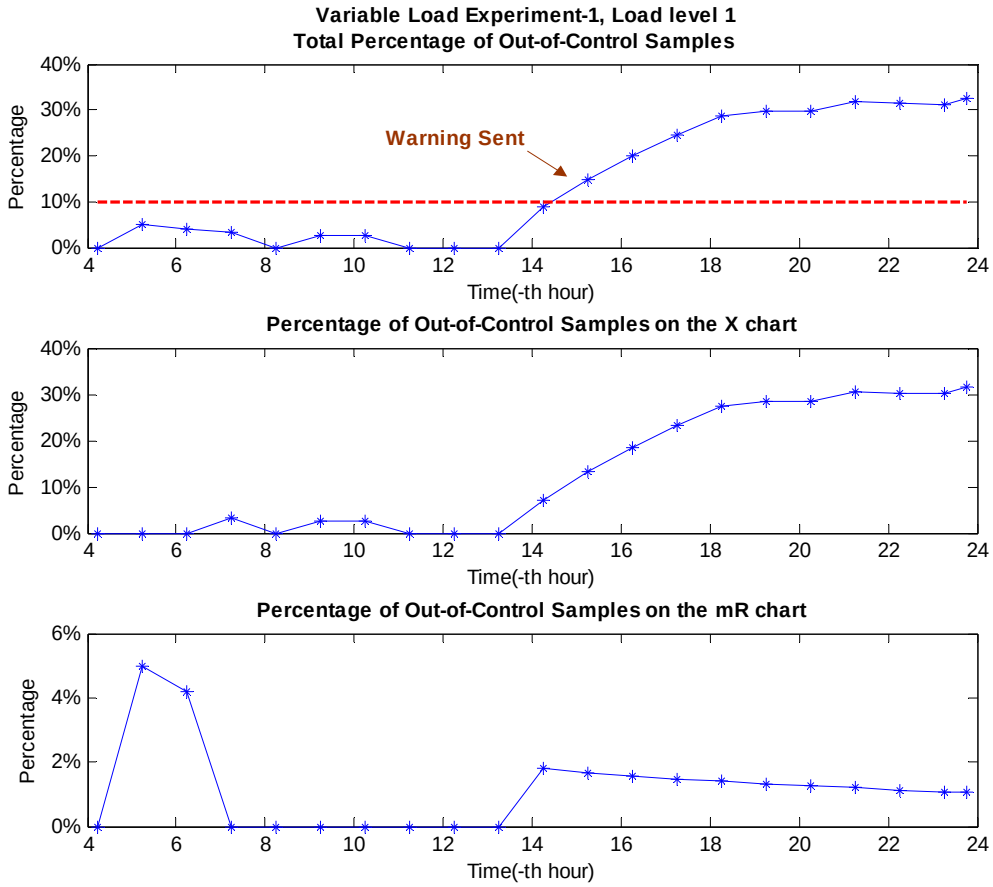


**Figure 7.11 The percentage of out-of-control samples under the first load level during Variable-Load Experiment 1**

Figure 7.12 shows the percentage of out-of-control samples for the second load level. The percentage of out-of-control samples increases from 3% to 9% in the operation at this load level *alone*. It should be pointed out that the noise cancellation algorithm processes the data from the two load levels separately (see Section 6.2, Chapter 6). For bearing fault diagnosis purposes, the SPC results for the second load level should be considered in conjunction with the results obtained from the previous load level, in order to properly track the bearing condition during the entire operation period. In other words, for real-time bearing condition monitoring, the percentage of out-of-control samples increases from 35% to 41% during the second half of the experiment, where the percentage 32% at the end of the first load level period has been carried on to the calculations for the second load level. Nevertheless,

the increase in the percentage of out-of-control samples at both load levels indicated the degradation of the bearing condition.

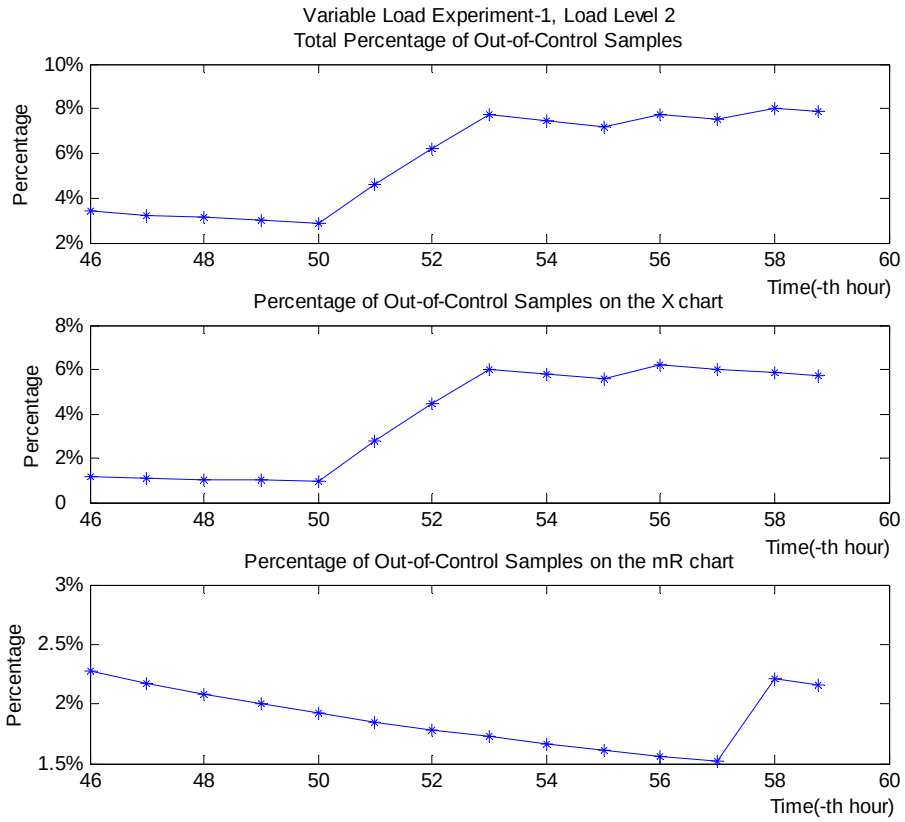


**Figure 7.12 The percentage of out-of-control samples under the second load level during Variable-Load Experiment 1**

### 7.5.4 VARIABLE LOAD EXPERIMENT TEST 2

Similar results to those of Variable-Load Experiment Test 1 are obtained for this experiment. The percentage of out-of-control samples increases significantly during the operation and, specifically, as shown in Figure 7.13, the percentage of out-of-control samples increases from 0% to nearly 20%, which indicated that the bearing health is degraded.

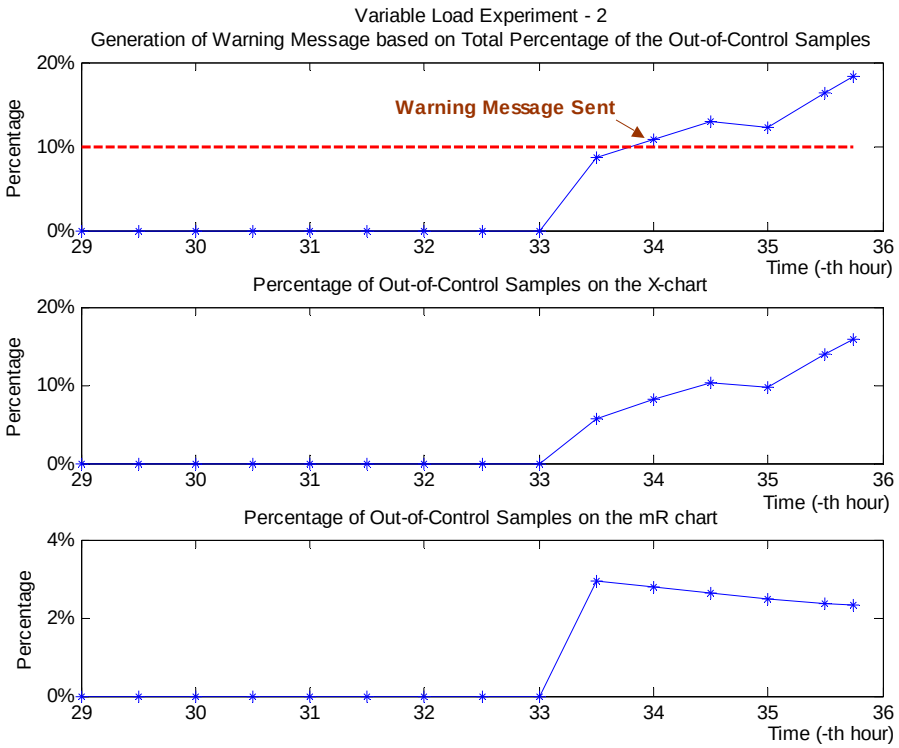


**Figure 7.13 The percentage of out-of-control samples increases during Variable Load Experiment 2**

Similar results are obtained from all other experiments performed in this research which are not shown here for conciseness.

## 7.6 SUMMARY

The main objective of this chapter is to develop a scheme to distinguish a deteriorated bearing condition from normal conditions, solely relying on stator current measurements. First, the difficulties in bearing fault detection and fault severity assessment solely based on stator current measurements were discussed. Then it was proposed that statistical methods such as the statistical process control can be applied to calculate the warning threshold for stator current measurements. The statistical process control was further evaluated and its principle was discussed. Based on the discussion, the process of determining the warning threshold for the samples of noise-cancelled stator current was

described. Finally, the results attained by applying the SPC tool to the data collected during the on-line experiments were presented. It was observed that the percentage of out-of-control samples increases significantly as the bearing condition degrades. The results demonstrated that it is possible to detect realistic bearing faults by detecting uncontrolled variation, specifically by detecting the percentage of out-of-control samples in the noise-cancelled stator current.

# CHAPTER 8
# CONCLUSIONS, CONTRIBUTIONS, AND RECOMMENDATIONS

## 8.1 SUMMARY AND CONCLUSIONS

The goal of this research was to advance the field of bearing condition monitoring for electric machines. Bearing faults account for approximately half of all machine failures; therefore, an early detection of faltering bearings is of practical importance.

Many methods have been proposed in the literature to monitor bearing condition; those methods include vibration, chemical, temperature, acoustic emission, sound pressure, laser, and current monitoring. Each monitoring method has its own advantages and disadvantages. Because of its unique properties stator current monitoring was chosen to be the main topic of this research. Current monitoring is non-intrusive, can be implemented remotely, and is convenient and inexpensive. However, detecting bearing faults via stator current monitoring is known to be a difficult task. The difficulty comes from the fact that bearing fault signatures are subtle in the stator current, and the fact that the research is limited in this area. For many realistic bearing faults, the fault frequencies are not predictable, which adds another level of difficulty.

Most available current-based techniques rely on the observability of certain frequencies in the stator current. Consequently, they are most effective for detecting single-point defects in bearing surfaces. However, for realistic bearing faults that are developed on-line in industrial settings, especially at an early stage, those frequencies are not observable and may not exist at all.

Therefore, there was no attempt to localize specific frequencies in the stator current in this work; instead, the problem of detecting realistic bearing faults has been restated as a low signal-to-noise ratio (SNR) problem. It is known that the dominant components in the stator current are not related to bearing faults, and subtle bearing fault signatures can be well masked by the dominant components. Following the signal-noise notion, it was desired to separate the bearing fault-related and non-related components in the stator current via noise cancellation techniques. By effectively removing those dominant, fault-non-related components, the remaining components related to the bearing faults were better accessible.

Due to its optimum property in the sense of producing the best estimate of a noise-interfered signal, Wiener filtering has been chosen to accomplish the noise cancellation. Since Wiener filtering is very common in practical applications, there are efficient algorithms like the Levinson-Durbin Recursion algorithm that solve for the unknown coefficients.

Once the fault-related components were separated, further analysis was applied. Specifically, it was desired to evaluate the bearing condition based on the magnitude of those components obtained in real time. By using a statistical tool such as Statistical Process Control, a warning threshold was computed and applied to the magnitude of those components. The warning threshold was used to distinguish a deteriorated bearing condition from normal conditions.

To validate the proposed noise cancellation method, on-line experiments have been performed. A unique feature of those experiments is that bearings were failed over time by increasing generalized roughness on the bearing surfaces. Thus, the bearing failure mechanism is similar to many realistic situations. A medium-size induction motor (20 hp)

was employed as the test motor, in contrast to most previous research studies where only small-size motors were involved. The size of test bearings is type 6309 2Z. The duration of experiments ranged from tens of hours to several weeks. Vibration measurements were collected as a reference for the bearing health.

Six constant-load experiments and two variable-load experiments have been performed. Over 10 bearings have failed during the tests and among them the data for 8 bearings were successfully recorded. The two variable-load experiments involved 5 load levels. To avoid the drastic influence from load changes on the stator current, the noise cancellation was applied to each load level separately, while the results were considered together. To realize the true non-intrusiveness, a current-based speed estimation algorithm was employed to obtain the load information. Significant changes have been observed in the machine vibration and in the noise-cancelled stator current as the bearing faults developed. The experimental results showed that the first-order correlation between the noise-cancelled stator current and the machine vibration was highest as 0.86; in 4 out of the 11 load sections, it was greater than 0.69; in 6 out of the 11 load sections, it was greater than 0.55; and in 9 out of the 11 load sections, it was greater than 0.43. Due to the complexity of the system, higher-order fitting models provided better results. For example, by assuming a nine-order polynomial fit between the noise-cancelled stator current and the machine vibration, the correlation coefficient between the two measurements was found to be 1.0 in 2 out of the 11 load sections, and equal to or larger than 0.8 in 6 out of the 11 load sections, larger than 0.6 in 9 out of the 11 load sections.

The results attained by applying the noise cancellation method to vibration signals further demonstrated that bearing fault-related components were not affected by the noise cancellation process. In addition, the performance of the proposed method was compared to the existing Mean Spectral Deviation method. In one of those experiments, the MSD

method failed to detect the bearing fault, while the proposed method clearly indicated the deteriorated bearing condition.

Experimental results also showed that as the bearing condition was degraded, significant uncontrolled variation occurred in the noise-cancelled stator current. By applying the statistical process control technique, it was observed that the out-of-control samples (of the noise-cancelled stator current) increased from 3% to over 20% in those experiments. *The results showed that it is possible to detect a deteriorated bearing condition by observing the percentage of out-of-control samples of the noise-cancelled stator current*.

For convenience, the maximum allowed percentage of out-of-control samples under normal bearing conditions was preset and served as the warning threshold. *Theoretically*, the out-of-control samples should be 0.3% for a sample set drawn from a normal distribution, since 99.7% of the samples fall within the three-sigma limit. For practical use, a margin should be provided considering the factors that could affect this number: the completeness of the noise components removal during the noise cancellation process, the size of the sample set, the accuracy of the assumption of the normal distribution, and the random effects from unknown sources. In the experiments performed in this research, 10% served the purpose, though this threshold should be adjusted to meet specific needs in practical applications.

## 8.2 CONTRIBUTIONS

The contributions of this research are summarized as follows:

- Surveys in the following areas have been performed:
    - Various bearing condition monitoring methods, considering implementation requirements,
    - Vibration-based bearing condition monitoring techniques,
    - Existing current-based bearing condition monitoring techniques, and
    - Various noise cancellation structures and algorithms.
- A new method to detect bearing faults via stator current monitoring has been developed and experimentally verified.
    - A new concept to formulate the bearing fault detection problem as a low signal-to-noise (SNR) problem was proposed. It follows that stator current noise cancellation is appropriate to solve the problem.
    - A detailed theoretical analysis of the stator current noise cancellation method based on Wiener filtering was presented.
    - The noise cancellation method successfully detected the degraded bearing conditions in the experiments performed in this research.
    - The proposed noise cancellation method is simple and easy to implement.
- A strategy to extend the proposed method to variable-load conditions has been developed and experimentally verified.
    - A current-based speed estimation algorithm was implemented to detect a load change.
    - The negative effects of load changes on bearing fault detection were minimized by applying the noise cancellation method to each load level separately, while the results were considered together.
    - True non-intrusive bearing fault detection was achieved by using the strategy.

- A method to determine warning threshold for current monitoring has been developed and experimentally verified.
    - The challenges in determining warning threshold for current monitoring were discussed. To minimize those difficulties, it was proposed that statistical methods should be applied.
    - The new monitoring method was based on the combination of the statistical process control and the noise cancellation technique.
    - Experimental results have shown that it is highly possible to detect bearing faults by detecting uncontrolled variation in the noise-cancelled stator current. Experimental results have shown that the percentage of out-of-control samples provides valuable information about the bearing condition. As the bearing conditions were degraded in those experiments, the percentage of out-of-control samples increased from 3% to over 20%.
- An existing experimental setup for generating generalized-roughness bearing faults was improved and a number of bearings have been failed by using this setup.
    - An isolation transformer was added to the original setup to prevent interference between the shaft current circuit and the measurement circuit. The interference could corrupt bearing data.
    - Different from most previous research studies, a medium-size motor has been used as the test motor. A medium-size motor could produce less prominent fault signatures in the stator current compared to small-size motors because of reduced bearing-machine size ratio and increased noise from the load.
    - A number of bearings have been successfully failed by using the setup. The faults are characterized by generalized roughness on the bearing surfaces, which is similar to most realistic bearing faults.

## 8.3 RECOMMENDATIONS

Some recommendations are listed for continuing investigation in this research field:

- More experiments need to be carried out to further evaluate the sensitivity and reliability of the proposed detection scheme on a wide range of electric machines of different motor size, load types, and installations. Small-size motors may have relatively prominent bearing fault signatures. For large-size motors, such as medium-voltage motors, new challenges may exist for current-based bearing fault detection.
- For electric machines under continuous non-stationary operations, bearing fault detection via stator current may be more challenging than in stationary situations. The effects of non-stationary operations on the stator current need to be investigated for bearing fault detection purposes.
- Further work is needed to investigate the applicability of other signal processing tools in characterizing the fault signatures injected by realistic bearing faults. Those tools include, but not limited to, Kalman Filtering, Wigner-Ville Distribution (WVD), and Homomorphic (cepstrum) Transformation.
- It is desired that a detection method should be able to detect bearing faults of both types: single-point defects and generalized roughness. Reliable techniques in detecting single-point defects are available in the literature. Therefore, some work remains to be done on how to incorporate the techniques developed in this research along with those techniques available in the literature. By doing so, a complete bearing condition monitoring solution can be realized.
- Some work remains to be done to determine how the detection methods developed in this research interact with other fault detection methods such as stator fault detection methods and rotor fault detection methods, if all these methods are going to be implemented in a same microprocessor in practice.

# BIBLIOGRAPHY


[1] IAS Motor Reliability Working Group, "Report of large motor reliability survey of industrial and commercial installations: Part I and Part II," *IEEE Transactions on Industry Applications,* Vol. 21, No. 4, pp.853 – 872, 1985.

[2] T. A. Harris. " Rolling Bearing Analysis". Second edition. ISBN: 0-471-79979-3, New York : Wiley, 1984.

[3] B. Li,, M.Y. Chow, Y. Tipsuwan, and J.C. Hung, "Neural-network based motor rolling bearing fault diagnosis," *IEEE Transactions on Industrial Electronics*, vol. 47, no. 5, pp. 1060-1068, Oct. 2000.

[4], R.L. Schiltz, "Forcing frequency identification of rolling element bearings," *Sound and Vibration*, pp. 16-19, May 1990.

[5] B. Yazici, and G. B. Kliman, "An adaptive statistical time-frequency method for detection of broken bars and bearing faults in motors using stator current," *IEEE Trans. Ind. Applicat.*, vol. 35, pp. 442–452, Mar./Apr. 1999.

[6] L. Eren, and M. J. Devaney, "Bearing damage detection via wavelet packet decomposition of the stator current," *IEEE Trans. Instrumentation*, vol. 53, pp. 431-436, Apr. 2004.

[7] M. E. H. Benbouzid, M. Vieira, and C. Theys, "Induction motors' faults detection and localization using stator current advanced signal processing techniques," *IEEE Trans. Power electronics*, vol. 14, pp. 14-22, Jan. 1999.

[8] M. E. H. Benbouzid, "A review of induction motors signature analysis as a medium for faults detection," *IEEE Trans. Ind. Electronics*, vol. 47, pp. 984-993, Oct. 2000.

[9] M. Blodt, P. Granjon, B. Raiso, and G. Rostaing, "Models for bearing damage detection in induction motors using stator current monitoring," *Ind. Electronics, 2004 IEEE International Symposium,* Vol. 1, pp. 383-388, May 2004.

[10] J. R. Stack, T. G. Habetler, and R. G. Harley, "Fault classification and fault signature production for rolling element bearings in electric machines," *IEEE Trans. Ind. Applicat.*, Vol. 40, pp. 735-739, May/June 2004.

[11] A. M. Knight, and S. P. Bertani, "Mechanical fault detection in a medium-sized induction motor using stator current monitoring," *IEEE Trans. Energy Conversion*,

Vol. 20, pp 753-760, Dec. 2005.

[12] *Mechanical Vibration—Evaluation of Machine Vibration by Measurements on Non-rotating Parts—Part 1: General Guidelines*, ISO 10816-1:1995(E), 1995.

[13] *Mechanical Vibration—Evaluation of Machine Vibration by Measurements on Non-rotating Parts—Part 3: General Guidelines*, ISO 10816-3:1998(E), 1998.

[14] Tavner, P.J. and J. Pennman, *Condition Monitoring of Electrical Machines*, Letchworth, England: Research Studies Press Ltd. 1987.

[15] *IEEE Standard for Petroleum and Chemical Industry – Severe Duty Totally Enclosed Fan-Cooled (TEFC) Squirrel Cage Induction Motors – Up to and Including 370 kW (500 hp),* IEEE Std 841-2001, 2001.

[16] B. Maru, and P. A. Zotos, "Anti-friction bearing temperature rise for NEMA frame motors," *IEEE Transactions on Industry Applications*, vol. 25, no. 5, pp 883-888, 1989.

[17] J. A. Henao-Sepulveda, M. T. Quinones, and Y. Jia, "Contactless monitoring of ball bearing temperature," *Instrumentation and Measurement Technology Conference*, Ottawa, Canada, May 2005.

[18] M. W. Hawman, and W. S. Galinaitis, "Acoustic emission monitoring of rolling element bearings," *IEEE Proceedings of Ultrasonics Symposium*, vol. 2, pp. 885-889, Oct. 1988.

[19] R. B. W. Heng, and M. J. M. Nor, "Statistical analysis of sound and vibration signals for monitoring rolling element bearing condition," *Applied Acoustics*, vol. 53, no. 1-3, pp. 211-226, 1998

[20] S. J. Yang, *Low-noise electrical motors*, Oxford University Press, New York, 1981.

[21] Y. Shao, and K. Nezu, "Bearing fault detection using laser displacement sensor," *SICE '96. Proceedings of the 35th SICE Annual Conference. International Session Papers*, pp. 1069-1072, 1996.

[22] H. R. Martin, and F. Honarvar, "Application of statistical moments to bearing failure detection," *Applied Acoustics*, vol. 44, pp. 67-77, 1995.

[23] S. A. McInerny, and Y. Dai, "Basic vibration signal processing for bearing fault

detection," *IEEE Transactions on Education*, vol. 46, no. 1, pp. 149-156, Feb. 2003.

[24] Randall, R.B, J. Antoni, and S. Chobsaard, "A comparison of cyclostationary and envelope analysis in the diagnostics of rolling element bearings," *IEEE International Conference on Acoustics, Speech and Signal Processing*, vol. 6, pp. 3882-3885, 2000.

[25] J. Shiroishi, Y. Li, S. Liang, T. Kurfess, and S. Danyluk, "Bearing condition diagnostics via vibration and acoustic emission measurements," *Mechanical System and Signal Processing*, 11(5), pp. 693-705, 1997.

[26] C. C. Tan, and Y. Okada, " Detection of rolling-element bearing signal corrupted by noise of similar frequency using adaptive noise cancellation," *International Conference on Information, Communications and Signal Processing, ICICS '97*, Sept. 1997.

[27] J. R. Stack, R. G. Harley, and T. G. Habetler, " An amplitude modulation detector for fault diagnosis in rolling element bearings," *IEEE Trans. on Industry Electronics*, Vol. 51, No. 5, pp. 1097-1102, Oct. 2004.

[28] C. C. Osuagwu, and D.W. Thomas, "Effect of inter-modulation and quasi-periodic instability in the diagnosis of rolling element incipient defect," *ASME Journal of Mechanical Design*, vol. 104, pp. 296-302. 1982.

[29] H. Ocak, and K. A. Loparo, "A new bearing fault detection and diagnosis scheme based on hidden Markov modeling of vibration signals," *IEEE International Conference on Acoustics, Speech, and Signal Processing, 2001. (ICASSP '01)*. Vol. 5, pp. 3141–3144, May 2001.

[30] R. R. Schoen, T.G. Habetler, F. Kamran, and R.G. Bartheld, "Motor bearing damage detection using stator current monitoring," *IEEE Trans., Ind. Applica.*, vol.31, no. 6, pp. 1274-1279, Nov./Dec. 1995.

[31] J. R. Stack, T. G. Habetler, and R. G. Harley, " Bearing fault detection via autoregressive stator current modeling," *IEEE, Trans., Ind., Applica.*, Vol. 40, pp 740-747, May/June 2004.

[32] R. R. Schoen, , B. K. Lin, T. G. Habetler, J. H. Schlag, and S. Farag, "An unsupervised, on-line system for induction motor fault detection using stator current monitoring," *IEEE, Trans., Ind., Applica.*, vol.31, no. 6, 1280-1286, Nov./Dec. 1995.

[33] L. Eren, A. Karahoca, and M. J. Devaney, "Neural network based motor bearing fault detection," *IMTC-Instrumentation and Measurement Technology Conference*, pp. 1657-1660, May 2004.

[34] J. Ilonen, J. K. Kamarainen, T. Lindh, J. Ahola, H. Kalviainen, and J. Partanen, "Diagnosis tool for motor condition monitoring," *IEEE, Trans., Ind., Applica.*, Vol. 41, No. 4, pp.963-971, Jul./Aug. 2005

[35] J. R. Stack, T. G. Habetler, and R. G. Harley, "Experimentally generating faults in rolling element bearings via shaft current," *IEEE, Trans., Ind., Applica.*, Vol 41, pp. 25-29, Jan./Feb. 2005.

[36] S. M. Kuo, D. R. Morgan, "Active noise control: a tutorial review," *Proceedings of IEEE*, Vol. 87, Issue 6, pp. 943-973, June 1999.

[37] M. H. Hayes, *Statistical Digital Signal Processing and Modeling*. New York: Wiley, ISBN 0-471 59431-8, 1996.

[38] J. R. Stack, "Fault signature detection for rolling element bearings in electric machines," *PhD Dissertation*, Georgia Institute of Technology, Nov. 2002.

[39] J. L. Silva, and A. J. M. Cardoso, "Bearing failures diagnosis in three-phase induction motors by extended Park's vector approach," *Industrial Electronics Society*, IECON 2005, 32nd Annual Conference of IEEE, Nov. 2005.

[40] B. Chaplin, "The cancellation of repetitive noise and vibration," in *Proc. Inter-noise*, 1980, pp. 699–702.

[41] B. Widrow, J. R. Glover, J. M. McCool, J. Kaunitz, C. S. Williams, R. H. Hern, J. R. Zeidler, E. Dong, and R. C. Goodlin, "Adaptive noise canceling: Principles and applications," *Proc.IEEE*, vol. 63, pp. 1692–1716, Dec. 1975.

[42] S.J. Elliott, P. A. Nelson, "Active noise control," *Signal Processing Magazine, IEEE*, Vol. 10, Issue 4, October 1993 Page(s): 12-35.

[43] I. Veit, A Lightweight Headset with Active Noise Compensation, *Proceedings of Inter-Noise, pp. 1087-1090,* 1988.

[44] Ch Carme, A new Filtering method by Feedback for ANC at the ear, *Proceedings of Inter-Noise, pp. 1083-1086,* 1988.

[45] T. K. Moon, and W. C. Stirling, *Mathematical methods and algorithms for signal processing,* Prentice Hall, Upper Saddle River, New Jersey, ISBN 0-201-36186-8, 2000

[46] S. Haykin, *Adaptive Filter Theory*, 4th edition, Prentice Hall, ISBN: 0-13-090126-1, September, 2001

[47] A. V. Oppenheim, R. W. Schafer, *Discrete-Time Signal Processing,* 2nd Edition, Prentice Hall, Upper Saddle River, New Jersey, ISBN: 0-13-754920-2, 1999.

[48] Q. Xie, and H. K. Kwan, "Multichannel Lattice Structure for Adaptive Noise Cancellaiton," *Proceedings of 2004 International Symposium on Intelligent Multimedia, Video and Speech Processing*, October 20-22, 2004 Hong Kong

[49] Y. C. Chen, H.C. Wang, and T. J. Su, "Particle Swarm Optimization for Image Noise Cancellation," *Innovative Computing, Information and Control, 2006, ICICIC '06, First International Conference on*, Volume 1, 30-01 Aug, 2006 Page(s):587 – 590

[50] S. Wu, and M. J. Er, "Dynamic Fuzzy Neural Networks – A Novel Approach to Function Approximation," *IEEE Trans. Systems, Man, and Cybernetics – Part B: Cybernetics*, Vol 30, No. 2, April 2000

[51] M. J. Er, Z. Li, H. Cai, and Q. Chen, "Adaptive Noise Cancellation Using Enhanced Dynamic Fuzzy Neural Networks," *IEEE Trans. Fuzzy Systems,* Vol. 13, No. 3, June 2005

[52] S. A. Billings and C. F. Fung, "Recurrent radial basis function networks for adaptive noise cancellation," *Neural Networks,* vol. 8, pp. 273–290, 1995.

[53] M. J. Er, W. M. Wong, and S. Q. Wu, "A comparative study of different methods for realizing DFNN algorithm," *in Proc. 38th Conf. Decision Control*, Phoenix, AZ, Dec. 1999, pp. 2461–2462.

[54] C. Y. Chang, and K. K. Shyu, "A self-tuning fuzzy filtered-U algorithm for the application of active noise cancellation," *IEEE trans. Circuits and Systems I: Fundamental Theory and Applications*, Vol. 49, Issue 9, Sep 2002, Page(s): 1325-133

[55] D. Kundur, and D. Hatzinakos, " Blind image deconvolution," *IEEE Signal Processing Magazine, IEEE,* Vol. 13, Issue 3, May 1996 Page(s): 43-64

[56] W. Lu, and J. Gai, "Blind deconvolution of spotted image based on slice selection of

third-order moment," *Electronics Letters*, Vol. 39, Issue 3, May 1996 Page(s): 43-64

[57] Z. Ding, and G. Li, "Single-Channel blind equalization for GSM cellular systems,", *Selected Areas in Communications, IEEE Journal on*, Vol. 16, Issue 8, Oct 1998, Page(s): 1493 – 1505

[58] R. R. Obaid, T. G. Habetler, "Current-based algorithm for mechanical fault detection in induction motors with arbitrary load conditions," *Industry Applications Conference, 2003, 38th IAS Annual Meeting,* Vol. 2, 12-16 Oct. 2003, Page(s): 1347 – 1351

[59] K. D. Hurst, T. G. Habetler, "Sensorless speed measurement using current harmonic spectral estimation in induction machine drives," *IEEE Trans. On Power Electronics,* Vol. 11, Issue 1, Jan. 1996 Page(s): 66 – 73

[60] K. D. Hurst, T. G. Habetler, "A comparison of spectrum estimation techniques for sensorless speed detection in induction machines," *IEEE Trans. On Industry Applications*, Vol. 33, Issue 4, July – Aug. 1997 Page(s): 898 – 905

[61] D. J. Wheeler, D. S. *Chambers, Understanding statistical process control*, 2nd edition, Tennessee: Knoxville, ISBN: 0-945320-13-2, SPC Press, 1992

[62] J. S. Oakland, *Statistical Process Control*, 4th edition, Butterworth-Heinemann, ISBN: 0 7506 4439 7, 1999

[63] T. P. Ryan, *Statistical methods for quality improvement*, 2nd edition, A Wiley-Interscience Publication, John Wiley & Sons, Inc., ISBN: 0-471-19775-0, 2000

[64] H. L. Harter, and N. Balakrishnan, *Tables for the Use of Range and Studentized Range in Tests of Hypotheses,* CRC Press, 1998

[65] W. A. Shewhart, *Economic Control of Quality of Manufactured Product*, Amer Society for Quality Press, Milwaukee, Wisconsin, ISBN: 0-87389-076-0, 1980

[66] The MathWorks, Inc., *MATLAB® Version 7.0 (R14) User Manual*, September, 2004

[67] Cohen, J. (1988). *Statistical power analysis for the behavioral sciences* (2nd ed.) Hillsdale, NJ: Lawrence Erlbaum Associates. ISBN 0-8058-0283-5.

[68] C. M. Riley, "Current-based sensorless vibration monitoring of small AC machines,"

*PhD Dissertation*, Georgia Institute of Technology, Aug. 1998.

[69] R. R. Obaid, "Detection of rotating mechanical asymmetries in small induction machines," *PhD Dissertation*, Georgia Institute of Technology, May 2003

[70] J. R. Cameron, W. T. Thomson, A. B. Dow, "Vibration and current monitoring for detecting airgap eccentricity in large induction motors," *IEE Proceedings* B, Vol. 133, No, 3, pp. 155-163, May 1986.

[71] W. Zhou, T. G. Habetler, B. Lu, R. G. Harley, P. Theisen, "Motor bearing fault detection via stator current noise cancellation," *Appl No. US 60/932742,* United States Patent and Trademark Office, June 2007

[72] W. Zhou, T. G. Habetler, and R. G. Harley, "Bearing Condition Monitoring Methods for Electric Machines: A General Review," *6th IEEE International Symposium on Diagnostics for Electric Machines, Power Electronics and Drives, IEEE SDEMPED '07,* Poland, September 6 – 8, 2007.

[73] W. Zhou, T. G. Habetler, and R. G. Harley, "Stator Current-Based Bearing Fault Detection Techniques: A General Review," *IEEE International Symposium on Diagnostics for Electric Machines, Power Electronics and Drives, IEEE SDEMPED '07,* Poland, September 6 – 8, 2007.

[74] W. Zhou, T. G. Habetler, and R. G. Harley, "Incipient Bearing Fault Detection via Stator Current Noise Cancellation using Wiener Filter," *IEEE International Symposium on Diagnostics for Electric Machines, Power Electronics and Drives, IEEE SDEMPED '07*, Poland, September 6 – 8, 2007.

# Vita

Wei Zhou was born in China in October, 1977. He received the Bachelor of Science Degree and Master of Science Degree in Electrical Engineering from Wuhan University, Wuhan, China, in 1999 and 2002, respectively.

From 2002 to 2003, he was with Guangdong Electric Power Design Institute (GEDI), Guangzhou, China, as a bulk power system planner. While there, he was involved in transmission network expansion planning and large generation integration studies for Southern China Power Grid. In August 2003, he began his studies at Georgia Institute of Technology, Atlanta, GA, where he has been pursuing his doctoral degree in electrical engineering. From 2003, he has been working on electric machine condition monitoring, as a Graduate Research Assistant in the Power group in the School of Electrical and Computer Engineering. He joined the Midwest Independent System Operator, as a Financial Transmission Rights Engineer in August 2007.